NASA
SPACE VEHICLE
DESIGN CRITERIA
(CHEMICAL PROPULSION)

NASA SP-8052

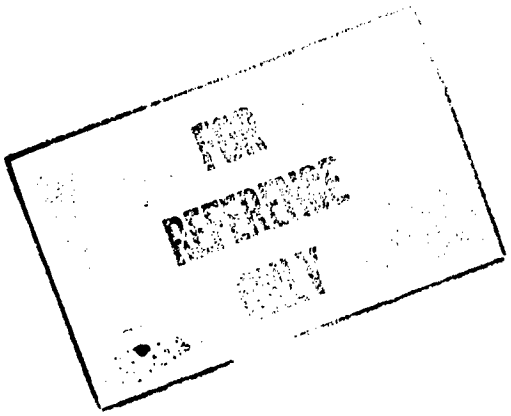

LIQUID ROCKET ENGINE TURBOPUMP INDUCERS

MAY 1971

NATIONAL AERONAUTICS AND SPACE ADMINISTRATION

FOREWORD

NASA experience has indicated a need for uniform criteria for the design of space vehicles. Accordingly, criteria are being developed in the following areas of technology:

Environment
Structures
Guidance and Control
Chemical Propulsion

Individual components of this work will be issued as separate monographs as soon as they are completed. This document, part of the series on Chemical Propulsion, is one such monograph. A list of all monographs issued prior to this one can be found on the last page of this document.

These monographs are to be regarded as guides to design and not as NASA requirements, except as may be specified in formal project specifications. It is expected, however, that these documents, revised as experience may indicate to be desirable, eventually will provide uniform design practices for NASA space vehicles.

This monograph, "Rocket Engine Turbopump Inducers," was prepared under the direction of Howard W. Douglass, Chief, Design Criteria Office, Lewis Research Center; project management was by Harold W. Schmidt and Lionel Levinson. The monograph was written by Jakob K. Jakobsen of Rocketdyne Division, North American Rockwell Corporation, and was edited by Russell B. Keller, Jr. of Lewis. To assure technical accuracy of this document, scientists and engineers throughout the technical community participated in interviews, consultations, and critical review of the text. In particular, J. Farquhar III of Aerojet-General Corporation, W. E. Young of Pratt Whitney Aircraft Division, United Aircraft Corporation, and M. J. Hartmann and C. H. Hauser of the Lewis Research Center individually and collectively reviewed the text in detail.

Comments concerning the technical content of this monograph will be welcomed by the National Aeronautics and Space Administration, Lewis Research Center (Design Criteria Office), Cleveland, Ohio 44135.

May 1971

GUIDE TO THE USE OF THIS MONOGRAPH

The purpose of this monograph is to organize and present, for effective use in design, the significant experience and knowledge accumulated in development and operational programs to date. It reviews and assesses current design practices, and from them establishes firm guidance for achieving greater consistency in design, increased reliability in the end product, and greater efficiency in the design effort. The monograph is organized into two major sections that are preceded by a brief introduction and complemented by a set of references.

The State of the Art, section 2, reviews and discusses the total design problem, and identifies which design elements are involved in successful design. It describes succinctly the current technology pertaining to these elements. When detailed information is required, the best available references are cited. This section serves as a survey of the subject that provides background material and prepares a proper technological base for the *Design Criteria* and Recommended Practices.

The *Design Criteria,* shown in italic in section 3, state clearly and briefly what rule, guide, limitation, or standard must be imposed on each essential design element to assure successful design. The *Design Criteria* can serve effectively as a checklist of rules for the project manager to use in guiding a design or in assessing its adequacy.

The Recommended Practices, also in section 3, state how to satisfy each of the criteria. Whenever possible, the best procedure is described; when this cannot be done concisely, appropriate references are provided. The Recommended Practices, in conjunction with the *Design Criteria,* provide positive guidance to the practicing designer on how to achieve successful design.

Both sections have been organized into decimally numbered subsections so that the subjects within similarly numbered subsections correspond from section to section. The format for the Contents displays this continuity of subject in such a way that a particular aspect of design can be followed through both sections as a discrete subject.

The design criteria monograph is not intended to be a design handbook, a set of specifications, or a design manual. It is a summary and a systematic ordering of the large and loosely organized body of existing successful design techniques and practices. Its value and its merit should be judged on how effectively it makes that material available to and useful to the designer.

CONTENTS

LIST OF FIGURES AND TABLES

LIQUID ROCKET ENGINE TURBOPUMP INDUCERS

1. INTRODUCTION

The inducer is the axial inlet portion of the turbopump rotor whose function is to raise the inlet head by an amount sufficient to preclude cavitation in the following stage. The inducer may be an integral part of the pump rotor or it may be mounted separately on the pump shaft upstream of the impeller. The principal objective in the design of an inducer is the attainment of high suction performance, but the achievement of maximum performance is limited by structural design considerations. The optimum design, therefore, is a compromise that provides adequate suction performance while maintaining structural integrity under all operating conditions. Such a design depends on simultaneous satisfactory solutions of hydrodynamic and mechanical problems.

The hydrodynamic problems involve obtaining the required suction specific speed and head rise of the inducer without introducing undesirable cavitation. Much work has been done on the theoretical hydrodynamic design of the inducer for an ideal fluid, which normally is assumed to resemble cold water in its effect on suction performance. However, it has not yet been possible to use test results on inducer performance with cold water to predict actual performance with the intended pump fluid. Other major unsolved problems involve obtaining satisfactory theoretical treatments for (1) three-dimensional effects, (2) the suction performance of inducer cascades with curved blades, (3) the effects of blade leading-edge sweep, and (4) the effects of tip clearance. In the absence of a satisfactory analytical basis for design, these hydrodynamic problems are solved empirically by utilizing experience with previous successful designs.

The mechanical problems involve maintaining the structural integrity of the blade leading edge and providing for blade and hub stresses due to blade loading, flow instabilities, and centrifugal forces. They include also proper choice of material, which must be compatible with both the pump operating fluid and the pump test fluid, and selection of the best way to assemble the inducer in the pump during fabrication. The achievement of an optimum inducer design requires a systematic survey of all mechanical design factors. This survey is based on a combination of fundamental theory and practical experience related to previously proven inducer designs and enables the designer to identify the effect of design variants on the overall performance, on ease of manufacture, on simplicity and reliability of assembly, and on strength and reliability of the chosen design.

In keeping with this approach, this monograph is based on a critical evaluation of available information on the hydrodynamics, mechanical design, development, and testing of pump inducers. Its purpose is to furnish well-established, specific design practices for pump inducers based on the present state-of-the-art technology. These practices are presented in a form matched to the needs of the design team, along lines following the natural and logical progression of the design effort. The material is arranged to reflect both the natural organization of work and the corresponding division of the design team to deal with hydrodynamics, mechanical design, material selection, and vibration and stress problems.

The design philosophy in the monograph is to seek an optimization of the hydrodynamic parameters to obtain the highest suction specific speed possible without violating structural and mechanical design constraints. The approach is to design for the maximum acceptable tip cavitation number by a mathematical optimization process. This establishes an optimum value for the flow coefficient and the corresponding fluid angle. To achieve a certain margin of operation, the blade suction surface is kept within the cavity boundary up to a flowrate somewhat higher than design requirements. The blade thickness, as given by the wedge angle between the pressure and the suction sides of the blade at the leading edge, increases with the ratio of incidence angle to blade angle. The bending stresses in the leading edge then decrease, even though the increased incidence angle raises the hydrodynamic load. Root bending stresses are lowered by the increase in wedge angle possible at the root section. Since the head rise obtained with flat-plate inducers is low, a simple radial-equilibrium check of the flow distribution is sufficient to verify that there is no backflow in the blade channel at the design point. By this approach, inducer design can achieve the most effective combination of hydrodynamic and mechanical factors.

2. STATE OF THE ART

Inducers are classified according to head-rise capability and also according to the shape of the meridional flow path. They are divided by head-rise capability into low head (head coefficent $\psi \leq 0.15$)[1] and high head ($\psi > 0.15$). The head-rise capability is a function of blade geometry (i.e., flat-plate, modified-helix, or vortex type). The low-head inducer blading is either flat-plate or flat-plate plus modified-helix, depending on hub-tip contours and ψ value. The high-head inducer blading is a combination of flat-plate, modified-helix, and vortex-type blading with splitter vanes. The high-head inducer may be divided into the inducer proper and the discharge blade section; it is actually an axial-flow impeller with an integral inducer covering a solidity between 2.0 and 2.50. When inducers are classified according to meridional cross section, they are divided into four basic types: (1) cylindrical tip and hub; (2) cylindrical tip, tapered hub; (3) tapered tip and hub; and (4) shrouded with or without a hub.

Figure 1 gives six characteristic examples of the basic inducer types taken from actual practice. Examples (a) to (d) are low-head inducers, and (e) and (f) are high-head inducers. Notice that all the inducers with the exception of (c) maintain a constant tip diameter at the inlet for an axial length corresponding to a solidity of 1 or higher. This design practice benefits the suction performance by maintaining optimum conditions until the blade cavity has collapsed (type (c) was designed before this practice was established). Table I summarizes design and performance parameters of these inducers.

The shrouded inducer with a large forward sweep of the blade is also known as the hubless inducer because of its appearance (fig. 2). The blading is thus supported by the shroud, which in turn is supported and driven either through the rear portion of the inducer blading by the inducer short hub or, in the case of a truly hubless design, by attachment to the impeller shroud. The front hubless portion and the rear hub portion of the inducer are machined separately and joined by welding.

Thus, the hubless inducer differs from the conventional inducer in that its blading is supported by the shroud instead of by the hub; also, if the conventional inducer is considered a screw, then the hubless inducer must be considered a nut. The hubless inducer concept is associated with several assumed advantages: (1) it eliminates tip vortex cavitation; (2) it centrifuges eventual bubbles toward the center, where they may collapse harmlessly; and (3) it offers the possibility of using an extremely large forward sweep of the vanes to obtain a sweptwing effect similar to that of supersonic plane design.

[1]Symbols, subscripts, and abbreviations are defined in the Glossary.

Table I.—Basic Inducer Types: Design and Performance Summary

Rocket engine	Thor	J-2	X-8	X-8	J-2	J-2
Pump designation	Mark 3	Mark 15	Mark 19	Mark 19	Mark 15	Mark 15
Example in fig. 1	(a)	(b)	(c)	(d)	(e)	(f)
Pump fluid	Liquid oxygen	Liquid oxygen	Liquid oxygen	Liquid oxygen	Liquid hydrogen	Liquid hydrogen
Head type	Low	Low	Low	Low	High	High
Cross-sectional profile or geometry	Cylindrical tip and hub	Cylindrical tip, tapered hub	Tapered tip and hub	Shrouded	Cylindrical tip, tapered hub	Tapered tip and hub
Design flow coefficient ϕ_d(1)	0.116	0.109	0.106	0.05	0.0942	0.0735
Design head coefficient ψ_d(1)	0.075	0.11	0.10	0.063	0.21	0.20
Inlet tip blade angle β	14.15°	9.75°	9.8°	5.0°	7.9°	7.35°
Suction specific speed S_s in water(2)	28,500	34,300	31,200	58,000	43,200	44,200
Hub-tip ratio ν at inlet	0.31	0.20	0.23	0.19	0.42	0.38
Number of blades	4	3	3	2	4 + 4	4 + 4
Leading-edge sweep	Radial with rounded tips	Sweptback	Sweptback	Sweptforward	Sweptback	Sweptback

(1) Based on inlet tip blade speed.
(2) At 10% head dropoff from noncavitating head.

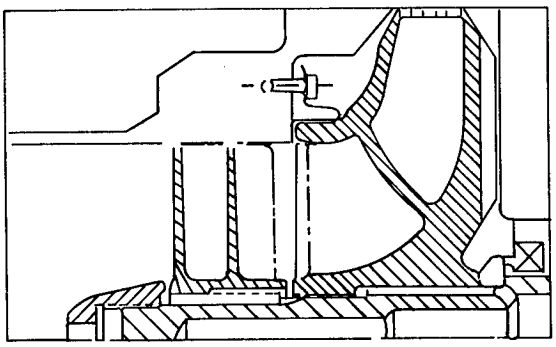

(a) Low-head inducer with cylindrical tip and hub

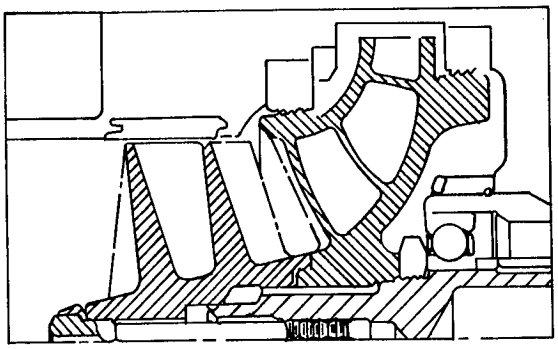

(b) Low-head inducer with cylindrical tip, tapered hub

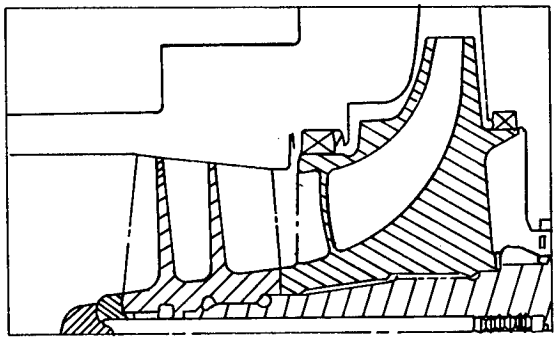

(c) Low-head inducer with tapered tip and hub

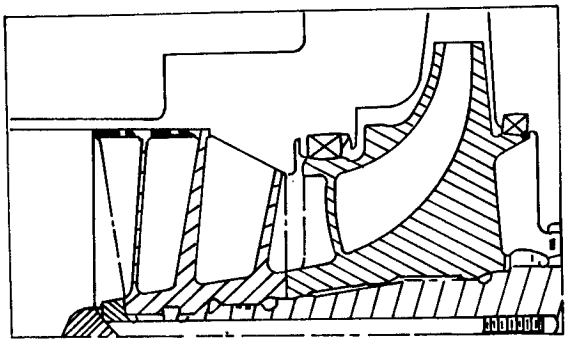

(d) Low-head inducer, shrouded

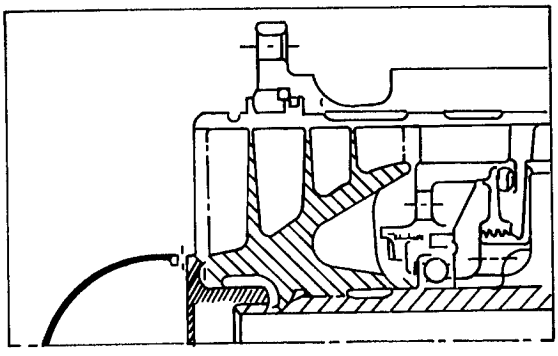

(e) High-head inducer with cylindrical tip, tapered hub

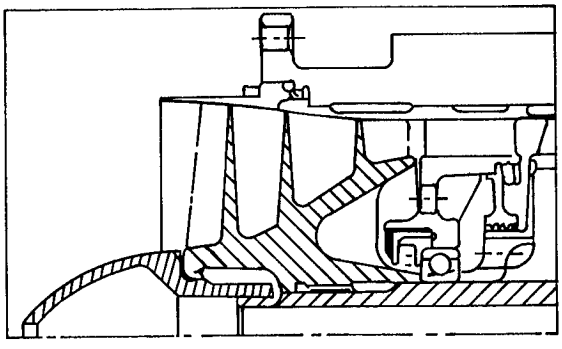

(f) High-head inducer with tapered tip and hub

Figure 1.—Basic inducer types.

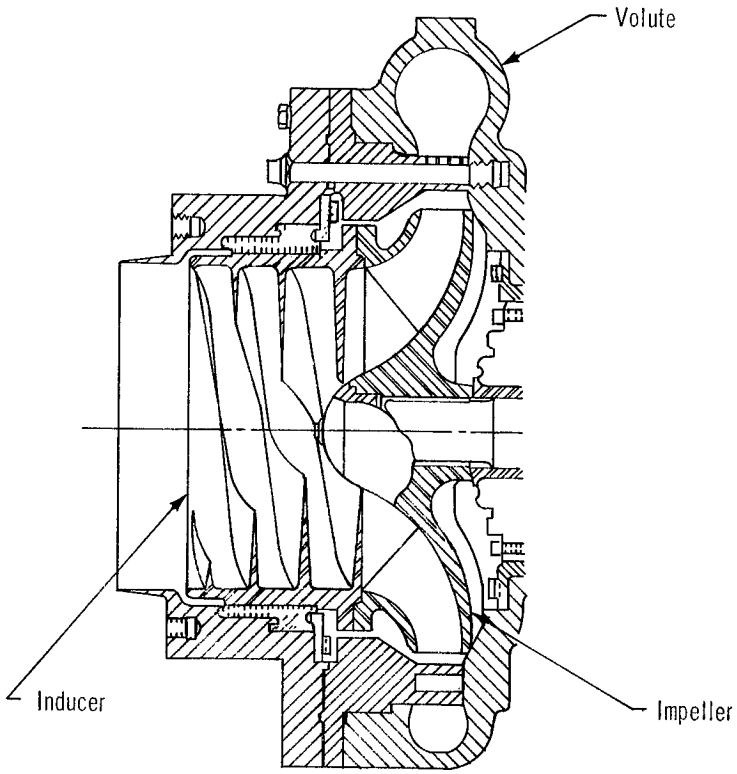

Figure 2.—Hubless inducer.

The concept, however, also has serious disadvantages: (1) the hubless inducer is difficult to manufacture, and the vanes cannot be properly machined to obtain the desired accuracy and surface finish; and (2) structurally the free floating ring of the shroud cannot carry high-speed centrifugal forces, and the inducer is reduced to a low-speed device.

Experimentally the hubless inducer has shown suction performance about equal to that of the conventional type, but somewhat worse efficiency and head coefficient. As a consequence of the performance limitations, manufacturing problems, and space requirements, the hubless inducer is not a serious contender to the conventional hub-type inducer and cannot be considered a state-of-the-art item.

2.1 Inducer Inlet-Eye and Leading-Edge Geometry

The inducer design is optimized with respect to system considerations. Suction specific speed S_s and suction specific diameter D_s are the characteristic parameters that describe the inducer suction performance in terms of shaft rotative speed n, flowrate Q, inducer inlet tip diameter D, and critical or required net positive suction head NPSH:

$$S_s = n\,Q^{1/2}\,(\mathrm{NPSH})^{-3/4} \tag{1a}$$

$$D_s = D\,Q^{-1/2}\,(\mathrm{NPSH})^{1/4} \tag{1b}$$

Details involved in determining the values of n, Q, and NPSH are provided in the design criteria monograph "Turbopump Systems for Liquid Rocket Engines."

In general, the flowrate is fixed by the engine specific impulse and thrust level. The available NPSH is a function of structural considerations that involve tank pressure and the minimum needs of the pump suction performance. The shaft speed is limited by various system considerations concerning the turbopump design. To minimize the weight of the turbopump, the shaft speed is generally chosen as high as is permitted by considerations of mechanical design of the turbopump unit and the swallowing capacity of the inducer. This swallowing capacity is limited by the vapor cavitation or by combined vapor–dissolved gas cavitation that takes place in the liquid adjacent to the suction side of the inducer blades at the leading edge. The cavitation is most severe at the blade tip, where blade speed is highest. As blade speed increases, the cavity at the leading edge becomes larger and increasingly blocks the flow. When the blade speed exceeds the value associated with the maximum obtainable suction specific speed, head rise is lost. The solution to this cavitation problem lies in careful attention to the design of the inducer inlet configuration, with special emphasis on the hydrodynamic aspects of the blade leading-edge geometry that determine the suction performance of the inducer.

2.1.1 Inlet Casing

The configuration of the inducer inlet casing is dictated by systems considerations. The preferred shape is the axial inlet in line with the inlet duct (fig. 1). This arrangement provides unobstructed flow into the inducer; it requires an overhung impeller driven from the rear through the pump scroll.

Space and systems limitations may require a 90° bend that features either single or dual inlets on opposite sides of the casing; this requirement also exists when the pump is driven from the front end (figs. 3 and 4).

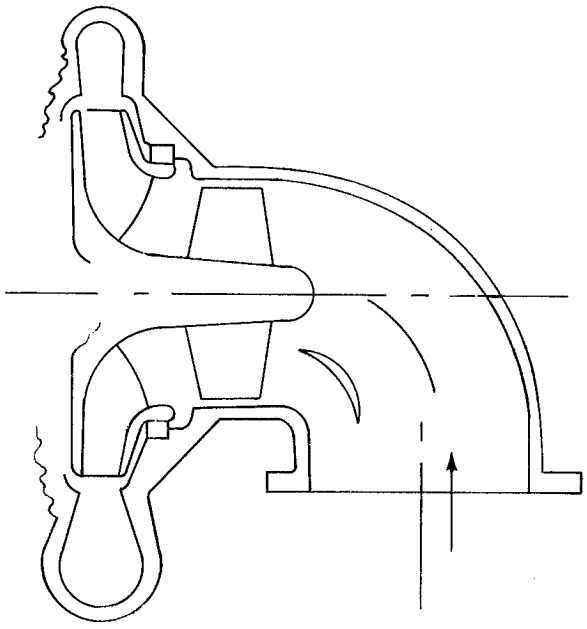

Figure 3.—Inlet elbow.

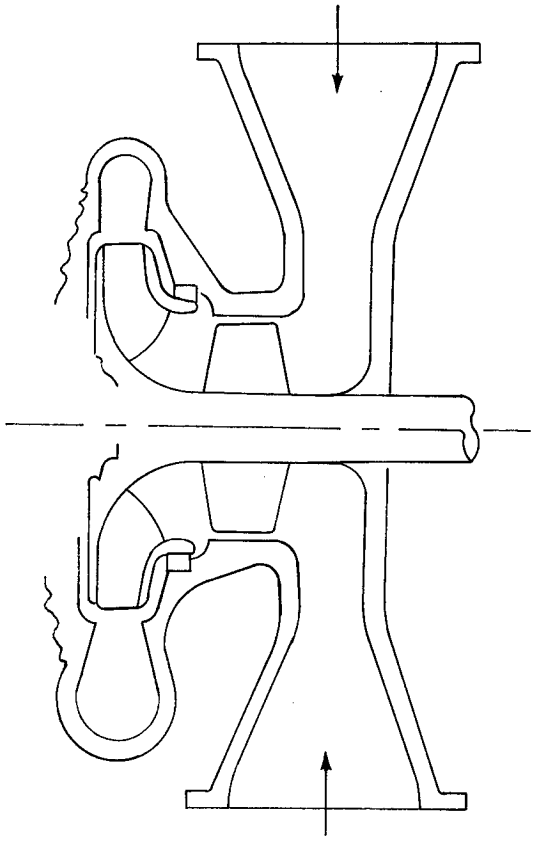

Figure 4.—Dual inlet.

The arrangement of the inlet casings for a propellant pump with fuel and oxidizer pumps back-to-back, driven through an intermediate reduction gear from an offset turbine, is shown in figure 5. Notice the combination of a mitered bend and a cascade of turning vanes to obtain a compact and efficient elbow.

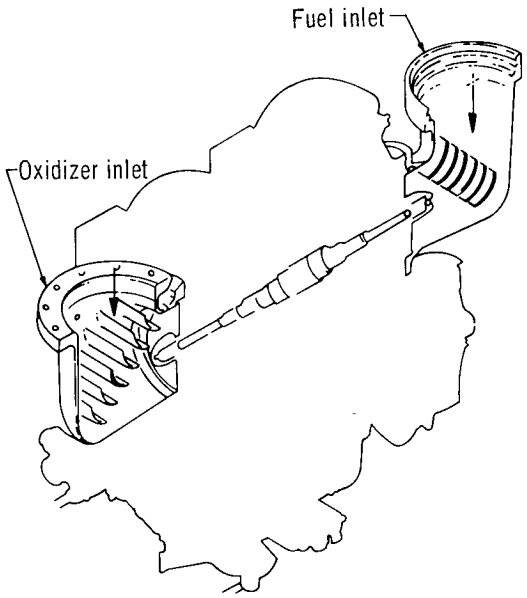

Figure 5.—Arrangement of inlet casings.

The use of vanes to obtain a uniform circumferential flow distribution for a dual inlet pump is shown in figure 6.

Development of an inlet elbow is shown in figure 7, which compares the original, unsatisfactory configuration with the final, improved configuration. The original configuration, without vanes, had unstable flow and backflow at the inner radius of the elbow. Addition of two turning vanes alone did not stabilize flow because of the abrupt turning at the original inner radius. The elbow was redesigned with an extended turning region aided by three turning vanes. The final design shown in figure 7 was effective in producing stable flow. This inlet elbow is used with the dual inlet casing of figure 6.

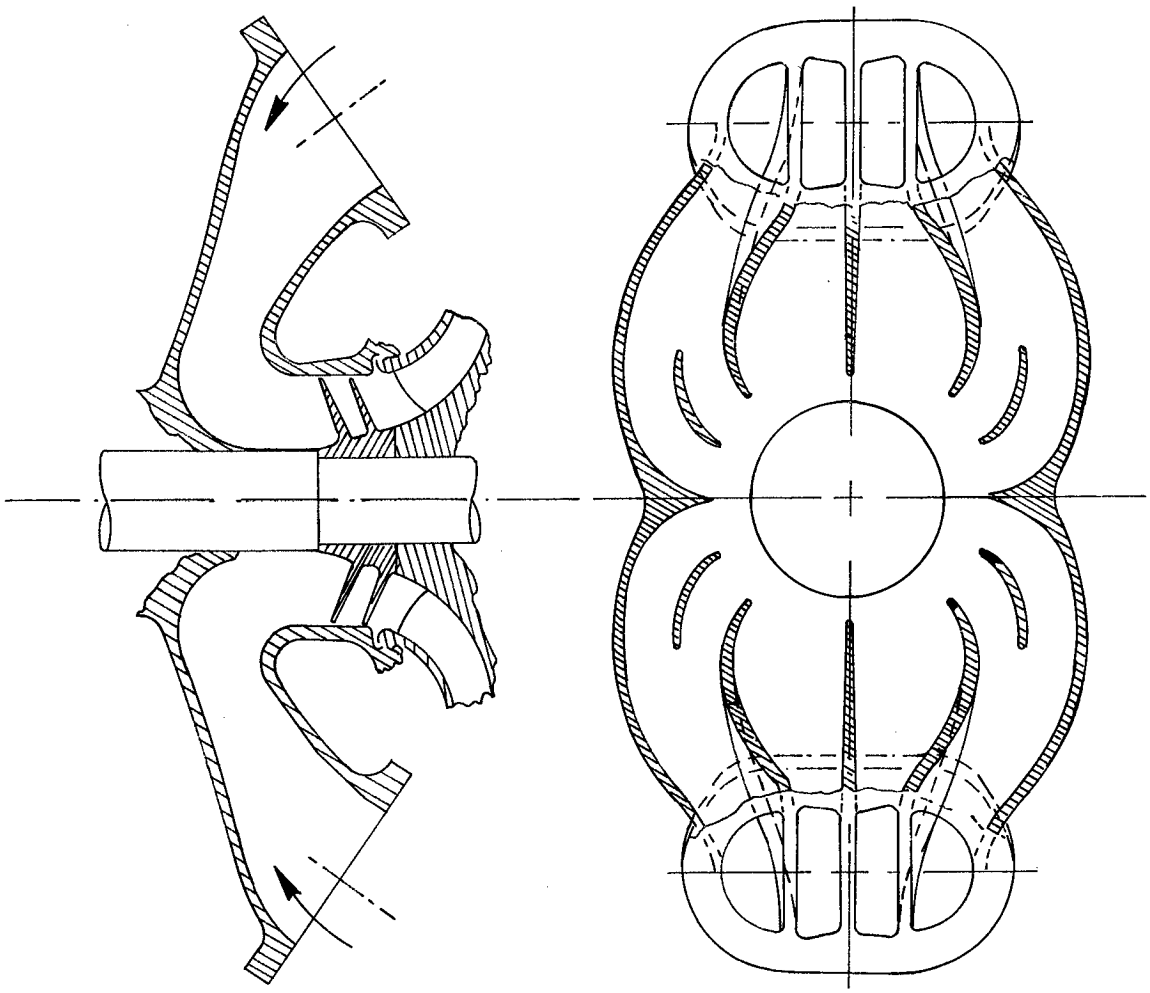

Figure 6.—Dual inlet casing.

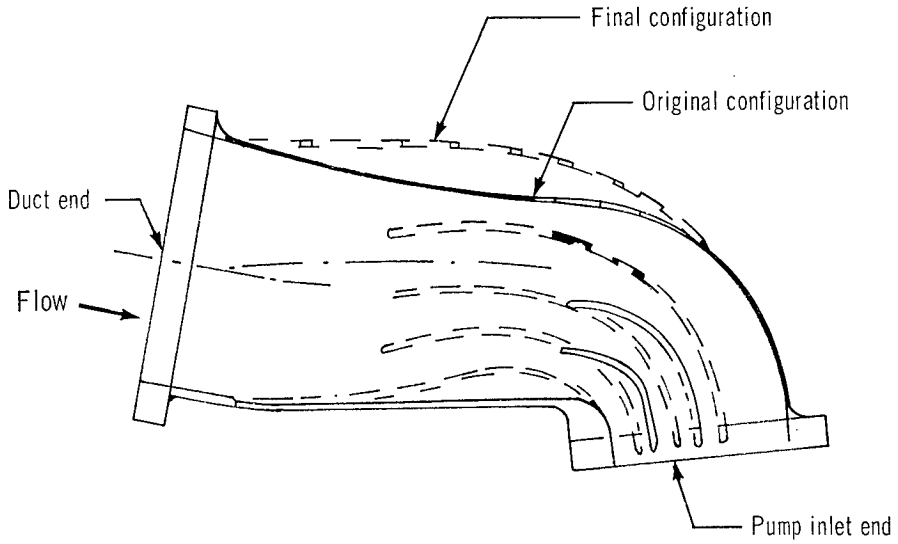

Figure 7.—Inlet elbow development.

2.1.2 Hub Size and Shape

The inducer hub diameter on the inlet end is determined primarily by the structural requirement that the hub withstand the loads from torque transmittal and the loads from the combined fluid and mass forces acting on the blades (and possibly on the hub itself in high-head inducers). In addition, the final size selected for the hub must allow for the installation and use of a spinner nut or axial bolt large enough for axial retention of the inducer.

When the pump is driven from the rear, the inducer hub diameter on the inlet end can be kept small; normally the hub-to-tip diameter ratio ν is in the range $\nu = 0.2$ to 0.4. When the pump is driven from the inlet end, the full pump torque must be transmitted through the inducer hub. In this case, the hub-to-tip diameter ratio falls normally in the range $\nu = 0.5$ to 0.6.

The contour of the inducer hub depends on the hub inlet and outlet diameters. The inlet diameter normally is chosen as small as possible consistent with structural considerations discussed in section 2.7.3. The outlet diameter is chosen to match the component following the inducer; for low-head inducers this is the impeller eye, and for high-head inducers it is an axial stage. The resulting hub contour for a low-head inducer normally is a straight taper of 8° to 12°. High-head inducers combine a low-head inducer section with a mixed-flow integral or separate section that generates additional head and matches the axial stage following it. The hub contour in this case consists of a straight taper for the inducer section, with a curved, smooth transition between this taper and the discharge diameter and slope of the mixed-flow section.

2.1.3 Inlet Tip Diameter and Contour

The most suitable inlet tip diameter D is derived from the relationship between suction specific speed S_s, blade tip cavitation number K, and flow coefficient ϕ by mathematical consideration of optimum flow conditions for maximum suction performance. For an inducer with zero prewhirl, these relationships are given by the following equations:

$$\tau = K + K\phi^2 + \phi^2 \tag{2}$$

$$S'_s = 8147\, \phi^{1/2}\, \tau^{-3/4} \tag{3}$$

$$S_s = S'_s\,(1 - \nu^2)^{1/2} \tag{4}$$

where S'_s is the corrected suction specific speed obtainable for zero hub-to-tip radius ratio ν and $\tau = 2g(\mathrm{NPSH})/u^2$ is the cavitation parameter. For an inducer with zero prewhirl and a fixed hub-to-tip radius ratio the consideration of optimum flow conditions leads to the so-called Brumfield criterion (refs. 2-5) for the optimum flow coefficient ϕ_{opt}:

$$K = \frac{2\,\phi^2_{opt}}{1 - 2\,\phi^2_{opt}} \tag{5}$$

which solved for ϕ_{opt} in terms of K gives

$$\phi_{opt} = \sqrt{\frac{K}{2\,(1 + K)}} \tag{6}$$

The corresponding suction specific speed then is a mathematical maximum given by

$$\max S'_s = \frac{5055}{(1 + K)^{1/4}\, K^{1/2}} \tag{7}$$

showing that theoretically the suction specific speed is limited only by the minimum cavitation number K^* at which the blade will operate. Values of K^* as low as 0.01 to 0.006 have been obtained experimentally for very thin blades and small blade and wedge angles ($\beta \cong 5°$, $\alpha_W \cong 2°$).

The inducer inlet tip diameter D follows from the definition of the flow coefficient $\phi = c_m/u$, where $c_m = Q/A$ when inlet flow area A and blade tip speed u are expressed in terms of D. With proper consideration of units, there results

$$D = 0.37843 \left[\frac{Q}{(1 - \nu^2)\, n\, \phi}\right]^{1/3}, \text{ ft} \tag{8}$$

where

Q = flow, gpm
n = shaft speed, rpm

The optimum value for D follows from equation (8) by using the optimum value for ϕ from equation (6).

To obtain the maximum suction performance, the inlet tip diameter must be held constant and equal to its optimum value at the inlet (as determined above) for an axial distance equal to one axial blade spacing downstream of the leading edge. This design practice leaves the partial cavity on the blade undisturbed until the channel section is reached.

To ensure the uniform inlet velocity assumed in the optimization, the diameter of the duct or housing upstream of the leading edge is held constant for a length equal to at least one axial spacing. Thus, the housing diameters both downstream and upstream of the blade leading edge are held constant. In most cases, these diameters are the same; but they may differ because of special considerations such as the effects of leakage flow or the use of a shroud.

The design approach outlined in this section must be modified for the hubless inducer because a nonuniform velocity distribution is induced at the blade leading edge by the strong forward sweep of the blading featured in the hubless inducer. No state-of-the-art design approach is known at present. A cross section of an actual design of an experimental hubless inducer is shown in reference 1, but no design approach is indicated.

2.1.4 Fluid Thermodynamic Effects

For an ideal fluid, which is as approximated by cold water, hydrocarbon and amine fuels, and other low-vapor-pressure fluids, the limitation on suction performance is always leading-edge cavitation in the inducer. With certain fluids there is observed a thermodynamic suppression head (TSH) that acts to decrease the critical NPSH requirements of the inducer (refs. 1, 6-25). Among the fluids known to exhibit this effect are liquid hydrogen, liquid oxygen, storable oxidizers such as N_2O_4, and hot (over 200° F) water. For liquid hydrogen this effect may be so strong that the swallowing capacity is limited only by cavitation in the inlet duct; i.e., by $c_m^2/2g = (\mathrm{NPSH})_{\mathrm{tank}}$, where c_m is the meridional velocity, calculated for single-phase flow and $(\mathrm{NPSH})_{\mathrm{tank}}$ is the minimum available net positive suction head in the tank at operating conditions.

Thermodynamic suppression head is an effect brought about by the decrease in fluid vapor pressure and additionally, in the case of two-phase flow, by the decrease in fluid density. The phenomenon of TSH is best defined and understood in the following mathematical formulations.

The basic condition for pump suction performance is that

$$(\text{NPSH})_{\text{required}} \leqq (\text{NPSH})_{\text{available}} \tag{9}$$

The $(\text{NPSH})_{\text{required}}$ is determined by the characteristic pump suction specific speed $S'_s{}^*$, which is obtained from pump performance with an ideal fluid (approximated in practice by cold water). From equations (1) and (4), with Q' as defined in equation (24)

$$(\text{NPSH})_{\text{required}} = (n\, Q'^{1/2}/S'_s{}^*)^{4/3} \tag{10}$$

assuming that the pump characteristic suction performance is independent of the pump fluid.

By definition, the net positive suction head is the excess of fluid total pressure p_{total} above vapor pressure p_v divided by the fluid density ρ_F at the prevailing local conditions. It follows then that the pump sees the value

$$(\text{NPSH})_{\text{available}} = \left(\frac{p_{\text{total}} - p_v}{\rho_F} \right)_{\text{at inducer leading edge}} \tag{11}$$

where p_{total}, p_v, and ρ_F are the local values measured at the inducer inlet; they are different from the values at the tank and depend on the flow conditions.

For the hypothetical ideal fluid, the NPSH value is of constant magnitude (except for line friction loss) throughout the inlet system from tank to inducer inlet under all flow conditions; i.e.,

$$(\text{NPSH})_{\text{ideal fluid}} = \left(\frac{p_{\text{total}} - p_v}{\rho_F} \right)_{\text{tank}} - H_{\text{loss}} \tag{12}$$

where p_{total}, p_v, and ρ_F are the values in the tank at its outlet, and where H_{loss} is the line head loss due to friction.

By definition, the thermodynamic suppression head is determined by the following equation:

$$(\text{NPSH})_{\text{available}} = (\text{NPSH})_{\text{ideal fluid}} + \text{TSH}, \quad \text{or TSH} = (\text{NPSH})_{\text{a}} - (\text{NPSH})_{\text{if}} \tag{13}$$

In practice, $(\text{NPSH})_{\text{available}}$ has never been measured directly, but its value has been inferred from the measured pump suction performance with various liquids by assuming that the equal sign applies in equation (9) when head breakdown occurs.

Various semiempirical correlations of TSH with fluid properties and pump parameters have been attempted (refs. 24 through 27). These correlations are based on a relationship between the thermal cavitation parameter α, the thermal diffusivity of the liquid $\mathbf{K}_L$, and the size and speed of the pump.

The thermal cavitation parameter and diffusivity are functions of the fluid properties only; i.e.,

$$\alpha = \frac{J L^2}{T c_L \frac{\rho_L}{\rho_v} \left(\frac{\rho_L}{\rho_v} - 1 \right)} \tag{14}$$

and

$$\mathbf{K}_L = \frac{k_L}{\rho_L c_L} \tag{15}$$

where

J = energy conversion factor, 778.2 ft-lb/Btu
L = latent heat, Btu/lb
c_L = specific heat of liquid, Btu/lb-°R
T = fluid bulk temperature, °R
ρ_L = liquid density, lb/ft^3
ρ_v = vapor density, lb/ft^3
k_L = thermal conductivity of liquid, Btu/(sec-ft-°R)
$\mathbf{K}_L$ = thermal diffusivity of liquid, ft^2/sec
α = thermal cavitation parameter, ft

Holl (ref. 22) combined the parameters α and $\mathbf{K}_L$ to form the thermal factor β:

$$\beta = \frac{\alpha}{\sqrt{\mathbf{K}_L}}, \text{ sec}^{1/2} \tag{16}$$

By hypothesis, TSH is a function of the fluid thermodynamic cavitation properties, the fluid velocity U_c on the cavity boundary, and the length L_c of the cavity. The variables TSH, α, $\mathbf{K}_L$, U_c, and L_c form a set of three independent, physically significant, dimensionless groups through which the functional relationship is expressible. One set of three basic groups includes (TSH/α), (L_c/α), and $(U_c L_c/\mathbf{K}_L)$, from which other sets are formed by combination, e.g., (TSH/L_c), (L_c/α), and $(\beta^2 U_c/L_c)$. The application of dimensionless groups to the analysis of pump performance studies requires a relation between a set of basic groups, e.g.,

$$\frac{(\text{TSH})}{L_c} = C\,(L_c/\alpha)^{m1}\,(\alpha U_c/\mathbf{K}_L)^{m2}\,(L_c/S)^{m3} \tag{17}$$

where the constant C and the exponents $m1$, $m2$, and $m3$ are determined by tests on similar pumps, S is the blade spacing, and U_c is a function of the blade tip speed u. So far, no such relationship with well-established values for the constants and exponents has been found.

A cavitation number K_c, based on the cavity pressure instead of the liquid bulk vapor pressure, has been defined (refs. 24 through 27):

$$K_c = \frac{p_s - p_c}{\rho_F \, w^2/2 \, g} \tag{18}$$

where

p_s = fluid static pressure, lb/ft^2
p_c = fluid vapor pressure in cavity at leading edge, lb/ft^2
ρ_F = fluid density, lb/ft^3
w = fluid velocity relative to blade at tip, ft/sec
g = gravitational constant, 32.174 ft/sec^2

Venturi cavitation studies show that K_c is approximately constant while the conventional cavitation number K varies when both are measured over a large range of liquids, temperatures, velocities, and venturi sizes, provided the geometric similarity of the cavitated region is maintained (i.e., the ratio of cavity length to diameter, L_c/D_c, is constant). The studies on venturi cavitation have produced information useful in understanding the problem of thermal suppression head in pumps. On the basis of these studies, attempts have been made to predict actual values for TSH for various fluids used in pumps (ref. 25). The correlations obtained, however, do not allow successful prediction of pump performance without the availability of reference data, i.e., data on the actual performance of the pump with a liquid having TSH effects.

Fluid thermodynamic effects on suction performance are considered in the design phase by a correction on the available NPSH value. An empirical allowance for TSH is added to the tank NPSH value (less the inlet line head loss). The assumed TSH value is based on previous experience with the fluid. No theoretical prediction is attempted at present. Presently established empirical values for the Mark 10 (F-1 engine) liquid-oxygen pump (inducer tip speed: 300 ft/sec) and the Mark 15 (J-2 engine) liquid-hydrogen pump (inducer tip speed: 900 ft/sec) are as follows:

Mark 10-0: TSH = 11 ft, at 163° R
Mark 15-F: TSH = 250 ft, at 38° R

These values are used with considerable reservation, however, when applied to other pumps, because the occurrence of thermodynamic suppression head is not well understood and the effect of a change in the characteristic parameters is not known. The TSH value of a fluid increases with temperature almost as a linear function of vapor pressure (ref. 20). Tests also indicate the existence of a speed and fluid velocity effect increasing the TSH with speed (rpm) at fixed flow coefficients (refs. 28 and 29).

Another common practice to allow for the fluid thermodynamic effect empirically in the design phase is to assume a value (based on experience) for an NPSH factor Z, defined by

$$Z = \frac{2\,g\,(\mathrm{NPSH})_{\mathrm{tank}}}{c_m{}^2} \tag{19}$$

which corresponds to a TSH correction of

$$(\mathrm{TSH}) = \frac{(Z_{\mathrm{opt}} - Z)c_m{}^2}{2g} \tag{20}$$

giving the total required NPSH value

$$(\mathrm{NPSH})_{\mathrm{required}} = (\mathrm{NPSH})_{\mathrm{tank}} + (\mathrm{TSH}) = \frac{Z_{\mathrm{opt}}\,c_m{}^2}{2g} \tag{21}$$

where

$$Z_{\mathrm{opt}} = 3\,(1 - 2\,\phi^2{}_{\mathrm{opt}}) \cong 3 \tag{22}$$

for small ϕ_{opt}.

Present liquid-hydrogen pumps are able to pump two-phase hydrogen at pump-inlet vapor volume fractions up to 20 percent at design liquid flow coefficient. The basic limit to pumping two-phase hydrogen occurs when, at high flow coefficients, the flow area within the inducer blade passages becomes less than upstream flow area. When this occurs, both two-phase flow and pure saturated liquid flow will choke (ref. 30). Further experimental investigations aimed at establishing proper criteria for two-phase flow are in progress.

2.1.5 Blade Profile

In a well-designed inducer cascade, the blade profile does not interfere with the free-streamline boundary of the cavitating flow at the blade leading edge.

If so-called real fluid effects due to viscosity of the fluid and surface roughness of the blade are neglected, the flow in cavitating inducers may be adequately described by potential flow models with a simplified geometry. These models all are based on the assumption of a two-dimensional, irrotational, steady flow of an incompressible, inviscid fluid through a two-dimensional cascade of blades. The cascade and flow conditions represent those of the actual inducer at some fixed radial station.

A set of physically significant, characteristic parameters relating to the state of the fluid, the entering and leaving flows, and the geometry of the cascade is illustrated in figure 8.

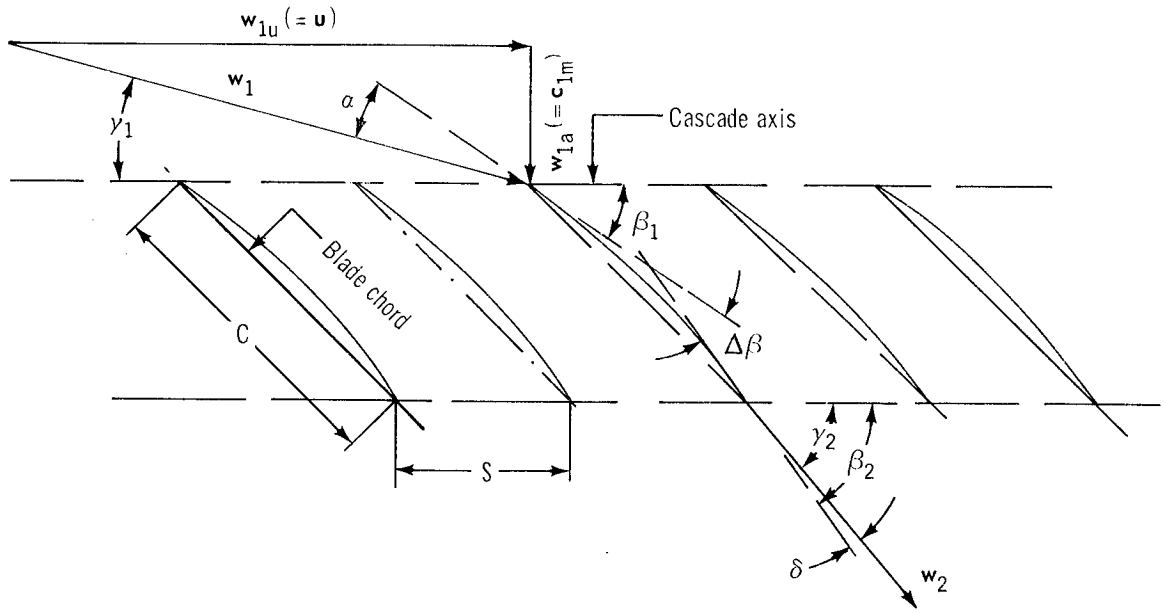

Figure 8.—Cascade and flow parameters.

The cascade geometry parameters are blade angle β, blade camber $\Delta\beta$, chord length C, and cascade spacing S. Subscripts 1 and 2 or, occasionally and more distinctly, LE and TE denote the leading and trailing edges, respectively. The entering and leaving flows are characterized by the relative velocities w_1 and w_2 and the angles γ_1 and γ_2 of these flows with the cascade axis. The velocity components normal and parallel to the cascade axis are w_m (or w_a) and w_u, respectively. These two components commonly are designated meridional and tangential components, referring to the equivalent usage for inducer flow. The meridional flow may or may not be axial but, by common usage, is always referred to as meridional because the cascade represents the meridional flow picture of the inducer. The cascade velocity w_1 is the vector sum of the two components represented by the blade velocity u and the fluid meridional velocity c_m at the inducer inlet. The inlet velocity c_m is assumed uniform over the inlet area; hence

$$c_m = \frac{4Q'}{\pi D^2} \tag{23}$$

where Q' is a corrected flowrate expressed by

$$Q' = \frac{Q}{(1 - \nu^2)} \tag{24}$$

giving the equivalent swallowing capacity of a hubless inducer.

Various models for the flow in flat-plate cascades with cavitating flow have been proposed and studied. These models differ essentially in the manner of cavity closure. There is no unique solution for a constant-pressure cavity of finite length, because the cavity can be terminated in a variety of ways. Among these cavity models are a re-entrant jet, an image plate on which the free streamline collapses, and the free-streamline wake model where the flow gradually recovers pressure on a solid boundary that resembles a wake. Experimental and visual observations indicate that, of all these models, the free-streamline wake model (wake model, for short) simulates to some extent the actual wake downstream of the cavity terminus, where intense mixing may be seen. The wake model of the flat-plate cascade with semi-infinite blades yields the simplest possible simulation of the important flow features of a cavitating inducer with partial cavitation. The theory is described and derived in detail in reference 31. For supercavitating flow with an infinite cavity, existing solutions (refs. 32 and 33) treat cascades with a finite chord length and arbitrary camber.

The wake model gives a good approximation to the cavitating flow in the inducer and is a useful tool for the inducer designer in calculating the cavity boundary. The main difficulty lies in the evaluation of the free-streamline theory as a function of cavitation number and angle of incidence of the inducer flow; the analysis involves the numerical evaluation of some complex variable relationships for the cavity shape. A computer program written to accomplish these objectives for any given inducer blade is available (ref. 34).

The cavity velocity w_c follows from Bernoulli's law and the definition of the cavitation number, giving

$$w_c = w_1 \sqrt{1 + K} \tag{25}$$

Similarly, combining this with the stagnation point condition for the velocity ratios results in

$$w_2 = \frac{w_c}{F + (F^2 - 1)^{1/2}} \tag{26}$$

where F stands for the expression

$$F = \frac{(1 + K)^{1/2} \sin \beta + (1 + K)^{-1/2} \sin (\beta - 2\alpha)}{2 \sin (\beta - \alpha)} \tag{27}$$

The wake or cavity height h_c is found from

$$\frac{h_c}{S} = \sin \beta - (w_1/w_2) \sin (\beta - \alpha) \tag{28}$$

which determines the maximum blade thickness that may be contained in the cavity with proper shaping of the leading edge (fig. 9).

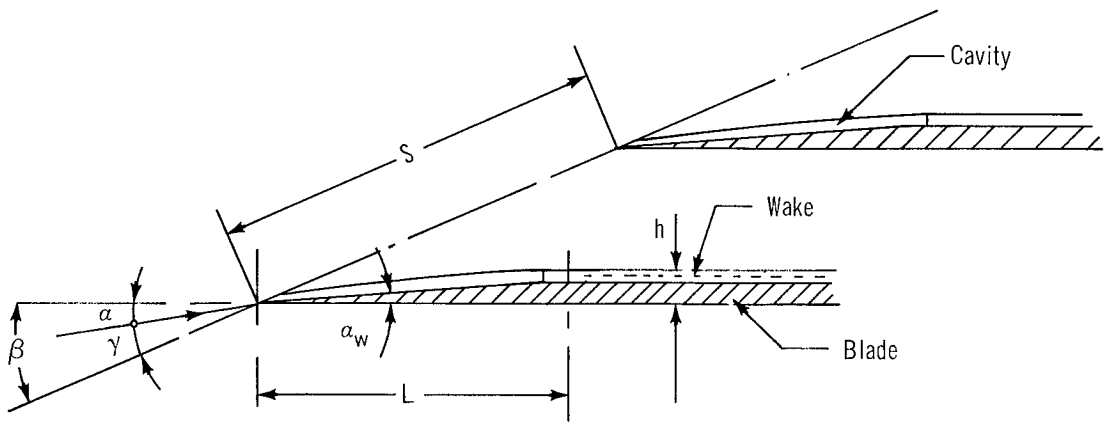

Figure 9.—Blade in cavity.

For the extreme case of supercavitation, the free streamline approaches a wedge shape at the leading edge with an angle equal to the angle of incidence α.

The cavitation number K attains its minimum value at supercavitation:

$$K_{min} = \frac{2 \sin \alpha \sin (\beta - \alpha)}{1 + \cos \beta} \tag{29}$$

When $\alpha = 0$ or $\alpha = \beta$, then $K_{min} = 0$; but these values are not realistic, because in the first case there is no deflection of the flow and in the second case there is no throughflow in the cascade. The equation does bring out clearly that, to obtain small cavitation numbers, the blade angle should be small.

At $\alpha = \beta/2$ a maximum value of K_{min} is obtained:

$$\max K_{min} = \tan^2 \frac{\beta}{2} \tag{30}$$

which also shows the need for small blade angles β to get small values of K. Because of blade thickness and boundary-layer blockage, in actual operation with a real fluid the attained values of K are approximately two to three times greater than the maximum values of K_{min}.

2.1.6 Blade Leading-Edge Sharpness

The radius of curvature of the free streamline r_{FSL} at the leading edge constitutes an upper limit for the permissible nose radius of the blade profile. In practice this radius is very small and, in case of supercavitation, $r_{FSL} = 0$. This means that the blade should be knife-sharp at the leading edge, in agreement with experimental evidence. When ultimate suction performance is required, the leading edge is made knife-sharp. However, a practical limit on the radius of the leading edge is the value $t/100$, where t is the maximum thickness of the blade profile. For large inducers (e.g., those used in the J-2 and F-1 engines), common practice is to leave the edge 0.005 to 0.010 in. thick.

2.1.7 Blade Sweep

The radial shape of the leading edge affects both the suction performance and the blade load and bending stress. Sweeping back and rounding off the radial contour of the leading edge has resulted in increases of 10 to 25 percent in suction specific speed (refs. 35 and 36). Structurally, the sweepback removes the corner flap and redistributes the blade load, thus reducing the possibility of failure. The blade wrap is reduced, but the reduction can be allowed for in the design by a slight increase in axial length. On shrouded inducers, the leading edge is usually swept forward to avoid sharp corners and to provide fillets where the blade meets the shroud.

2.1.8 Blade Cant

Canting of the blade is done for mechanical reasons only. At high blade loadings, the blade is canted forward to partially counterbalance hydrodynamic and centrifugal bending forces; also, canting produces a double curvature, which makes the blade stiffer and stronger. The backward or forward sweep of the leading edge is obtained by a face cut on the inducer blading such that forward canting of the blade results in a sweepback of the leading edge and a backward cant angle results in a forward-swept leading edge. Machining of the blade space is easier when the blade is perpendicular to the hub taper.

2.1.9 Blade Angle

The inducer suction performance is a function of the blade angle β at the leading edge.

The flow incidence angle α is chosen to minimize blade blockage. Experience indicates that for design purposes the ratio α/β is a characteristic parameter that varies with blade thickness as necessary to keep the blade inside the cavity. Values for this ratio range from a low of 0.35 for thin blades to a high of 0.50 for thick blades; the mean of 0.425 is a common design value.

2.1.10 Blade Lead

For an inducer, the best inlet configuration is the so-called flat-plate inducer, which has constant lead both radially and axially. The lead of the blade is given by

$$\Lambda = 2\pi r \tan \beta \cdot \tag{31}$$

where r is the radial coordinate on the blade.

The fluid velocity relative to the blade w varies along the radius according to the velocity diagram based on the flow coefficient at the blade tip and the inlet velocity c_m. The blade angle must vary correspondingly along the radius to maintain optimum values of α/β. For a uniform flow with zero prewhirl and small blade angles, this variation agrees well with the commonly used flat-plate inducer blade-angle variation with radius (i.e., $r \tan \beta = \text{constant}$), which is easy to manufacture.

2.1.11 Blade Thickness

The blade thickness t is determined from a combination of hydrodynamic and structural design considerations.

Hydrodynamically, the blade thickness is designed to lie inside the cavity (ref. 4) and wake of the cavitating flow at design NPSH and at 10 to 20 percent over design flow. Structurally, the blade is designed to resist the worst combination of centrifugal and pressure forces. To reduce stress concentrations at the root section, a generous fillet is provided at the hub juncture.

The result is a blade that tapers along its length from a maximum thickness at the hub to a minimum thickness at the tip.

2.1.12 Blade Camber

The head-rise capability of the flat-plate inducer is fixed at about $\psi \cong 0.075$ by the limited fluid turning angle of a straight cascade. For higher head coefficients, a cambered blade profile is required. Experiments have shown that suction performance may be maintained with a cambered blade when the blade angle at the leading edge

β_{LE} is the same as for the flat-plate cascade. In order to maintain the same cavity development, the cambered blade starts with zero curvature, and the camber gradually increases from zero at the inlet to the required amount at the discharge. The variation of the curvature follows a smooth monotone curve from zero at the leading edge to a maximum at the trailing edge. The simplest distribution of camber is given by the circular arc with the blade angle increasing steadily from β_1 to β_2 and constant curvature from inlet to outlet. A circular-arc blade has been used for small amounts of camber (i.e., a few degrees); but this blade does not satisfy the recommended variation of curvature from zero at the inlet to a maximum at the outlet, and there is some loss of suction performance. It is common practice to assume some distribution of camber on the rms (root-mean-square) diameter and calculate the corresponding head-rise distribution as a check.

2.1.13 Blade Surface Finish

A considerable amount of research (refs. 37 and 38) has been carried out on the effect of surface roughness on cavitation inception and hydraulic efficiency. It has been found, for example, that, when the measured efficiency of a hydraulically smooth specimen with a 2 μ in. surface finish (ASA) was compared with the measured efficiency of specimens that had 160 μ in. finishes, efficiency was reduced 5.9 percent with chordwise striations and 7.2 percent with spanwise striations (ref. 37). Early occurrence of incipient cavitation as an effect of surface roughness has also been observed.

2.1.14 Blade Number

When high-density fluids are pumped, the hydraulic loads on the blades require large blade chords to provide adequate bending strength. In addition, the hydrodynamic requirement for a small ratio of blade thickness to blade spacing to accommodate the blade thickness inside the cavity makes a large spacing necessary. These requirements for long chord length and large blade spacing are equivalent to a requirement for low blade numbers.

The choice of blade number affects the axial length of the inducer, which is proportional to the blade chord length. The possibility of alternate blade cavitation makes an odd number of blades desirable (ref. 39). Alternate blade cavitation is one of several possible cavitation patterns.

One-bladed inducer designs have been considered, but were given up because of balancing problems. The best suction performance is obtained with a small number of blades, normally between two and five. A three-bladed inducer is the preferred design if design considerations such as solidity, aspect ratio, and axial length permit. The blade number N is chosen with matching requirements of the impeller in

mind. Preferably, the impeller blade number is made a multiple of N to promote symmetry of flow. When the impeller blade number is a prime, however, no such choice is possible.

2.1.15 Cascade Solidity

The solidity of the inducer cascade σ affects the suction performance through its effect on blade loading and deviation angle (refs. 40 and 41). Solidity is given by

$$\sigma = \frac{C}{S} \cong \frac{L_{ax}}{\Lambda} \tag{32}$$

as a function of chord length C and blade spacing S and also as a function of blade axial length L_{ax} and blade lead Λ. For a flat-plate inducer, the solidity stays essentially constant over radius except for effects of blade sweepback. A high solidity improves the suction performance and tends to counteract cavitation-induced oscillations. For best suction performance, current practice requires $\sigma \geq 2.0$ to 2.5 at all blade sections from tip to hub, and low values for blade loading and deviation angle. This condition gives the leading-edge cavity sufficient time to collapse undisturbed by pressure fields from channel loading of the blade. By experience, any infringement on this condition has resulted in unsatisfactory performance. For instance, the employment of splitter vanes or increased camber to gain additional head rise in this inlet region has been unsuccessful.

2.2 Inducer Flow-Channel and Blade Geometry

The head rise and efficiency of the inducer depend to a great extent on the flow conditions in the channel region of the blading, i.e., the region where the blades overlap. The special problems of pump inducers with high head rise require careful design of the channel region of the blade. The blade geometry and the contours of the meridional flow passage constitute special problems for efficient design.

2.2.1 Channel Flow

The flow conditions in the channel region may be estimated for an incompressible fluid by an approximate calculation based on four assumptions:

(1) Constant radial lead,

$$\lambda = r \tan \beta = \text{constant} \tag{33}$$

(2) Simple radial equilibrium,

$$\frac{dh}{dr} = \frac{c_u^2}{r\,g} \tag{34}$$

where h is fluid static head.

(3) Perfect guidance (fluid follows blade),

$$\gamma = \beta \tag{35}$$

(4) Zero loss (100-percent efficiency),

$$H = h + \frac{c^2}{2g} = H_1 + \frac{u\,c_u}{g} \tag{36}$$

where H is the total head and H_1 is the total head at station 1.

The blade cant angle is assumed to be zero or small. Under these assumptions, the flow at an arbitrary axial station l is given by the equation for the local head coefficient,

$$\frac{d\,\psi_l}{\psi_l} + \frac{2r\,dr}{r^2 + \lambda^2} = 0 \tag{37}$$

with the solution

$$\psi_l = \frac{C_\psi}{r^2 + \lambda^2} = \frac{C_\psi}{\lambda^2}\sin^2\beta = \frac{C_\psi}{r^2}\cos^2\beta \tag{38}$$

where C_ψ denotes a constant of integration that must satisfy the continuity condition. The local velocities are given by

$$c_a = (1 - \psi_l)\lambda\omega \tag{39}$$

$$c_u = \psi_l r\omega \tag{40}$$

where ω is the angular velocity of the inducer and $\lambda\omega$ and $r\omega$ are, respectively, lead velocity and blade velocity of the inducer.

The parameters λ and C_ψ may vary with the axial station. The local total head-rise ΔH is

$$\Delta H = C_\psi \omega^2 \frac{\cos^2\beta}{g} = \Delta H_{ms} \frac{\cos^2\beta}{\cos^2\beta_{ms}} \tag{41}$$

where ΔH_{ms} is the headrise at some convenient radial reference station, preferably the rms radius. The constant C_ψ depends on the blade blockage at the axial station considered. For a tapered blade, the integrations can be performed and the constant expressed in closed form. The local blade thickness is given by

$$t_1 = a - br \tag{42}$$

where

$$b = \frac{t_H - t_I}{r_T - r_H} \tag{42a}$$

and

$$a = t_H + b\, r_H \tag{42b}$$

Then, for an inducer with blade number $= j$, the constant is given by

$$C_\psi = \frac{I_{A1} - j\, I_{B1} - (Q/\lambda\omega)}{I_{A2} - j\, I_{B2}} \tag{43}$$

where I_{A1}, I_{A2}, I_{B1}, and I_{B2} are given by

$$I_{A1} = \pi\,(r_T{}^2 - r_H{}^2) \tag{43a}$$

$$I_{A2} = 2\pi \ln \frac{\sin\beta_H}{\sin\beta_T} \tag{43b}$$

$$I_{B1} = \frac{a\lambda}{2}\left[\frac{\cos\beta}{\sin^2\beta} - \ln\left(\tan\frac{\beta}{2}\right)\right]_H^T - \frac{b\lambda^2}{3}\left[\sin^{-3}\beta\right]_H^T \tag{43c}$$

$$I_{B2} = -\left[\frac{a}{\lambda}\ln\left(\tan\frac{\beta}{2}\right) + b\,\frac{1}{\sin\beta}\right]_H^T \tag{43d}$$

The subscripts T and H denote tip and hub, respectively, and

$$\left[f(\beta)\right]_H^T = f(\beta_T) - f(\beta_H) \tag{44}$$

2.2.2 Discharge Flow

The normal low-head inducer design is used as the inlet portion of the pump impeller, which may be radial, axial, or mixed-flow type. The flow passes directly from one rotating component to another without intervening stators. As a result, no matching problems are encountered except, possibly, that of finding an optimum relative location of the two sets of blades that will prevent wakes from blades in

the upstream rotor from hitting blades in the downstream rotor. However, this normal low-head inducer design may be combined with a high head-rise channel region following the inducer proper to form a so-called high-head inducer. The matching of this combination with the following component, a stator, presents a problem, because the stator needs a radially constant head across the passage in order to operate efficiently. For this condition to exist, the inducer discharge must be a free vortex flow with a rotation that is given by the expression

$$r\,c_u = \text{constant} \tag{45}$$

This condition is difficult to obtain physically with the inducer blades, because the rotation of a helical inducer is given by

$$\frac{r + \lambda^2}{r\,c_u} = \text{constant } (=\omega C_\psi) \tag{46}$$

For free-vortex-flow blading, the hub angle becomes greater and the tip angle smaller than for a helix with a radially constant lead. This configuration results in different wrap angles for hub and tip and a corresponding manufacturing problem. One solution to this problem is to divide the inducer into two or more parts, with the front part consisting of the actual inducer and an extended channel region and the other parts consisting of axially interrupted blading. These inducer parts may either be on separate hubs or be machined on the same hub. If separate pieces, they must be fastened together or fastened separately to the shaft. The head is calculated for a number of streamlines, assuming simple radial equilibrium; this method has been shown to give close agreement (refs. 42 and 43) with measured values for the axial velocities. The axisymmetric blade-to-blade solutions are more accurate but are seldom used for axial flow because of their complexity.

2.2.3 Impeller-Inducer Matching

The inducer discharge dimensions must match those of the impeller eye. The requirements for the impeller eye diameter and the inducer discharge diameter may be conflicting because of head-rise limitations, in that an increase in the impeller eye diameter will decrease the impeller head but an increase in inducer discharge diameter will increase the inducer head, and vice versa. For these reasons, the exact matching of inducer discharge diameters and impeller inlet eye diameters may be impractical. With sufficient axial clearance between the two components, however, a reasonably smooth boundary of the flow passage may be drawn.

The axial clearance distance (inducer-impeller or inducer-stator) is dictated mainly by mechanical design considerations such as minimum length and weight of pump and rotor and assembly requirements. However, for inducer-stator combinations (as in axial-flow pumps), the minimum permissible clearance for safe running must be maintained. The magnitude of the permissible axial clearance depends on the stiffness of the rotor and the casing, on the rigidity of the bearings, on the differential

thermal expansion of rotor and stator, and possibly on distortions due to load and temperature. Hydrodynamic matching between inducer and impeller also requires a certain minimum clearance of the magnitude of the blade gap, which equals L_{ax}/σ. For good suction performance, the axial spacing between inducer and impeller blades is kept at least as large as this blade gap.

2.2.4 Trailing-Edge Sharpness

Sharpening of the trailing edges is not critical. Trailing-edge sharpening is used particularly in applications where it is important that the blade wake and drag of the inducer be minimized. The trailing-edge sharpening increases the head rise and improves the efficiency of the inducer. The preferred blade sharpening is centerline faired.

2.2.5 Trailing-Edge Contour

The trailing-edge contour normally is not critical and often is left straight radial. The major consideration in contouring the trailing edge is the proximity of stators, coupled with the possibility of blade flutter. The structural integrity of the blade is improved by cutting off the outer corner of the blade at the sacrifice of some solidity.

2.2.6 Discharge Angle

The fluid turning angle $\Delta\gamma$ along a streamline follows from the Euler equation for the head rise

$$g\,\Delta H_{net} = \Delta\,(u\,c_u)\,\eta_{bl} \tag{47}$$

The equation is solved for the tangential velocity component at the discharge c_{u_2}, to determine the velocity triangle and the fluid discharge angle γ_2. The blade efficiency η_{bl} is assumed to be 0.85.

For low-head inducers it is satisfactory to determine the lead of the inducer based on the rms station only. For high-head inducers with free vortex flow, the lead of the inducer is determined for a minimum of two radial stations, one close to the hub and the other close to the tip, to define the blade completely.

2.2.7 Deviation Angle

The blade angle varies along radius according to $\lambda = r \tan \beta$, where the lead ($\Lambda = 2\pi\lambda$) should be determined for the mean (i.e., rms) diameter D_{ms} from the

required headrise. The discharge blade angle $\beta_{ms,TE}$ is the sum of the fluid angle $\gamma_{ms,TE}$ and the deviation angle δ at this station. The deviation angle δ is an expression of how well the blading guides the fluid. The value of δ may be estimated from rules developed for compressor blades by Carter (ref. 44) and by other investigators (refs. 45 and 46). None of the studies on deviation angle was made for inducers, but Carter's rule has given reasonably good results when modified to allow for the different flow conditions in inducers and compressors. Carter's rule is

$$\delta = M(\beta_{TE} - \beta_{LE})/\sigma^b \tag{48}$$

where

σ = solidity
b = exponent, a function of inlet blade angle β_{LE} with values in the range from 0.5 to 1.0; approximate value of b for inducers is 0.5
M = coefficient, a function of stagger angle and the location of maximum thickness; approximate values of M for inducers are 0.25 to 0.35

Carter's rule is derived from an empirical correlation between cascade parameters and experimental deviation angles for purely two-dimensional flow with constant blade height and the incidence angle of impact-free entry, essentially zero for thin blades. Sometimes a modified form of the rule, based on fluid turning angle $\Delta\gamma$, is used for flat-plate inducers with

$$\delta = 0.10 \text{ to } 0.20\,\Delta\gamma \tag{49}$$

However, because the flow is not two-dimensional and because the flow area and blade height of inducers vary from inlet to discharge, the application of Carter's rule to inducer blades involves various corrections. The blade camber usually is referred to a zero-action blade camber $\Delta\beta_0$, such that the active blade camber is given by

$$\Delta\beta_{active} = \Delta\beta - \Delta\beta_0 = \beta_{TE} - \beta_{TE,0} \tag{50}$$

Also, the incidence angle α is included with the blade camber, so that the deviation angle is found from

$$\delta = \frac{M(\alpha + \Delta\beta_{active})}{\sqrt{\sigma}} \tag{51}$$

where

$$\Delta\beta = \beta_{TE} - \beta_{LE} \tag{52}$$

and, with approximation,

$$\Delta\beta_0 = \beta_{TE,0} - \beta_{LE} \cong \left[\frac{A_1}{A_2} \left(\frac{r_1}{r_2} \right)_s - 1 \right] \beta_{LE} \tag{53}$$

which follows from continuity of flow for a helical inducer. The ratios (A_1/A_2) and $(r_1/r_2)_s$ are, respectively, the ratio of inducer inlet area to discharge area and the ratio of the radii at inlet and discharge of a stream surface s containing the blade section, e.g., at tip, hub, and rms stations.

On high-head inducers, Carter's rule is used to find the deviation angle of the vortex-type blading constituting the channel region of the inducer, such that the required camber angle of this part of the inducer blading can be established.

2.2.8 Clearance Losses

The inducer performance is strongly dependent on the effect of clearance losses. The leakage flow through the clearance has a disturbing effect on the main flow entering the blading, tending to cause early separation. It is the source of the first visual occurrence of cavitation and lowers the suction performance correspondingly at partial head dropoff, but not at supercavitation.

The clearance losses are a function of the ratio c/L of radial clearance to blade length or, preferably and more precisely, of the ratio of clearance to passage height $(D - d)/2$. This latter expression is particularly appropriate in extreme cases where the clearances are large. A study of inducers with cylindrical tip contour indicates that the loss in performance may be estimated from the following empirical relationships:

The effect on S_s follows from

$$S_s = S_{s,0}\left(1 - k_s \sqrt{c/L}\right) \tag{54}$$

and the effect on ψ follows from

$$\psi = \psi_0\left(1 - k_\psi \sqrt{c/L}\right) \tag{55}$$

where (from experiments) $k_s = 0.50$ to 0.65 and $k_\psi = 1.0$. The subscript 0 refers to zero clearance.

The clearance effect is compensated for in design by additional blade length and work input.

2.2.9 Shrouding

Shrouding of inducers serves three principal functions: control of clearance; reinforcement of structure; and protection of blades, liner, and housing from erosion or cavitation damage.

(1) Clearance control.—By use of a shroud, the blading may be run with zero clearance losses except for the leakage past the shroud; this leakage is controlled by using close-clearance wearing rings of a suitable material with good rubbing and wearing qualities, e.g., polychlorotrifluoroethylene (Kel-F).

(2) Structural reinforcement.—By proper design, the shroud can be made to distribute the blade forces more uniformly, both among the blades and over the axial extent of the blading. Also, the shroud absorbs some of the bending load that otherwise would have to be carried by the blade root. With cambered blades, the stiffening effect of a shroud is especially strong; blade vibrations are prevented or dampened, and the stress level due to bending is reduced.

(3) Erosion or cavitation damage protection.—In certain cases the flow around the end of the blades, in the clearance space, has produced cavitation erosion of a nonmetallic lining (e.g., Kel-F) used to improve rubbing characteristics of the blading. Cavitation erosion will destroy such a soft liner in a very short time. The only solution then is to use a shrouded rotor. Shrouding of inducers occasionally is used as a fix for design shortcomings discovered in the development period. Tests on similar inducers with and without shrouds have shown the shrouded inducer to have slightly worse performance (refs. 47-49). The shroud may or may not cover the full axial length of the blading (see sec. 2.4.7).

2.2.10 Blade Geometry Description

For fabrication of an inducer with the desired blade geometry, the geometry must be expressed in terms suitable for manufacturing and inspection purposes, i.e., the blade shape must be described by coordinates that can be obtained by direct measurements on the inducer. It is common practice to convert the blade description in terms of blade angles, blade thickness variation, and leading- and trailing-edge geometry into a set of coordinates for both pressure and suction sides of the blade. This conversion ordinarily is done by a manufacturing division department for master dimensions; a special computer program is used. It may be done on the drafting board by making an accurate layout of the blading. A tolerance band is always specified for the theoretical coordinates to ensure repeatable performance of the inducers.

2.3 Inducer Inlet Line

Inducer cavitation performance is dependent on the inlet flow conditions that in turn are dependent on the inlet-line configuration and the inducer operating point. These relationships are discussed in the sections below.

2.3.1 Inlet-Line Configuration

Any configuration that causes a loss in NPSH or creates a nonuniform flow distribution will be detrimental to the inducer suction performance. To obtain smooth flow into the inducer eye, the inlet-line area is blended smoothly into the inducer inlet area without any sudden diameter changes or breaks in the wall contour. Any projection of a rib or stud into the inlet flow or imperfect matching of duct and inducer inlet-casing diameters has a detrimental effect on the suction performance and smooth operation of the inducer. Sudden expansion and contraction sections of the inlet line are avoided because of the high loss coefficients involved and the strong turbulence created. When turbopump installation in the engine system requires a bend in the line, a vaned elbow or a large-radius elbow with a low loss coefficient and a uniform exit-flow distribution is used, depending on space limitations (see also sec. 2.1.1.1).

2.3.2 Inlet-Line Fluid Velocity

It is important that no cavitation occur anywhere in the inlet line. To achieve this objective, the velocity of the fluid at any point in the line is kept below its velocity at the inducer inlet. Even fluids with large fluid thermodynamic effects, such as liquid hydrogen, are kept well below the maximum obtainable cavitating velocity of

$$c_{m,\max} = \sqrt{2g\,(\mathrm{NPSH})_{\mathrm{tank}}} \tag{56}$$

at which the static pressure equals the vapor pressure. Fluids that do not exhibit fluid thermodynamic effects do not exceed the value

$$c_m = \sqrt{\frac{2g\,(\mathrm{NPSH})_{\mathrm{tank}}}{3}} \tag{57}$$

2.3.3 Inlet-Line Heat Transfer

For cryogenic propellants, heat transfer from the atmosphere to the tank and the inlet line may raise the temperature of the fluid by an amount that significantly lowers the NPSH available to the inducer. An uninsulated liquid-oxygen line exposed to the atmosphere builds up an insulating layer of ice from the moisture in the air. Apart from the benefit derived from this effect, liquid-oxygen lines often carry thermal insulation to protect them against thermal radiation and convection heating in space. An uninsulated liquid-hydrogen line exposed to the atmosphere does not develop an ice layer but acts as a condenser, liquefying the air around it. Thus, it has a high rate of heat transfer, and the duct fluid experiences a rise in temperature of several degrees.

It is common practice to reduce such heating of hydrogen by using a vacuum-jacketed inlet line. The line, including bellows, is a double-wall design.

2.3.4 Bypass Flow

The balance piston bypass flow of axial-flow liquid-hydrogen pumps can create undesirable effects if not reintroduced in a careful manner. Whenever the geometry of the inducer and the relative pressure level of the bypass fluid permit, this fluid is discharged behind the inducer. Otherwise, it is reintroduced into the main flow either through a hollow inducer shaft and spinner into the center of the inlet duct or through a duct back to the inlet duct in a manner that causes a minimum of disturbance to the main flow.

2.3.5 Backflow and Prewhirl

Backflow occurs at low flow (about 90 percent or less of design value) as a result of local head breakdown in the tip region. The detailed effects of backflow on inducer performance have not yet been established. Since backflow is a phenomenon of uncontrolled flow, it is desirable to attempt to reduce it or to control its effects.

Incorporating a backflow deflector in the inlet line (fig. 10) may improve the suction performance at low flow (refs. 50-52). Below nominal flow (i.e., between 20 and 90 percent of design flow) where backflow becomes significant, the deflector results in increased head, reduced critical NPSH, and lower amplitudes of low frequency oscillations. Above nominal flow, the deflector has a detrimental effect.

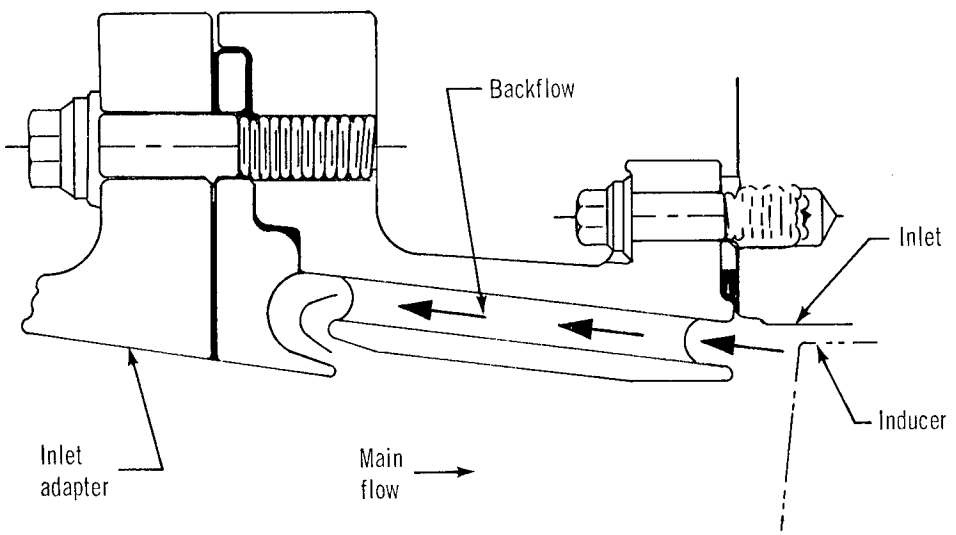

Figure 10.—Backflow deflector configuration.

Data using the backflow deflector are limited, however, and further development work is needed on deflector design and operation.

Backflow at the inducer inlet may cause erroneous inlet pressure readings if the data station location is close to the inducer inlet. In this event, it is difficult to obtain reliable NPSH values in suction performance tests. To get inlet pressure readings that are not influenced by upstream flow disturbances caused by the inducer, the data station is located, when possible, at least 20 diameters upstream of the inducer. The accuracy of the NPSH values is also improved by the use of an inlet section having a locally enlarged area that muffles the backflow generated by the inducer at low flows and low NPSH. This design is purely a device for improving pressure measurement. It does not improve flow conditions in general and, in fact, may cause a slightly increased head loss of the flow. The design is incorporated only for measurement purposes and is removed when no longer required.

Prewhirl of the inlet flow may be generated through momentum transfer by mixing the inlet flow with high-velocity fluid taken from the pump discharge and injected through a ring of orifices in a tangential direction upstream of the inducer. Prewhirl introduced in this manner has improved flow distribution and reduced flow instabilities that occur when the pump is throttled. At throttled conditions, the suction performance was increased a maximum of 50 percent with the use of about 10-percent recirculation (refs. 53-55). The use of prewhirl by mixing is still an experimental feature and has not yet become an established design practice. When pumping liquid hydrogen, heating of the pump fluid due to recirculation may become a limiting factor, but no data to that effect are available.

2.4 Mechanical Design and Assembly

All the fundamental considerations for performance, structural integrity, and manufacturing must be coordinated into a complete and unified layout providing all the information needed for the manufacturing process. Mechanical design and assembly constitute the backbone of inducer design.

2.4.1 Hub Configuration

Figures 11 and 12 show the typical hub configuration for low-head, low-speed applications and high-head, high-speed applications. Hydrodynamically, the hub diameter should be small on the inlet end and should match the fluid passage of the downstream component (impeller, axial flow blade, etc.) on the discharge end. Structurally, however, the hub must be sized to sustain the loads imposed, i.e., the hub radial thickness must provide a foundation capable of developing the necessary centrifugal and bending strength of the blades along the blade-hub junction. The hub normally is made somewhat longer than the blade plus the fillets to allow room for machining and tool runout.

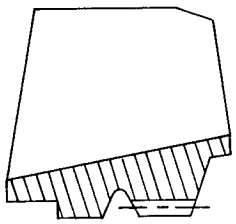

Figure 11.—Conventional low-head inducer hub.

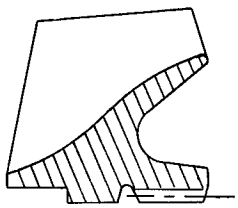

Figure 12.—High-head inducer hub.

2.4.2 Blade Root Juncture

The fillet at the blade root is a purely structural means to avoid or reduce stress concentrations (ref. 56), improving fatigue life correspondingly. Hydrodynamically the fillet represents a deviation from the true blade profile desired; it protrudes through the cavity and disturbs the flow. Where stress concentrations cannot be avoided, their effect may be minimized by polishing or shot peening (ref. 57) the blade surface.

2.4.3 Shaft Dimensions

The pump shaft is part of the general pump design, but the inducer end of the shaft is determined by the inducer designer to fit the requirements of the inducer drive and attachment. These requirements include adequate splines or keyways to drive the inducer, means for axial retention (spinner nut or bolt), possibly a hollow shaft to provide for return flow, and any special provisions for assembly and retention of rotating parts.

The impeller torque normally is much greater than that of the inducer, which means that the shaft and hub under the impeller must be larger than those under the inducer. The torque load is strongly dependent on pump speed and flowrate, and may have cyclic variations during periods of flow instabilities. The inducer power torque load can be transmitted to the hub from the driving shaft by several methods. Shear pins or keys are normally used for low-torque applications, and splines are used for high-torque applications.

2.4.4 Piloting

Radial piloting is a major concern in high-speed rotating hardware where rotor balancing and critical speeds are of importance. Positive piloting even under maximum operating conditions constitutes an established practice.

2.4.5 Axial Retention

Studs and bolts used for axial retention of inducer rotating parts are highly loaded to provide the clamping force necessary to withstand the maximum inducer axial forces that occur during operation. Great care is taken not to overstress fasteners during assembly; precalculated amounts of stretch are used as a measure of the actual preload.

The axial retention of the inducer is the major factor in preventing any relative motion between two parts that can cause fretting corrosion at the interface. Relative motion is particularly critical for oxidizer pumps, where the heat generated might initiate an explosion. To prevent any relative motion, the axial preload is kept high enough to provide positive axial piloting at all times, and the method of applying the preload is controlled accurately. When this procedure is not possible, fretting is minimized by the use of various types of surface treatments such as plating or the use of a dry-film lubricant with the oxidizer.

An example of an arrangement for axial retention is shown in figure 13.

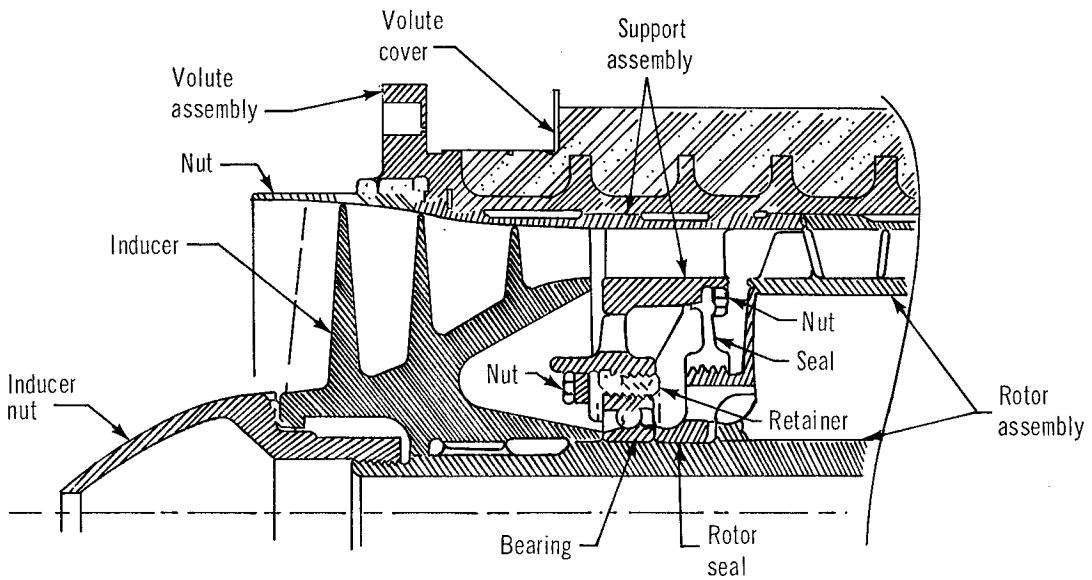

Figure 13.—Axial retention arrangement.

2.4.6 Clearance Effects

The blade tip clearance, the gap between the inducer blade tip and the pump inlet-tunnel inner surface, is a critical parameter (sec. 2.2.8). When the clearance is inadequate, shaft loads may cause inducer deflections such that interference with the housing will occur. The resultant interference may induce loads of such a magnitude that blade failures occur or sufficient heat is generated to cause chemical reactions or explosions in the case of oxidizer pumps. The effect of blade rubbing

is strongly dependent on the blade and housing material and the fluid environment. For instance, high-speed rubbing of titanium blade tips against the steel housing in fuel inducers has not produced unusual wear or galling.

The dimensions of the matching components, rotor and housing, where rubbing might occur are of critical importance in the estimation of the effect of stress and strain and of thermal expansions and distortions on the running clearances. A detailed study of these effects precedes the final determination of the blueprint dimensions of rotor and housing.

Cryogenic pumps often are tested initially in water. In this test condition, the rotor assembly runs at a temperature much different from that of the pump operating conditions, with a large effect on running clearance. Therefore, great care is taken to identify, calculate, and account for all possible deflections, displacements, and thermal expansions and distortions so that the effective clearances are at all times within the operational design allowables.

2.4.7 Shroud

As discussed in section 2.2.9, a shroud is often used to obtain clearance control. However, in high-speed inducers, a shroud cannot support itself as a free-floating ring but must be carried by the blades. This limitation restricts the use of a hubless inducer to low-speed applications. Present manufacturing practices allow the shroud to be welded or brazed onto the blade tips or allow the inducer to be cast as one piece. Inducers can be cast with very little machining or cleanup required except for the leading-edge and trailing-edge fairing, which should be kept smooth. The leading edge is usually swept forward on shrouded inducers to avoid sharp corners and to provide fillets at the shroud-to-blade junctures. The shroud may or may not cover the full axial length of the blading.

2.4.8 Misassembly

In the assembly of built-up rotors, the possibility of misassembly exists whenever a part can be mounted in more than one position. Various practices are used to preclude the possibility of misassembly. These usually take the form of minor modifications to the hardware that prevent mating the parts when they are not in the correct position.

2.4.9 Rotation Direction

All the various components of a rotating assembly obviously must be designed for the same direction of rotation. It is an established practice to coordinate design efforts and avoid problems of mismatched direction of rotation by making a preliminary axonometric projection of the assembly that shows clearly the direction of rotation (fig. 14). Copies are furnished to all designers on the job.

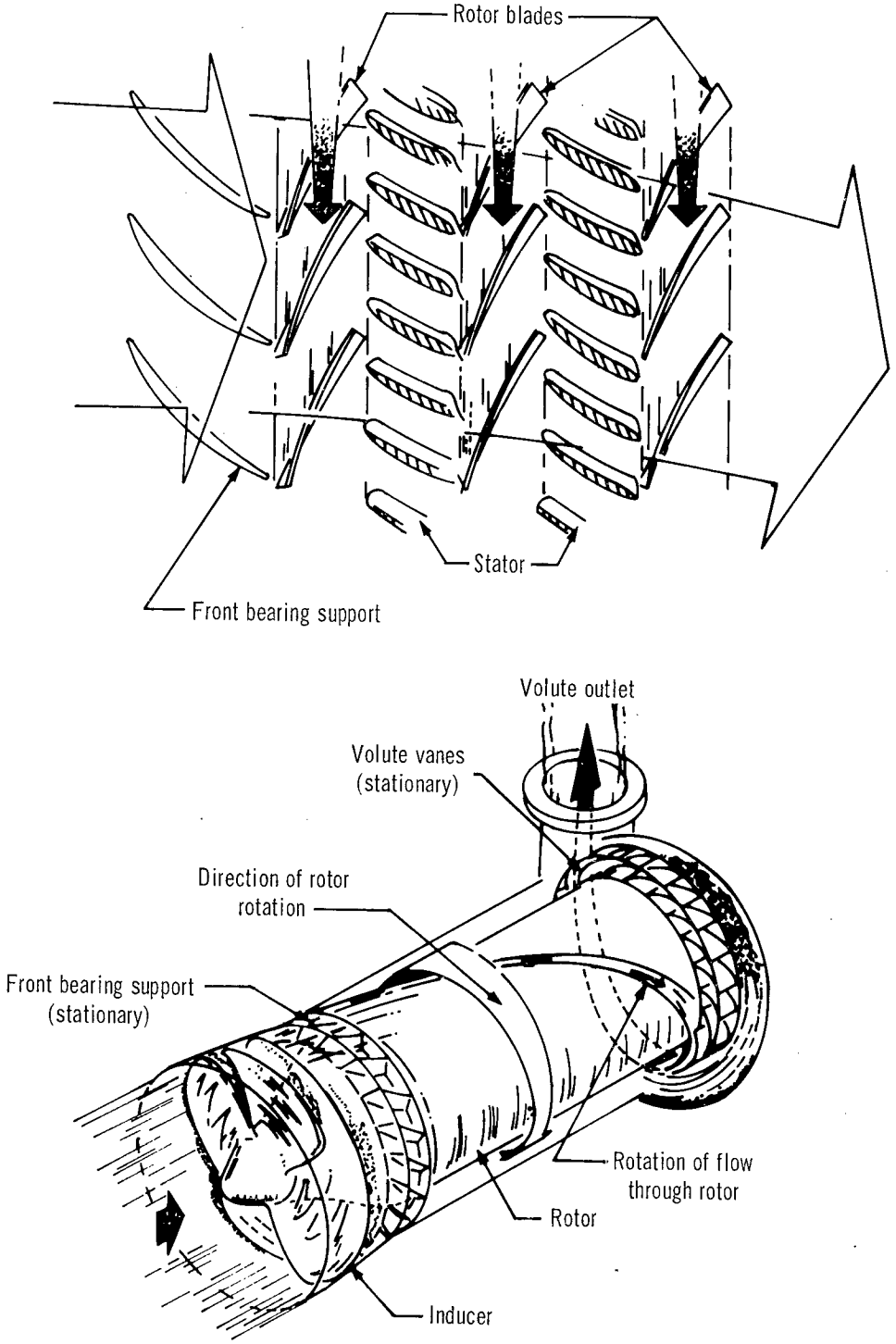

Figure 14.—Turbopump flow pattern.

2.4.10 Inducer Balancing

Because the inducer is part of a high-speed rotor system, it must be well balanced to obtain stable running. Inducer components are balanced separately to specified limits, depending on pump size and speed, mainly by removal of material. Material is removed either by drilling holes in the hub parallel to the axis or by thinning and fairing the blade tip. The conventional way of balancing is to remove material from the heavy side of the part. In aerospace designs, however, space and weight limitations often do not provide sufficient material to allow removal for balancing. Sometimes weighting must be used instead. For instance, for aluminum parts, the addition of lead plugs can increase the possible amount of correction by a factor of 3 to 4.

For oxidizer pumps the danger of entrapping contamination always exists. For that reason, holes or crevices in the inducer (such as tapped holes for the addition of screws) are undesirable because contaminants may collect there. Only metal removal is used as the method for balancing these pumps. Although with hydrocarbon fuels and hydrogen there is little or no concern with respect to chemical compatibility of the propellant with contaminants, there is a potential for the reaction of hydrazine base fuels with contaminants such as iron or rust (ref. 58). These materials can catalyze the decomposition of monomethylhydrazine, and the resultant gases can cause cavitation in turbomachinery.

2.4.11 Cavitation-Induced Oscillations

In most inducers, pressure and flow oscillations occur over some region of the operating NPSH and flow range. The oscillations of concern are in the low-frequency range, 5 to 40 Hz, and are the direct result of the hydrodynamic coupling of the inducer with the flow system of which it is a part. These oscillations can be of sufficient magnitude to impair the inducer performance in a pumping system. No specific criteria for absolute stability are known. Although there have been observations on trends or effects that are considered beneficial (refs. 59-67), the understanding and successful prediction of these cavitation-induced oscillations require further research.

Three methods, none of them a proven and consistent success, have been tried (refs. 59-67) to eliminate or reduce the inducer-generated pressure oscillations:

(1) Drilling holes in the blades.—The holes tend to stabilize the cavity and thus eliminate oscillation. Hole drilling is still very much an art in that there is little knowledge of how cavity behavior is affected by holes. Inducers of different designs do not act alike, and the required hole pattern is unpredictable from one inducer design to another. Rebalancing of the inducer is required if holes are drilled.

(2) Physically attaching wedges to the inducer blade.—These wedges are attached to the suction side of each blade near the tip. The purpose of the wedge

is to provide a solid surface upon which the blade cavity can close, thus stabilizing its position. This practice may be harmful to the suction performance. Rebalancing of the inducer is required if wedges are attached.

(3) Increasing the tip clearance.—This practice is the most ineffective and most harmful. It degrades the suction performance (NPSH) and, in most cases, does not change the pressure oscillation pattern.

2.5 Material Selection

The material selected for pump inducers must possess a combination of strength, chemical reactivity, and special properties suitable for the intended use.

The use of given values for the strength properties of the inducer material must take into account the effect of random variations in materials composition, the effect of variations in treatment from batch to batch, and the spread of test results. To put the design procedure on a firm basis in this respect, it has become an established practice to base the design stress level on the minimum guaranteed properties in accordance with principles stated in reference 68 (par. 1.4.1.1, Basis A).

2.5.1 Strength

Inducer materials normally are selected from the alloys of stainless steel, titanium, and aluminum. The respective specific densities of these preferred alloys are approximately 8.0, 4.5, and 2.7; they therefore represent a wide spectrum of material densities. The strengths of these materials vary somewhat in the same order as the densities. For applications involving inertia loading, the strength-to-density ratio (often somewhat misleadingly called strength-to-weight ratio) is an important parameter for material selection; for other types of loading (e.g., hydrodynamic, static preload in assembly, thrust forces), the strength itself is the important parameter. In particular cases where minimum blade thickness is of overriding concern for high suction performance and where the hydrodynamic loading causes large bending moments, the material with the highest strength is preferred.

The selection of a specific material from those listed above is further limited by considerations of chemical reactivity, cavitation erosion, and the need for special properties such as ductility, notch toughness, etc.

2.5.2 Chemical Reactivity

Material selection for pump inducers is governed by considerations of compatibility with the pump fluid and operation. Of special concern are the explosion hazard for oxidizer pumps, hydrogen embrittlement for liquid-hydrogen pumps, and general corrosion effects.

Titanium alloys are preferred for fuel inducers because of their high strength-to-density ratio and superb resistance to cavitation erosion. They are not used for oxidizer pump applications because of chemical reactivity; they propagate fire violently or show rapid reaction when ignited by high-temperature friction conditions.

Titanium alloys offer no problem with hydrazine, UDMH, and water (refs. 69 through 73), but they are not compatible with liquid fluorine or liquid oxygen or with a mixture of these fluids (FLOX). Ignition has been observed at different impact levels on titanium alloys tested in liquid fluorine; similar tests on titanium samples in oxygen have shown that ignition in liquid oxygen is even more severe than in liquid fluorine. In all tests with fluorine, even though the reaction was initiated, it failed to propagate itself; whereas in oxygen (in 1 test out of 26) the ignition became general and the sample was burned completely (ref. 74).

IRFNA causes rapid intergranular corrosion of titanium alloys. The corrosion products are pyrophoric and present an extremely dangerous explosive hazard. Titanium alloys used with uninhibited nitrogen tetroxide (brown N_2O_4) undergo stress corrosion cracking. In addition, titanium alloys are not compatible with N_2O_4 when used in rotating components where rubbing or fretting can occur. High-speed rubbing in N_2O_4 has caused ignition of the titanium alloy; however, unlike the pyrophoric reaction with oxygen, the fire does not propagate once the rubbing ceases.

Aluminum alloys are compatible with the cryogenic liquids: hydrogen, oxygen, nitrogen, FLOX, and fluorine. At room temperature they are satisfactory with water, IRFNA, UDMH, and N_2O_4. One aluminum alloy (7075-T73) is free of stress corrosion cracking and is selected where residual stresses have been imposed on the part. However, aluminum alloys are susceptible to cavitation erosion.

K-Monel and Inconel 718 are often used in inducers for low-speed, cavitating oxidizer pumps. The blades can be thinner than those of aluminum, and the resistance to cavitation erosion is much higher.

Steel inducers used for development testing in the water test facility tend to deteriorate quite rapidly because of rusting. To protect the shiny surface that facilitates the visual observation of the cavitating flow in the inducer, some form of rust protection may be used. This protection also helps maintain the shape and sharpness of the leading edge.

Titanium and aluminum alloys may be quite sensitive to exposure to certain chemical cleaning fluids or solvents that can cause stress corrosion, with correspondingly impaired fatigue strength for later application. Use of such fluids and solvents is avoided.

2.5.3 Special Properties

The thermal environment in cryogenic pumps creates problems of brittleness and

loss of elongation in materials otherwise acceptable for use in inducers. The content of interstitial elements such as oxygen, hydrogen, and nitrogen adversely affects the ductility and notch and fracture toughness of titanium alloys at cryogenic temperatures. Therefore, there has been established an extra-low-interstitial (ELI) grade of the Ti-5Al-2.5Sn alloy (and also the Ti-6Al-4V alloy) in which the interstitial elements oxygen, nitrogen, and hydrogen and the substitutional element iron are controlled at lower-than-normal contents. Ti-5Al-2.5Sn ELI alloy forgings are employed for pumping liquid hydrogen in several experimental fuel pumps. The Ti-5Al-2.5Sn ELI alloy was selected because of its high strength-to-density ratio at the temperature of liquid hydrogen ($-423°$ F); notch toughness and ductility remain at acceptable levels down to $-423°$ F.

The resistance to cavitation damage is an important consideration in material selection for high-suction-specific-speed inducers. However, because of the short operating time of rocket engine turbopumps, it is more of a problem in the development stage than in the actual mission.

Inducers made from annealed Ti-6Al-4V forgings are used to pump RP-1. The Ti-6Al-4V alloy replaced an aluminum alloy inducer of the same design because of its greater strength and significantly greater resistance to cavitation erosion. Because the inducer operates at ambient temperatures, Ti-6Al-4V of normal interstitial content is used in this application.

The finished surface of aluminum inducers is no harder than Rockwell B88 and requires some surface protection to reduce handling damage and cavitation erosion. Aluminum inducers normally are protected with an anodic coating. When the inducer is operated in fluorine or in any of the storable propellants IRFNA, N_2O_4, and UDMH, the coating will dissolve slowly. This dissolution does not present a problem in normal operational use, but when the inducer is used repeatedly, as in development programs, the coating is renewed after use to maintain surface protection.

After the critical requirements of strength, ductility, and erosion resistance have been satisfied, there remain the manufacturing considerations. Here, ease of machining, forging and casting characteristics, and weldability dictate the choice of material. Titanium alloy machining is similar to that of stainless steel. However, relatively high tool pressures are required for cutting titanium and, as a result, cutting tool must have quite rigid supports. Furthermore, the elastic modulus of titanium alloys (16.5×10^6 psi) is nearly one-half that of iron- and nickel-base alloys. Titanium alloy workpieces thus are more likely to flex under high tool pressures. On this account, tooling fixtures must hold the workpiece rigidly and the cutting tools must have rigid support. The combination of high tool pressures and high flexibility of the workpiece can make the machining of complex passageways and of cantilevered blades extremely difficult. Machining costs for parts made from titanium alloys are much greater than for comparable parts made from aluminum alloys. However, titanium alloys are considered much easier to machine than such alloys as Inconel 718 or Rene′ 41. Titanium alloys have a much smaller degree of work hardening than do austenitic stainless steels and a much lower surface hardness (e.g., R_C 36 vs. 50) than do high-strength steels (e.g., 4340) of comparable strength-to-density

ratios. Forging titanium alloys is more difficult than forging aluminum alloys and most steels. Titanium alloys are readily weldable by gas, tungsten arc, or electron beam processes. Titanium casting is not yet an established, state-of-the-art practice.

2.6 Vibration Considerations

The typical inducer is exposed to oscillatory pressure loading during operation. The oscillating pressures are induced by flutter, cavitation, upstream obstructions, or other pressure-wave generators that exist in the pumping system. Because inducer blade failures are typically fatigue-oriented, effort to prevent resonant vibration of the blade is warranted. Designs relying on built-in damping due to shrouds have not been too successful. The typical high-head inducer blades, which are designed for high-speed operation, normally are rigid enough to place their natural frequencies well above the cavitation-induced, high-amplitude, low-frequency pressure oscillations (1 to 100 Hz).

A vibration analysis of an inducer design is difficult because of the uncertain knowledge of the amplitude and frequency of the exciting forces and the complexity of the mathematical analysis required to determine the response of the elastic structure in terms of resonant frequencies and damping properties. Despite the difficulties, a vibration analysis is essential to achieving a design that minimizes the probability of inducer blade failures due to high-frequency fatigue.

2.6.1 High-Frequency Fatigue

The most common cause of blade failure in turbomachinery is fatigue fracture induced by high-frequency alternating stresses, which are proportional to the vibration amplitude of the blade. To prevent fatigue failure, the oscillatory stresses are kept below the endurance limit (level of stress at which the material can endure an unlimited number of cycles). Ideally, the blade frequency and response to a forcing function should be predicted by analytical means, and the stress level and fatigue life calculated on this basis. As noted, this analysis usually is not possible for inducer blades because of the complexity of the analysis and the unknown nature of the forcing function (refs. 75 and 76). However, inducer fatigue or vibration failures have been few; in general, the main part of canted inducer blades has proven much too rigid to be prone to vibration failure (ref. 77). The critical parts of the blade in this respect are the leading-edge and trailing-edge regions (ref. 78).

2.6.2 Resonance

Because of the uncertainties involved in determining the oscillatory stress levels in inducer blades, it is common practice to avoid operation at resonant frequencies. This is done by modifying either the forcing frequencies or the blade natural frequencies by various means such as changing the number of wake generators (ribs,

vanes, etc.), changing the shaft speed, or making the blade stiffer. By experience, only first- and second-order harmonics have proven critical in inducer operation.

2.6.3 Self-Induced Vibration

Another source of vibration failure is self-induced vibration that causes blade flutter at the inlet corner of the blade. This flutter has not been a serious problem, but it is best avoided or minimized by trimming back the blade to remove the corner portion that is susceptible to flap. Blade flutter at the trailing edge has not been a problem in inducer-impeller combinations, but it is a consideration in inducer-stator combinations.

2.6.4 Determination of Blade Natural Frequencies

Theoretically, the blade natural frequencies are determined by the blade geometry and material. In practice, however, certain corrections and modifications are applied to the theoretical or nominal values to account for the effect of blade dimensional tolerances, the stiffening effect of the centrifugal force, variations in material elastic properties with temperature, and virtual-mass effects caused by the surrounding medium.

Variations in blade geometry due to dimensional tolerances affect the blade natural frequencies and produce frequency bands. The frequency increases when the root has maximum thickness and the tip minimum thickness, and decreases when the converse is the case. Therefore, the blade frequency may have any value inside the band of frequencies corresponding to the blade tolerance band.

The centrifugal force on the blade has a restoring component that adds to the elastic force, resulting in a stiffer blade. As a consequence, natural frequencies tend to increase as speed is increased.

The material elastic properties vary with temperature, and at operating temperatures these properties may be quite different from those at ambient conditions. The effect of the change on the blade natural frequency is considered when the results of vibration tests in air are reduced to inducer operating conditions.

The blade resonant frequency is directly proportional to the square root of the blade stiffness and inversely proportional to the square root of the mass in motion. When the blade vibrates, the mass in motion consists of the mass of the blade and the mass of some fluid in a space near the blade (i.e., the virtual mass). Because of the effect of the virtual mass vibrating with the blade, the blade frequency changes when the temperature (and therefore the material modulus of elasticity E) changes as well as when the fluid density (and therefore the mass in motion) changes. Calculating the mass of the blade is trivial, but no method exists for calculating the

virtual mass. The virtual-mass effect is estimated from the results of vibration experiments normally conducted in a convenient test fluid (for instance, water, if cryogenic applications are involved). The data are interpreted for the actual pump fluid by scaling the experimental results to account for the differences in fluid densities relative to the density of the blade material.

Analytical methods for calculating inducer blade frequency are complex. The exact solution of the partial differential equations governing the displacements and stresses due to time-dependent excitation forces usually cannot be obtained. Results obtained from numerical methods are limited and at best approximate. Therefore, the natural frequencies are always determined or verified by experimental methods.

2.7 Structural Considerations

The design of an inducer for maximum hydrodynamic performance must be tempered by structural design considerations. This section summarizes the critical considerations and methods involved in the structural analysis of the inducer design.

2.7.1 Blade Loading

The inducer blade loading analysis involves two distinct areas: leading-edge loading and channel loading. In low-head inducers, most of the head is developed in the leading-edge region; the remaining part of the blade is lightly loaded, and only the leading-edge loading need be considered. For high-head requirements, a large part of the head is developed in the channel region; the blade loading in that part of the inducer becomes large, and the channel loading must be included in the structural analysis. The leading-edge loading is calculated by a computer program such as that provided in reference 79. The channel loading is calculated by computer programs based on an axisymmetric or blade-to-blade solution of the noncavitating inducer flow. Another approach for determining the channel loading is to use the theory of simple radial equilibrium to calculate the pressure distribution on the blades (sec. 2.2.1).

The blade loading consists of both steady-state and alternating loads. Both kinds of loads arise from the same sources: inertia and fluid effects. High-performance inducers are designed to operate under partial cavitation. During part of component testing, the inducer is operated in deep cavitation with pressure forces approaching zero. To allow for this condition, the blade is also analyzed for centrifugal loads alone. Alternating (periodic and random) blade loads are induced by flow oscillations and instabilities. In addition, wakes and reflected pressure pulses from an obstruction (a bearing support or stator) can cause cyclic blade loading.

Because analytical values of the dynamic pressure loads are not available, a percentage of steady-state load normally is assumed to provide a margin of safety against high-frequency fatigue failure; the assumed value of 20 percent has given satisfactory results.

The inducer thrust, of concern for shaft and bearing design, is calculated from the flow conditions and the inducer layout. Unsymmetric flow in inducers has produced radial forces equal in magnitude to 30 percent of the axial thrust. The hydrodynamic blade loading depends on the density and the cavitation properties of the fluid. The temperature of the fluid is an important parameter in respect to material properties. Development tests of an inducer often are performed in a test fluid different from the pump design fluid. The effect on structural design may change stress levels and operating temperatures enough to make it desirable to use a different material for the development test model.

2.7.2 Blade Stress

Three methods to calculate the critical stresses in the inducer blade are available.

One method simplifies the analysis by dividing the blade into a series of independent pie-shaped beams, cantilevered from the inducer hub. Shell continuity is taken into account by an averaging technique and a plate correction factor. The beam loading is determined from the pressure profile for each segment. To correct for angular differences at hub and tip caused by blade twist, the effective center of curvature based on the hub and tip length for the blade is found for each segment. The pressure loading and bending moments are then calculated for an effective pie shape with center at the center of curvature. This analysis ignores tangential stress and circumferential beam action and tends to overestimate the bending moment at the hub.

The second method models the inducer as an axisymmetric shell of revolution (a canted blade being modeled by one or more conical shells for the critical sections) from which moments and stresses are obtained.

The third method is the most accurate, but also the most time-consuming. In this method the blade is divided into a number of finite triangular plate elements, for which a stiffness matrix is set up and solved for the displacement (refs. 80-82). The basic steps in the finite-element technique are as follows: The structure is divided into many elastic elements, which are connected to each other at their corners (called nodes). In general there are three displacements and three rotations and corresponding forces at each node. A square symmetric element stiffness matrix k_i is then determined. This matrix relates the column matrix of nodal forces f_i to a column matrix of nodal deflections δ_i by the matrix equation

$$f_i = k_i \delta_i \tag{58}$$

which expresses the equilibrium conditions for the ith element.

The particular method selected depends on cost and availability of computer facilities. To save cost and time, a simple beam or axisymmetric-type analysis is used to rough-size the blade. When the final design has been established, the stress analysis is refined by the finite-element method.

Regardless of the analytical technique used, the calculated stresses at the blade ends, where it joins hub or shroud, are amplified with a stress-concentration factor. This practice allows for stress concentrations at the blade root that have caused fatigue failures.

2.7.3 Hub Strength

Critical stress regions exist in the inducer hub at various locations. One critical area is in the vicinity of the blade root, where failures have occurred because of insufficient strength of the hub wall. Another critical area is the undercut or hollowed-out hub profile at the discharge end of high-head inducers. Stress concentrations here have caused fatigue failures in the hub as a result of discontinuities at the blade juncture or at holes and splines in the hub.

In general, little information on inducer burst speed is available. Thus, the only approach is to utilize data from disc testing together with parameters for material ductility and ultimate strength. The present state of the art of disc design is based on the experimental observation that the average tangential disc stress σ_{AT} is more characteristic of disc failure than the maximum calculated disc stresses. Essentially, failure occurs when the average tangential stress exceeds a certain fraction f_b of the ultimate tensile strength F_{tu} of the material. The value of f_b, which is called the burst factor, is determined experimentally as a function of the elongation of the material and a design factor f_d equal to the average tangential stress divided by the maximum tangential stress. Various configurations of discs classified by the design factor f_d have been tested and the experimental data plotted (ref. 83); the results are given in figure 21 (presented in sec. 3.7.3).

The average tangential stress is defined as the centrifugal force on one-half the disc divided by the cross-sectional area carrying this force. It may be obtained from the calculated elastic stress distribution by

$$\sigma_{AT} = \frac{1}{A_H} \int \sigma_t \, dA_H \tag{59}$$

where A_H is the area of the inducer-hub meridional cross section over which the integral is taken and σ_t is the local tangential stress. The speed at which the inducer hub would rupture or yield excessively because of centrifugal stresses is called the burst speed or yield speed, respectively.

2.7.4 Shaft Shear Section Strength

The inducer shaft shear section transmits the inducer torque. It is sized with consideration to the steady-state power torque, the alternating power torque, and the axial stress at the shear section (refs. 56, 68, and 84). Because the rotor alternating torque

is unknown, a rotor alternating shear stress equal to 5 percent of the steady-state shear stress was assumed for the Phoebus engine (Mark 9) and J-2 engine (Mark 15-F) axial-flow hydrogen pumps. This approximation has provided adequate reliability for these pumps.

2.7.5 Safety Factors

The structural integrity of a part customarily is ensured by establishment of a value greater than unity for the ratio of the stress capability of the part material to the calculated stress on the part. In specifying this ratio, or safety factor, it is the practice to consider only the minimum guaranteed values for material properties; these values are established by military standards or by equivalent statistical tests.

Some uncertainty exists concerning fatigue data. Before construction of the Goodman diagram (ref. 56), fatigue data obtained from polished laboratory specimens are modified to account for the effects of surface finish, temperature, erosive or corrosive environment, material grain size, surface residual stress from machining, and type of loading (tension-tension vs. bending).

Safety factors obtained for a particular design are dependent on the technique used in the stress analysis. Care must be exercised in comparing safety-factor values obtained from different sources.

2.7.6 Hub Stress Verification

Because the analytical methods for stress analysis and failure prediction are approximate in nature, an experimental verification is performed for highly stressed, complex components such as the inducer hub. The burst speed is determined by spin testing to failure an inducer provided with suitable instrumentation.

2.7.7 Inducer Proof Test

High-speed inducers are proof-tested by prespinning each part during the fabrication process to provide partial quality assurance. Prespinning each inducer has additional benefits in that local yielding occurs at areas of high strain concentration such as bolt holes, splines, and keyways. This yielding produces favorable residual stresses that effectively prestress the part and prevent the occurrence of yielding during operation.

3. DESIGN CRITERIA and Recommended Practices

3.0 Head-Rise Capability

The inducer shall generate sufficient head to prevent cavitation from impairing the suction performance of the impeller or stator following it.

For design purposes, an estimate of the NPSH requirement should be made by using either of two essentially different approaches: (1) the NPSH may be calculated from values of the suction specific speed previously measured for impellers of similar design, or (2) the NPSH may be based on an estimate of the cavitation number requirements for hydrofoils similar in form and profile nose radius to the actual impeller blades. A good way to make this latter estimate is to let

$$1 + K = C_p \tag{60}$$

where C_p is the pressure coefficient of a similarly shaped airfoil, which may be obtained from any collection of airfoil data (e.g., ref. 85). Then, use the energy equation to get

$$1 + \tau = (1 + K)(1 + \phi^2) = C_p\,(1 + \phi^2) \tag{61}$$

An approximate value of C_p for an uncambered airfoil is between 1.3 and 1.5. To estimate K, the single airfoil C_p should be corrected for blockage effects by increasing it in the ratio of the blockage factor squared.

The head generated by the inducer at a given speed is a function of the flow-channel and blade geometry. These subjects are treated in detail in sections 2.2 and 3.2.

3.1 Inducer Inlet-Eye and Leading-Edge Geometry

3.1.1 Inlet Casing

The inducer inlet casing shall provide free, uniform, and undisturbed axial flow into the inducer.

It is recommended that an axial inlet be provided by mounting the inducer on the end of the pump shaft, the inducer being driven from the rear through the scroll of the pump. If engine arrangement or space limitations prohibit the use of a straight axial inlet from the tank or at least several diameters of straight ducting to reduce flow distortions, the alternate solution is to use a dual inlet casing or a vaned elbow. The

casing should be carefully tailored, with smoothly contoured flow passages that match flow areas to local flow requirements so that velocity changes are reduced while the flow is gradually turned into the axial direction.

3.1.2 Hub Size and Shape

The inducer hub shall be as small as possible consistent with structural requirements, and its outlet end shall match the hub of the following stage.

To reduce blockage area for the flow and provide for best suction performance, it is recommended that the hub-to-tip diameter ratio be kept between 0.2 and 0.4 for rear drive and between 0.5 and 0.6 for front drive. Structural and mechanical suitability must be verified by analysis. The hub should be contoured from inlet to outlet so that the hub taper joins smoothly with the impeller hub taper and the hub diameters match. High-head inducers featuring an additional mixed-flow section should provide smooth transition between the taper of the inducer section and the taper of the stator section. Subsequent calculations of hydrodynamic blade loading may show a need for minor modifications of the hub contour.

3.1.3 Inlet Tip Diameter and Contour

3.1.3.1 Tip Diameter

The inlet tip diameter shall be derived from mathematical consideration of optimum flow conditions for maximum suction performance.

The inlet tip diameter should be obtained mathematically from the relationship between suction specific speed S_s, blade tip cavitation number K, and flow coefficient ϕ as follows:

(A) When the suction performance is specified in terms of Q, n, and NPSH, the blades must operate at the highest possible value (K_d) of the cavitation number K.

For an inducer with a fixed hub-to-tip radius ratio and no prewhirl, this condition leads to Brumfield's criterion (ref. 2) for the optimum flow coefficient, which, expressed in terms of the corrected suction speed of the inducer, gives the (cubic) equation in $(2\,\phi^2_{opt})$:

$$\frac{2\,\phi^2_{opt}}{(1 - 2\,\phi^2_{opt})^{3/2}} = \left(\frac{5055}{S'_s}\right)^2 \tag{62}$$

With good approximation, the solution may be expressed by S'_s as

$$\phi_{opt} = \frac{3574/S'}{(1 + \sqrt{1 + 6\,(3574/S'_s)^2})/2} \tag{63}$$

For the small values of ϕ_{opt} (about 0.10 or less) encountered in inducer design, the divisor approaches unity.

From equation (5),

$$K_d = \frac{2\phi^2_{opt}}{1 - 2\phi^2_{opt}} \tag{64}$$

From equation (8),

$$D_{opt} = 0.37843 \left(\frac{Q}{(1 - \nu^2) n \phi_{opt}} \right)^{1/3}, \text{ ft} \tag{65}$$

This procedure solves the problem of finding optimum operating conditions and the corresponding maximum operating cavitation number K_d for an inducer with a design point specified by Q, n, and NPSH.

(B) When only two of the three performance parameters—Q, n, and NPSH—are given, maximize the suction specific speed while assuming a certain blade cavitation number K^*.

This practice leads again to Brumfield's criterion, from which

$$\phi_{opt} = \sqrt{\frac{K^*}{2\,(1 + K^*)}} \tag{66}$$

which determines the inlet diameter, and

$$S'_{s,\,max} = \frac{5055}{K^{*1/2}\,(1 + K^*)^{1/4}} \tag{67}$$

showing that the suction specific speed is limited only by the K^* value, which should be as small as possible. The actual K^* value used is an empirical number and must be based on previous experience with similar designs.

The relationship between the important parameters K, ϕ, Z (secs. 2.1.4 and 3.1.4), and S'_s characteristic for suction performance may be presented in a very convenient manner by an S'_s-D'_s chart, where D'_s is the corrected suction specific diameter. Figures 15 and 16 show S'_s-D'_s diagrams covering the whole range of practical pump operation. The values satisfying the Brumfield criterion are plotted in the curve for optimum D'_s.

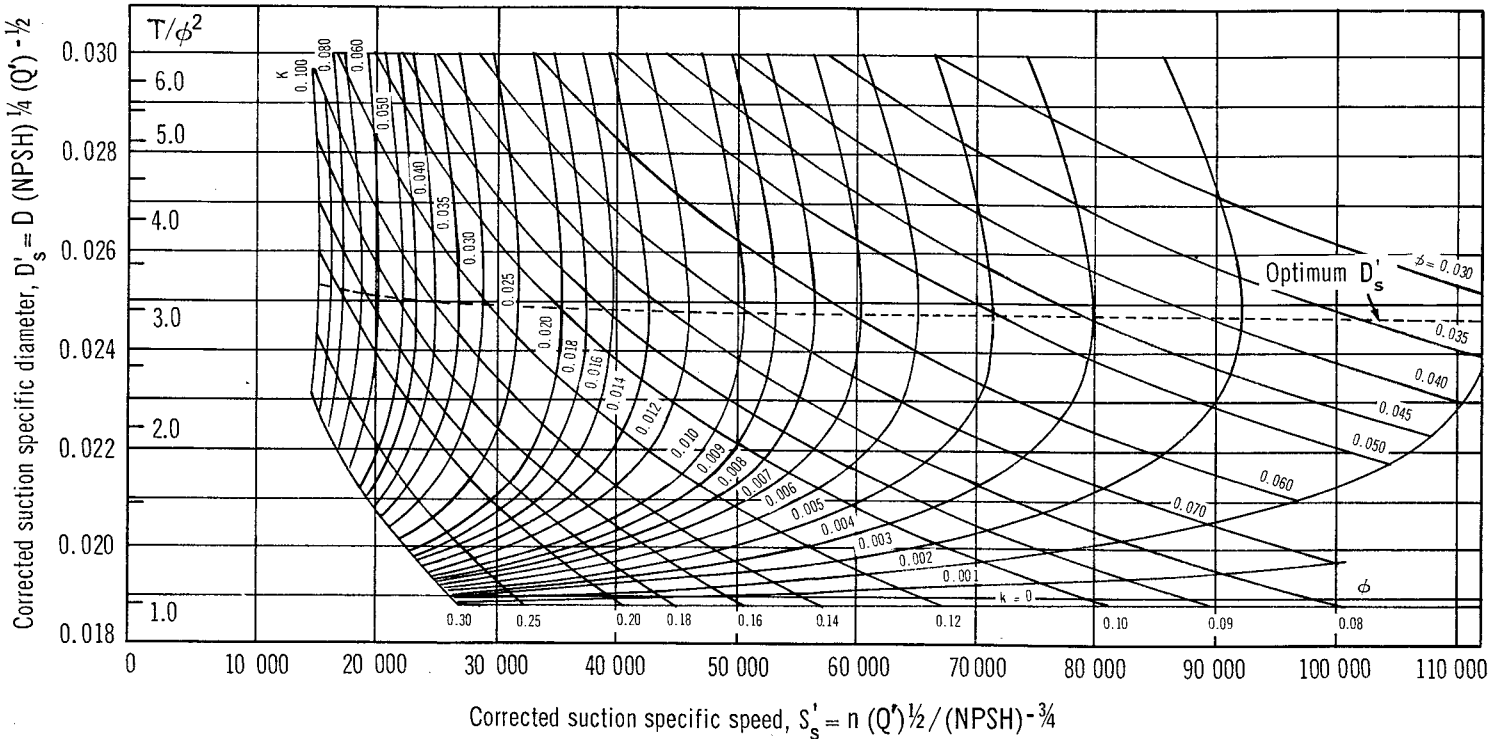

Figure 15.—S'_s-D'_s chart (zero pre-rotation), high-speed range.

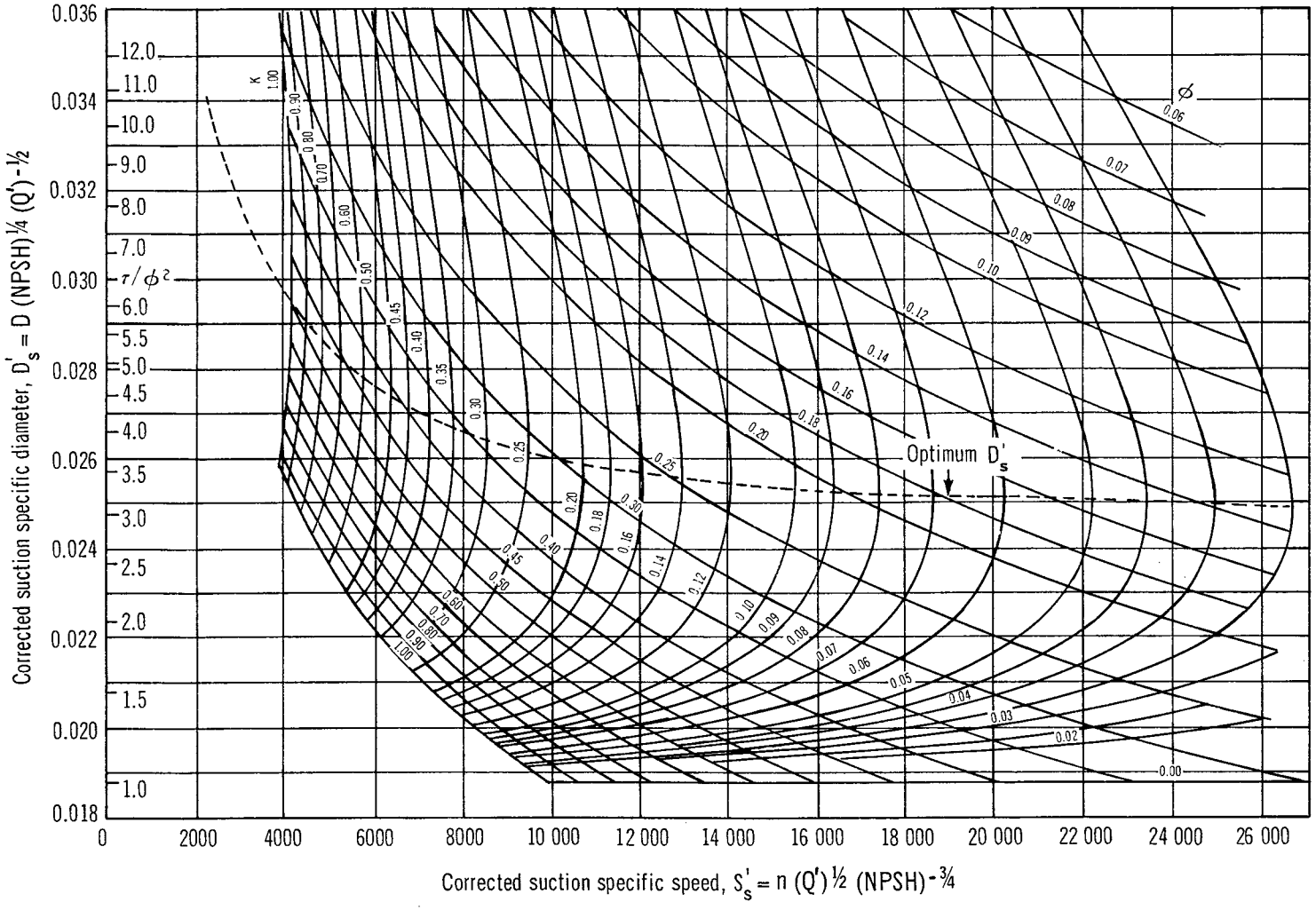

Figure 16.—S'_s-D'_s chart (zero pre-rotation), low-speed range.

The S'_s-D'_s diagram may be used in the following ways:

(1) To check the suitability of an existing design for suction performance at various operating points.
(2) To determine the effect on suction specific speed of changing the pump fluid for different values of Z.
(3) To determine optimum flow coefficient and inlet diameter required to meet suction performance specified in terms of the parameters n, Q, and NPSH.

3.1.3.2 Tip Contour

The inducer tip contour shall maintain the optimum flow conditions on the blade until the channel section is reached.

The tip contour should be held cylindrical at its optimum value at the inlet for an axial length at least equal to an axial blade spacing ($= \pi D/N \sin \beta$) and the inlet duct should be constant diameter on this length, both downstream and upstream of the leading edge for an inducer with a straight inlet. For an inducer with an elbow in the inlet, the upstream cylindrical length should at least be doubled for optimum suction performance.

3.1.4 Fluid Thermodynamic Effects

Fluids with high vapor head shall not produce unexpected fluid thermodynamic effects on suction performance.

Fluid thermodynamic effects, important for cryogenic fluids, should be accounted for by applying a TSH correction to the tank NPSH, then subtracting friction loss in inlet line to obtain the available NPSH at the inducer inlet:

$$(\text{NPSH})_{\text{available}} = (\text{NPSH})_{\text{tank}} + \text{TSH} - H_{\text{loss}} \tag{68}$$

The value of TSH cannot be predicted for an arbitrary inducer design and condition of operation; however, semiempirical correlations of TSH with fluid properties and pump parameters have been made. Tests of experimental inducers have shown that the fluid thermodynamic effects vary appreciably with the liquid, liquid temperature, rotative speed, flowrate, and inducer design. It is recommended that reference be made to recent technical literature to obtain experimental values of TSH for an inducer similar in design to the one being considered.

3.1.5 Blade Profile

The blade profile shall not interfere with the free-streamline boundary of the cavitation flow; that is, the blade must stay inside the cavity and wake at operating conditions.

It is recommended that the blade wedge angle α_w (fig. 17) be determined from

$$\alpha_w = \beta - \beta_w \tag{69}$$

where β is the blade angle and

$$\beta_w = \text{arc tan } (1.10\,\phi_d) \tag{70}$$

ϕ_d being the design flow coefficient. The numerical factor 1.10 in the equation means that the inducer blade will be inside the cavity for up to 110 percent of design flow and will present no additional blockage near the leading edge beyond that of the cavity.

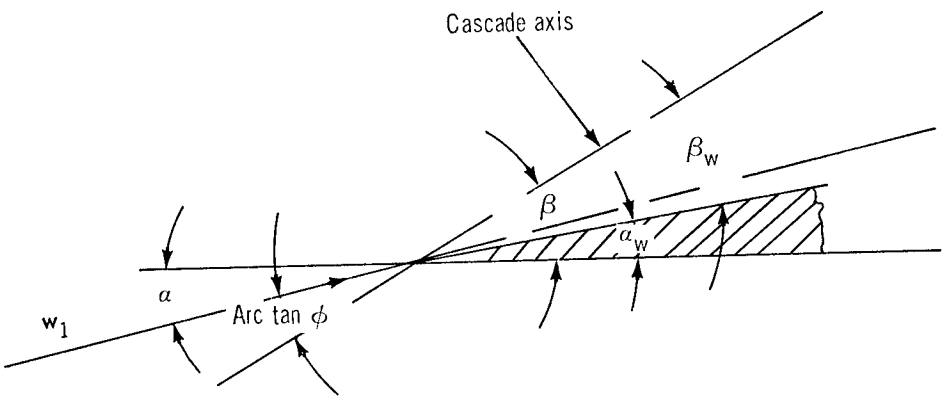

Figure 17.—Wedge angle.

If this factor is chosen larger than 1.10, the operating range becomes wider but the blade becomes very thin and may present a stress problem. The blade sharpening described is the so-called suction-side fairing of the blade (ref. 86). When stress conditions are severe and some suction performance may be sacrificed, the blade fairing may be modified by combining the suction-side fairing with a similar amount of sharpening on the pressure side to obtain centerline fairing. All sharpening should blend smoothly into the blade thickness. This simplified approach to leading-edge design has given good results. However, when very high suction performance and blade loading are required (over 40,000 S_s), the blade should be designed to match exactly the free-streamline boundary of the cavity at the highest flow (110 percent) so that the best guidance for the flow and the strongest leading edge may be obtained.

3.1.6 Blade Leading-Edge Sharpness

The blade leading edge shall be as sharp as consistent with practical limitations of strength and manufacturing considerations.

A practical measure for the sharpness of the blade is the maximum permissible leading-edge radius R_{LE} of the blade profile. It is recommended that the practical limit on leading-edge radius be

$$R_{LE} \leqq 0.01\, t \tag{71}$$

where t is the thickness of the blade profile at the particular radial station.

3.1.7 Blade Sweep

The leading-edge radial shape or contour shall improve suction performance and increase the mechanical strength of the blade.

The leading-edge radial shape or contour should be swept back for an unshrouded inducer and swept forward for a shrouded inducer. For structural reasons, the cutback in wrap angle at the tip for a sweptback leading edge should be equal to or greater than the wrap angle of the blade fairing at the hub. Then the blade will have reached its full thickness at the root when the leading-edge contour reaches the tip diameter and the blade forces attain their full value. The loss in solidity due to the cutback at the tip should be compensated for with a corresponding increase in axial length such that the solidity is maintained at its full value.

It is recommended that the leading-edge sweepback be an arc with a radius not less than the length of the blade fairing l_w. The outer part of the arc may be tangent to the inducer circumference for a minimum size sweepback (of radius l_w). The inner part of the arc should be radial, i.e., the leading edge should be radial next to the hub to provide room for the blade fairing.

3.1.8 Blade Cant

The cant angle shall be a compromise of its effects on blade bending stress, machining of the blade, and the leading- and trailing-edge geometry.

The inducer-blade cant angle should counterbalance pressure load and centrifugal force on the blade. For ease of machining, the blade should be perpendicular to the hub taper. The leading-edge sweepback at the blade tip,

$$\theta = r\,\Sigma\,, \text{ radians} \tag{72}$$

due to the canting of the blade, should be modified by the use of a conical face cut, according to the relationship

$$\Sigma = \frac{(1 - \nu)\,(\tan \alpha_{\text{cone}} + \tan \alpha_{\text{cant}})}{\lambda} \tag{73}$$

to obtain the desired amount of sweepback with the chosen cant angle α_{cant}. The cone angle α_{cone} is measured in the opposite direction of α_{cant}.

3.1.9 Blade Angle

The leading-edge blade angle β shall minimize blade blockage at optimum flow coefficient by meeting criterion 3.1.5.

Use the ratio of incidence angle to blade angle as a characteristic parameter α/β for design purposes. The ratio should be chosen in the range from a low value of 0.35 for thin blades to a high of 0.50 for thick blades. A mean value, 0.425, has gained preference. However, if a wide range of flow is required, the design value of α/β should be greater than the (optimum) 0.425 value to avoid blade blockage.

3.1.10 Blade Lead

The radial variation of the inducer leading-edge blade angle shall match the radial variation of the inlet velocity diagrams.

It is recommended that the inducer be designed as a flat-plate cascade at the blade inlet; i.e., at the leading edge, the blade pressure side should be part of the surface of a constant-lead helix $\lambda = r \tan \beta$, where $\Lambda = 2\pi\lambda$ is the lead of the helix and β is the local blade angle. This design produces optimum cavitation performance, essentially uniform over radius, and provides ease of manufacture. Its main disadvantages are high leading-edge loading and a low head rise (maximum $\psi \cong 0.075$).

3.1.11 Blade Thickness

The blade thickness variation shall be consistent with the radial variation of the cavity wake height so that the blade is entirely within the cavity at design conditions of speed, flow, and NPSH.

The blade thickness is determined almost entirely by mechanical considerations in regard to stress and vibration. The blade should be made thicker at the hub than at the tip. Usually the blade radial sections are formed by straight lines from the hub to the tip on both pressure and suction sides. They need not be straight lines, but

these are usually easier to define and to manufacture. However, for best hydrodynamic performance the blade thickness variation should match the variation of the cavity wake height at the critical NPSH design condition and 110 percent flow, calculated from the free-streamline wake theory. The blade root fillet (sec. 3.4.2) must also be taken into account as a factor in the thickness variation with an effect on flow.

3.1.12 Blade Camber

The blade camber shall produce the turning angle needed for the head-rise requirement while maintaining the suction performance of the flat-plate inducer.

For head coefficients beyond the capability of the flat-plate inducer ($\psi \approx 0.075$), a certain amount of blade camber ($\beta_2 - \beta_1$) is needed. The result is a modified, variable lead helical inducer, which starts out as a flat-plate inducer but whose camber gradually increases from zero at the leading edge to the required camber at the trailing edge. The variation of the blade curvature should follow a smooth, monotone curve from zero at the leading edge to a maximum at the trailing edge. Then the suction performance will be unaffected by the blade camber. The simplest distribution satisfying this condition is given by a linear variation of the curvature from inlet to outlet. The corresponding blade-angle variation is given approximately by a parabolic relationship:

$$\beta = \beta_1 + (\beta_2 - \beta_1)\,(z/L_{ax})^2 \tag{74}$$

where z is the axial coordinate and L_{ax} the axial length of the blade. It is common practice to specify the blade-angle distributions for the rms radius. The distribution of the blade angle along some meridional curve, contour, or streamline is related to the blade wrap angle θ through the slope equation

$$dz = \tan\beta\, d(r\theta) = \frac{\Lambda}{2\pi r}\, d(r\theta) \tag{75}$$

where Λ is the local lead and dz the change in axial coordinate for the infinitesimal change in blade wrap $d(r\theta)$. The corresponding wrap angle θ may be found by numerical methods from this first-order nonlinear differential equation between θ, z, β, and r such that the blade layout can be completed.

3.1.13 Blade Surface Finish

The blade surface finish shall be hydraulically smooth.

The required degree of surface finish cannot be attained by machining only. It is recommended that the blade be polished after machining to a finish of at least 25 μ-in. rms.

3.1.14 Blade Number

The number of inducer blades shall be as small as considerations of solidity and axial space permit.

The number of blades should be not less than two nor more than five, with three or four being preferred. An odd number of blades prevents alternate cavitation from occurring; three is therefore a preferred choice if other, more critical considerations permit. It is recommended that whenever possible the blade number N be selected so that the impeller blade number is a multiple of N. This relationship promotes symmetry of flow into the impeller.

3.1.15 Cascade Solidity

The solidity of the inducer shall be large enough to satisfy high suction performance and fluid turning requirements, without exceeding a suitable angle of deviation or introducing manufacturing problems due to small blade spacing.

For a low-head inducer, the solidity σ should be 2.5 for the inducer proper. For a high-head inducer, consisting of an inlet region featuring a flat-plate inducer of solidity 2.0 to 2.5 and an outlet region with increased camber featuring vortex-type blading with splitter vanes, the solidity of the outlet region or transition stage should be treated separately and may require consideration of the effects of deviation angle (sec. 3.2.7).

3.2 Inducer Flow-Channel and Blade Geometry

3.2.1 Channel Flow

The inducer shall provide a monotone increase in head along any streamline through the inducer without backflow at any station.

The head distribution should be calculated assuming simple radial equilibrium and perfect guidance of the fluid by the blades (eqs. (34) and (35)). In the application of this analysis to the actual inducer blade, a few modifications should be made to account for the effect of these assumptions. To account for the assumption of perfect guidance, one may assume that the deviation angle is distributed along the arc length of the blade, and then apply a correction factor to the axial distribution of the lead of the inducer helix. The calculated head distributed may be corrected by multiplication with an assumed value of the blade efficiency. The head distribution in the cavitating region of the blade should be calculated from the cavity theory, wake model (ref. 31). The transition between the two regions is not well understood, and there is a lack of experimental and analytical evidence of the flow conditions in the transition region.

It may be postulated without evidence that the blading should reach a solidity of $\sigma = 2$ or higher before any essential amount of blade camber is introduced, so that the cavity-collapse process behind the leading edge may progress undisturbed.

In interpreting the results obtained in calculating the flow distribution, it should be noted that $c_a = 0$ for $\psi = 1$; i.e., to avoid backflow, the local head coefficient ψ should be less than 1 at all stations. To alleviate any backflow problem discovered in the calculation, the blade camber should be modified and a new check performed. A simplified approach is permissible for low-head inducers, which are essentially flat-plate inducers with zero or very small channel loading. In this case, a one-dimensional check should be made of the flow at the rms diameter, checking the blade angle against the fluid angle at axial intervals through the inducer to correct for blockage effects due to tip and hub contour variations as well as blade blockage. The corresponding c_u values should also be calculated to ensure a monotone head rise throughout the length of the inducer.

3.2.2 Discharge Flow

The inducer discharge head and flow distribution shall satisfy the requirements of the impeller or high-head inducer following it.

In general, this requirement is no problem for low-head inducers used in conjunction with centrifugal impellers. However, there is a requirement for a uniform head-rise distribution at the discharge from the inducer that must be met when the inducer is used in a multistage axial pump with repeating stages.

The requirement of uniform head rise for high-head inducers results in the so-called free-vortex-flow type of rotation (eq. (45)). A deviation from the free vortex flow of about ± 5 percent is acceptable. To match the free-vortex-flow requirement, the inducer blade should be twisted at the discharge; i.e., it should be a double-definition blade with different leads at root and tip sections. Excessive twist, however, introduces stresses that must be analyzed and provided for. To avoid excessive twist of the long inducer blades, the blading should be divided into axial sections, thus simplifying both stress and manufacturing problems. The solidity should be increased by the addition of partial blades between the main blades.

3.2.3 Impeller-Inducer Matching

3.2.3.1 Basic Requirements

The inducer-impeller combination shall present a smooth meridional flow passage with an axial spacing consistent with hydrodynamic and mechanical requirements.

The inducer discharge hub and tip diameters should match the impeller inlet-eye dimensions closely enough that a smooth contour may be drawn. For easy clearance

control on unshrouded blading, the tip contour should be cylindrical if head-rise requirements of inducer and impeller permit.

3.2.3.2 Axial Clearance

Hydrodynamic matching between inducer and impeller shall include a minimum axial clearance of the same magnitude as the blade gap.

The minimum clearance should be of the maginitude of

$$\Delta z = \frac{2\pi r}{N} \sin \beta_{TE} \tag{76}$$

which for a flat-plate inducer reduces to

$$\Delta z = \frac{L_{ax}}{\sigma} \cong \frac{\text{lead}}{\text{blade number}} = \frac{\Lambda}{N} \tag{77}$$

3.2.4 Trailing-Edge Sharpness

The blade trailing edge shall be as thin as possible consistent with structural and manufacturing considerations.

A thin trailing edge is desirable for optimum performance, but not critical. A recommended value giving low drag for the trailing-edge radius R_{TE} is

$$R_{TE} = 0.02\, t \tag{78}$$

where t is thickness of the blade profile at the particular radial station.

The trailing edge normally is sharpened to $R_{TE} = 0.025$ to 0.050 in. The trailing edge should be centerline faired as designed but should be modified as necessary during the development stage to correct for an insufficient head rise. The length of the trailing-edge fairing is not critical, but the transition from the blade must be smooth with a gradual change in thickness.

3.2.5 Trailing-Edge Contour

The contour of the trailing edge shall be free of corners that are structurally inadequate and prone to blade flutter or oscillation.

Minimize the tendency of the trailing edge to flutter by using forward-swept fairings of 20° to 40° wrap angle. It is good practice to have the blade reach its full thickness

at the hub before the full radial blade height is reached. When the blade edges are contoured and faired, the inducer axial length should be increased to maintain the required solidity.

3.2.6 Discharge Angle

The fluid turning angle shall be based on the head-rise requirements of the inducer, allowing for blade losses.

For low-head inducers the turning angle $\Delta\gamma$ should be determined for the rms station such that the Euler head multiplied by an assumed blade efficiency of about 85 percent equals the required head rise.

For high-head inducers with free vortex flow, the turning angle should also be determined at both the root and the tip section so that a double-definition blade may be specified.

3.2.7 Deviation Angle

The trailing-edge angle $\beta_{ms,TE}$ shall minimize deficiencies in head rise.

The discharge blade angle should include a correction for the effect of an imperfect guidance in the form of a deviation angle δ, which may be estimated from Carter's rule (sec. 2.2.7) or from other sources (refs. 45 and 46) by a trial-and-error method. A normal target tolerance is 5 percent of design values. In regard to the discharge blade angle, this correction means that $\beta_{ms,TE}$ should be given by

$$\beta_{ms,TE} = \gamma_{ms,TE} + \delta_{ms} + 0.05\,\Delta\gamma_{ms} \tag{79}$$

where $\Delta\gamma_{ms} = \gamma_{ms,TE} = \gamma_{ms,LE}$ is the turning angle of the fluid at the rms station, ms. The customary tolerance on the blade angle is 1/2°. In some cases, limiting the deviation angle to 2° may produce more stable flow.

3.2.8 Clearance Losses

The effect of blade tip clearance on inducer performance shall be as small as possible.

For good suction performance, the blade tip clearance at the inlet should be as small as possible for a distance of at least one axial blade spacing. The clearance area should never exceed 3 percent of the flow area. For comparison purposes, clearance areas of 1 to 1.5 percent of the flow area are common practice.

The gain in performance from close clearances should be weighed against the difficulties encountered in maintaining such clearances. Recommended values of the ratio of radial clearance to blade length depend on the application and the actual design and materials used. Minimum practical values reached for fuel and oxidizer pumps are 0.005 and 0.020, respectively. Frequently, nonmetallic liners are used in the housings of inducers running in liquid oxygen so that close running clearances may be maintained without danger of sparking.

3.2.9 Shrouding

A shroud on the inducer, used when mechanical reasons so dictate, shall provide clearance control, structural reinforcement, or erosion damage protection.

When possible, a shroud should be made integral with the blading. When it cannot be made integral, it should be welded or brazed to the blading, and care should be taken to obtain a strong joint. Brazing is not recommended for high-operating-stress regions or for cryogenic applications.

When a shroud is used, the wearing-ring seal should maintain close clearances to preserve efficiency and suction performance. The inner diameter of the shroud should be flush with the inlet line outer diameter to minimize flow disturbances.

3.2.10 Blade Geometry Description

3.2.10.1 Specification Form

Final specification of the blade shape shall be suitable for fabrication and inspection purposes.

Give blade descriptions by coordinates to both blade surfaces rather than by blade angle and thickness distribution. Specify these coordinates at two parallel positions or cuts: one next to the hub but above the fillet, and the other near the tip.

Blade thicknesses are established at the two positions; all other thicknesses are a function of a straight-line tool cut between the two blade definitions. The inducer blade angles β should be defined initially at intervals along either one or two cylindrical or conical sections, according to the hydrodynamic design. A blade angle distribution called out at two stations implicitly defines a variable blade cant angle. From these definitions and from the blade fairing and the hub and tip geometry, the blade surface coordinates and the tool positions for both sides of the blade should be derived by computing and layout procedures. The coordinates and tool positions may be defined along either conical or cylindrical cuts as preferred by the manufacturer.

3.2.10.2 Tolerances

Tolerances on blade coordinate dimensions shall be specified and held at values consistent with good manufacturing practice.

In accordance with current practice, tolerances on blade coordinates should be clearly specified as ± 0.010 in. on large inducers (10 in. diameter or larger), and proportionately less for small inducers. Maintenance of these tolerances throughout manufacture should be ensured by careful and consistent inspection.

3.3 Inducer Inlet Line

3.3.1 Inlet-Line Configuration

The inlet-line design shall minimize the drop in NPSH resulting from line losses and shall provide the inducer with a uniform inlet flow distribution.

Every attempt should be made to avoid sharp bends and steps in the inlet line. The inlet line should be kept as short and straight as possible. If a bend is required, either a vaned or a large-radius elbow with a low loss coefficient and a uniform exit-flow distribution should be used, the choice depending on space limitations. Ribs and struts at the inducer inlet should be avoided, as they may cause wakes or eddies to enter the inducer. Gentle transitions between sections of varying cross section should be provided. Bellows in the line should have an internal liner to smooth the flow.

3.3.2 Inlet-Line Fluid Velocity

The inlet-line design shall maintain fluid velocity below the level that could cause cavitation anywhere in the line.

It is recommended that the line be designed so that the maximum velocity of the fluid at any point in the line stays at least 10 to 15 percent below the maximum possible velocity of $\sqrt{2g(\mathrm{NPSH})_{\mathrm{tank}}}$ for liquid hydrogen and below $\sqrt{2g\,[(\mathrm{NPSH})_{\mathrm{tank}}/3]}$ for all other propellants. Bellows and compensators in the inlet line should not produce vena contracta effects or other local cavitation due to flow around sharp corners. The peak velocities occurring at these places under normal operating conditions should be calculated carefully and verified by measurements whenever possible. When the velocities exceed the recommended limits, the line design must be modified to reduce these local speeds.

3.3.3 Inlet-Line Heat Transfer

Heat transfer to the fluid in the inlet line shall not reduce the available NPSH for the inducer below acceptable levels.

It is recommended that heat transfer to both the tank and the inlet line be investigated carefully. The amount of line insulation required to reduce the fluid temperature rise to allowable levels should be determined before final design specifications for the pump and inducer are made.

3.3.4 Bypass Flow

The reintroduction of leakage or bypass flows from bearings or balance-piston operation shall cause a minimum of disturbance to the main flow.

If possible, all bypass flows should be reintroduced after the inducer. Otherwise they may be fed through a hollow shaft and spinner into the center of the inlet line, where they cause the least disturbance.

3.4 Mechanical Design and Assembly

3.4.1 Hub Configuration

3.4.1.1 Wall Thickness

The hub wall shall be adequate to absorb the blade bending moments and the blade centrifugal pull, and shall have adequate hoop capability to carry the centrifugal force induced by its own mass.

The hub radial thickness should be at least $\sqrt{1/2}$ times the blade thickness to carry the blade bending moments. If the hub has a center hole with a diameter approaching the hub diameter, it is recommended that the hub radial thickness be equal to or greater than the blade thickness to accommodate both the bending moments and the centrifugal forces.

3.4.1.2 Diameter

The hub shall be of sufficient diameter and thickness to hold the shaft and transmit the shear load from the keys or splines.

The hoop discontinuity and stress concentration effects caused by the key way or spline teeth on the hub inner diameter must be considered when the hub is sized

in accordance with procedures set forth in the design criteria monograph "Liquid Rocket Engine Turbopump Shafts and Couplings."

3.4.1.3 Wall Contour

If the discharge diameter is greater than required by structural considerations, the hub configuration shall minimize the weight.

If the hub discharge diameter is large (with or without the center hole), the hub should be profiled and hollowed out as shown in figure 18 to minimize weight while maintaining an adequate margin on the burst speed.

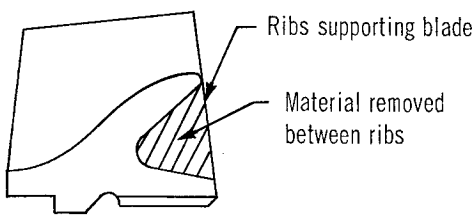

Figure 18.—Hub profile.

3.4.1.4 Axial Length

The inducer hub axial length shall be sufficient to permit full runout of the blade-to-hub fillet radius at leading and trailing edges during machining.

It is recommended that at each end of the hub an axial length equal to at least twice the fillet radius be added to the axial length of the blading.

3.4.2 Blade Root Juncture

The fillet at the blade root-to-hub juncture shall satisfy structural requirements but have minimum effect on the hydrodynamic performance of the blade.

The blade fillet should be a compromise among structural, hydrodynamic, and manufacturing considerations. A practical compromise is a circular fillet of radius equal to the blade thickness t. Better still in both structural and hydrodynamic respects, but more complicated to make, is an elliptical fillet with the radius joining the blade equal to t and the radius joining the hub equal to $t/2$.

When hydrodynamic requirements limit the fillet size, the fillet should be shot peened to improve fatigue resistance. Shot peening should also be used as a development tool to improve the fatigue resistance of inducers that experimentally have shown a tendency to fail by fatigue of the blade junctions.

3.4.3 Shaft Dimensions

3.4.3.1 Size

The inducer shaft size shall be adequate to carry the torque, preload, shear, and bending loads imposed on it at the worst operating condition.

Shaft size should be established in accordance with procedures set forth in the design criteria monograph "Liquid Rocket Engine Turbopump Shafts and Couplings." When sizing the shaft, allow for possible later modifications of the inducer design by adding 10 to 15 percent to the diameter required by structural analysis.

3.4.3.2 Torque Transmission

The torque transmission device shall be sized for the maximum torque load, considering potential cyclic variations.

Shear pins or keys normally are limited to low-torque applications. Splines are recommended for high-torque applications. Preferably, the arrangement of keys or splines should allow assembly in only one position so that proper balancing is maintained after reassembly.

3.4.4 Piloting

The inducer shall be piloted radially in the pump rotor assembly at all operating conditions.

When the design involves centrifugal stresses large enough to cause the inducer to come loose on the shaft, an inverted or external type of piloting is recommended. In this design, the inducer is piloted inside a groove or in a hole in the center of the shaft (fig. 19).

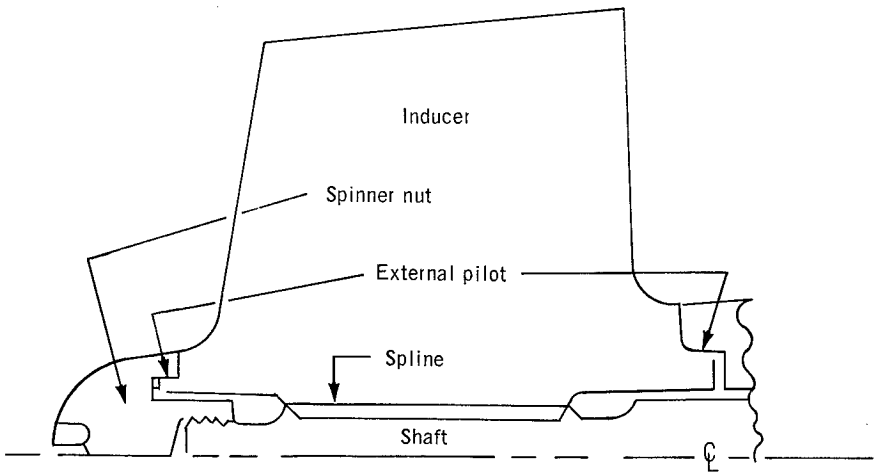

Figure 19.—External piloting.

3.4.5 Axial Retention

3.4.5.1 Axial Preload

The axial preload at assembly shall be adequate to withstand maximum hydrodynamic forces including dynamic forces, thermal contraction, centrifugal contractions including "Poisson's" contractions, and unbalance.

Dynamic forces cannot be known in advance; they may be estimated to be 30 percent of the steady hydrodynamic forces. Thermal contractions should be calculated on the basis of a slow chilldown period and should include the effects of differential expansion or contraction due to differences in thermal expansion coefficients. In the event of a fast chilldown, thermal effects due to different rates of cooling should be considered and evaluated.

Radial stresses due to centrifugal loads produce a radial elongation of the material with an accompanying contraction in the axial direction (the Poisson effect). These dimensional changes should be determined from the general stress condition by using the Poisson ratio of the material (this ratio has the approximate value of 0.3 for most materials of construction). The Poisson effect may produce loose fits that otherwise would not be expected, and it therefore must be carefully evaluated for the materials and stresses involved (ref. 87).

Unbalance should be identified by dynamic balancing, and then compensated.

3.4.5.2 Fastener Unloading

Bolts and studs in rotating assemblies shall not yield or unload under operating conditions.

Avoid any permanent deformation that would cause the assembly to come loose. Bolts and studs should be installed by measured amounts of stretch wherever practical. Three general methods may be employed:

(1) If both ends of a bolt are accessible, it may be measured with large outside micrometers. Usually the rotor parts being clamped undergo measurable compression, and therefore individual bolts in bolt circles must be progressively stretched.
(2) Stud stretch is generally measured by determining the change in length of a concentric center hole. This hole must pass through the entire working length of the stud.
(3) If measurement along a center hole is not practical, the increased protrusion of the nut end may be measured. Compression of the clamped parts must then be accounted for, or determined to be negligible.

The effect of chilling of parts by cryogenic propellants must be analyzed, and the combined effect of the axial shortening of rotating parts due to Poisson's effect coupled with radial growth due to centrifugal force must be accounted for. Such effects are particularly important when assemblies are composed of various materials with different coefficients of thermal contraction and different moduli of elasticity.

3.4.5.3 Preload Control

The inducer axial retention preloads at assembly shall be sufficient to preclude separation and fretting during operation and shall be accurately controlled.

To achieve uniform axial preloading of through-bolts, measure the bolt elongation or the nut rotation. The use of bolt torque measurements in critical load applications is not recommended because the variation in friction coefficient makes this method an unreliable index to preloading.

3.4.5.4 Galling, Fretting, and Seizing

Parts in rotating assemblies shall not experience galling, fretting, or seizing.

It is recommended that threaded joints and mating surfaces be coated with a suitable lubricant (ref. 88) or that they be silver plated. The tendency of titanium to

gall and seize has not yet proved to be a problem in inducer applications; however, whenever possible, a dry-film lubricant that is chemically compatible with the propellant should be used.

To eliminate or reduce fretting of the shaft and hub splines, a spline drive should have interference-fit pilot diameters at each end of the spline, or the spline teeth should have an interference fit under all operating conditions. For oxidizer applications, it is recommended that the radial pilot surfaces be coated with an acceptable lubricant (ref. 88) or that they be silver plated. When the radial stack interference fit requirements are evaluated, the relative thermal contractions, the centrifugal deflections, and the steady-state and oscillatory hydrodynamic loading extremes should be identified and included in the calculations.

3.4.6 Clearance Effects

The blade tip or shroud radial and axial clearances shall be as small as possible, but always sufficient to preclude detrimental rubbing between inducer and housing under any operating condition.

Pump rotating parts must not be allowed to rub metal-to-metal in oxidizer pumps.

Practically attained minimum values of the inducer clearance-to-blade length ratio are 0.5 percent for fuel and 2.0 percent for oxidizer applications. When closer clearances are required for oxidizer applications, a Kel-F liner or its equivalent should be used for the inducer casing. Since Kel-F has poor wearing properties at room temperature, it should not be used for water tests. The use of a Kel-F coating is shown in figure 20.

For pumps in which efficiency is not important, a large clearance can be used to prevent rubbing. For most rocket pumps, however, efficiency and suction performance are important enough to justify a more sophisticated design. The preferred practice is to house open impellers or inducers in a nonmetallic "tunnel"; with this arrangement, slight rubbing can be allowed. For shrouded impellers or inducers where nonmetallic wearing rings are used, multiple lands should be provided in the wearing rings to sustain rubbing with the lowest resisting torque.

The calculation of minimum required clearances must consider (1) manufacturing tolerances; (2) differential thermal expansion of inducer and housing including possible distortions occurring during chilldown and operation; (3) change in dimensions produced by operating conditions (e.g., centrifugal strain of blade and hub and deflections due to bending of the blade); (4) potential radial shaft and bearing deflections resulting from unbalanced inertia forces and radial hydrodynamic loads; and (5) potential axial displacements resulting from thermal and mechanical causes, if the inducer tip contour is not cylindrical.

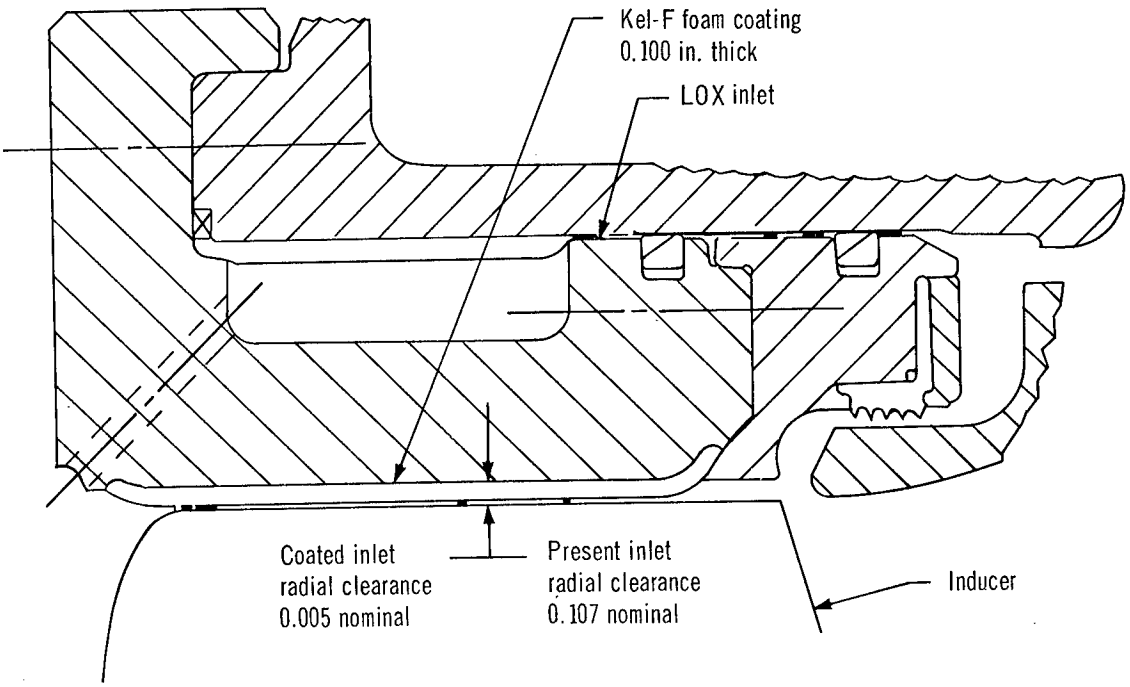

Figure 20.—Liquid-oxygen inducer, reduced tip clearance.

The maximum hydrodynamic loads should be considered in selecting the inducer tip clearances. The radial load should be considered equal to 30 percent of the inducer axial thrust unless better values are available. The following practices are recommended to minimize the possibility of interference rubbing:

(1) Provide adequate running clearances for steady-state operation.
(2) Design to minimize housing deflections.
(3) Account for all extremes of thermal deflections.
(4) Account for loads induced by engine malfunction, such as discharge valves not opening or closing in programmed sequence.

If models of cryogenic pumps are to be tested in other fluids, make proper allowance for different stackups, fits, and clearances. To get comparable test results, the design should be modified to maintain the clearance-to-blade length ratio c/L while running in the test fluid.

3.4.7 Shroud

The thickness of the shroud and its attachment to the blades shall be adequate for centrifugal loading effects from the shroud's mass and for the effect of the blades.

The inducer shroud thickness should be the minimum consistent with the centrifugal forces and the loads at the shroud-blade junction, as determined by a detailed stress analysis of the compound stress conditions in the shroud-blade structure combined with a knowledge of material properties.

The method of attachment of the shroud to the blading must be such that all junction loading can be adequately transferred to the blade. Integrally machined or cast shrouds are recommended. Attaching the shroud by welding is acceptable when the weld is inspected carefully by X-ray or other means. Brazing is not recommended for high-operating-stress regions or for cryogenic applications.

3.4.8 Misassembly

The design of rotating assemblies (rotors, turbine discs, blading, spacers and other symmetrical or near-symmetrical parts) shall preclude backward installation.

When only one orientation for a part is permissible, preclude misassembly in one of the following ways:

(1) Stepped land sizes on studs.
(2) Missing tooth (and mating space) on splines.
(3) Nonsymmetrical hole patterns for multiple bolt or stud fastening.
(4) Fixed dowel pins or keys (used mostly for stationary parts or lightly loaded rotary parts).

3.4.9 Rotation Direction

The direction of inducer rotation shall be consistent with the direction of rotation of the pump rotor assembly.

To avoid any inadvertent mismatch of the direction of rotation for the various components of a turbopump, preparation of an axonometric schematic of the complete rotor assembly, showing direction of rotation, should be the first order of business for the layout designer. Provide copies to all those involved with design and assembly.

3.4.10 Inducer Balancing

Inducer dynamic balance shall satisfy requirements imposed by the pumping system.

A two-plane dynamic balancing should be performed on a balancing machine of suitable size. Further balancing of the entire pump or turbopump assembly should be done as required.

Typical turbopump practice for speeds of around 30,000 rpm is to balance to within 0.01 oz-in. per balance plane for a two-plane balance on a part weighing 10 to 15 lb.

For oxidizer pumps, balancing should be accomplished through metal removal only; holes or grooves for weight addition should not be used.

Metal removal on hydrodynamic surfaces should be within the tolerance band of the surface. The cut must be faired smoothly into the blade surface.

3.5 Material Selection

Material strength properties used in material selection shall be the minimum guaranteed properties.

The minimum guaranteed material properties are established as military standards. Because of the statistical nature of the distribution of test results for material properties, a one-sided tolerance factor for evaluating compliance of test data with specifications should be used. Values of 99 percent for conformance or probability and 95 percent for confidence level are recommended (ref. 68, par. 1.4.1.1, Basis A). All materials should be compared on the basis of the minimum guaranteed properties in accordance with these recommended values for statistical significance.

3.5.1 Strength

The inducer material shall possess the best strength-to-density ratio for the particular inducer needs, provided it meets all the criteria in sections 3.5.2 *and* 3.5.3.

The strength properties should include the ultimate, yield, elongation, and endurance limits of the material. In the choice of material, the relative importance of these limits for the application in question should be considered. Aluminum and titanium forgings are the preferred inducer material choices for minimum weight but are subject to limitations noted in sections 3.5.2 and 3.5.3.

The titanium alloy Ti-5Al-2.5Sn ELI is recommended for liquid-hydrogen inducers. The Ti-6Al-4V titanium alloy, although stronger, should not be used at liquid hydrogen temperatures because its notch toughness and ductility below −320° F fall to levels unsatisfactory for rotating components. Annealed Ti-6Al-4V forgings are recommended for pumping RP-1; although the alloy is heat treatable to higher strength levels, the relatively thick hub sections and complex blade configurations preclude heat treatment. Where cavitation erosion is not a problem, the recommended material for oxidizer inducers is one of the four aluminum alloys: 7079-T6, 7075-T73, 2024-T4, and 2014-T6; any of these may be used for fuel pumps, both liquid hydrogen and RP-1.

3.5.2 Chemical Reactivity

3.5.2.1 Compatibility

The material shall be compatible with the pump fluid and shall have no tendency to react chemically at operating conditions.

It should be known or demonstrated by test that the material has no tendency to react chemically with the pump fluid. Environmental hydrogen embrittlement caused by the gaseous phase should be a special concern in choosing materials for liquid-hydrogen pumps. Explosion hazards should be of special concern in choosing materials for oxidizer pumps.

Titanium alloys should not be used with liquid fluorine, with mixtures of liquid fluorine and liquid oxygen (FLOX), with oxygen, with IRFNA, or with nitrogen tetroxide (N_2O_4). With each, there are known corrosion and explosion hazards.

Titanium alloys must not be used in oxidizer pumps. Recommended materials for oxidizer pumps are aluminum alloys, stainless steels 304 and 347, K-Monel, or Inconel 718.

Aluminum alloys are recommended for use with the cryogenic liquids (hydrogen, oxygen, nitrogen, FLOX, and fluorine) and at room temperature with water (for testing), IRFNA, UDMH, and N_2O_4. Anodic coatings of the aluminum alloys should be used to reduce handling damage and cavitation erosion. The minimum protection would be a chromic acid anodic coating about 70 μin. thick. A better protection would be a 300-μin. coating of sulfuric-acid or flashhard anodizing. Even though protection increases with thickness, a thickness greater than 500 μin. should not be used, for it will lower the fatigue resistance. However, all these coatings will slowly dissolve in liquid fluorine, IRFNA, UDMH, and N_2H_4; therefore, the coatings should not be used for extended running periods with these fluids, as in development program testing, unless the surface protection can be renewed periodically.

Steel inducers should be nickel plated for rust protection when used in the water-test facility.

3.5.2.2 Stress Corrosion

The inducer material shall possess acceptable resistance to stress corrosion.

When residual stresses are imposed by the manufacturing method or by assembly, the 7075-T73 aluminum alloy should be preferred to the 2014-T6 aluminum alloy, which has a low stress-corrosion threshold. Similarly, titanium alloys should not be used in brown N_2O_4 (i.e., uninhibited nitrogen tetroxide containing over 1.00 percent nitric oxide).

3.5.2.3 Degradation by Fluids

Inducer materials such as titanium and aluminum alloys shall not experience degradation from fluids or solvents used during cleaning, processing, or operation.

Cleanliness of the parts is of the utmost importance prior to any welding or thermal treatment of titanium; however, halogenated solvents should never be used prior to any welding or thermal treatment. Methanol causes stress corrosion in titanium alloys at room temperature; it should never be employed for any processing, testing, or operational service in contact with titanium alloys.

3.5.3 Special Properties

3.5.3.1 Cavitation

The resistance of the inducer material to cavitation damage shall be adequate for the intended use.

A steel alloy such as K-Monel or Inconel 718 is recommended for low-speed, cavitating oxidizer inducers. A titanium alloy is recommended for cavitating fuel inducers. Aluminum alloys should be avoided wherever cavitation erosion may affect the useful life and performance. When aluminum alloys are used, they should be protected with anodic coatings as described in section 3.5.2.1.

3.5.3.2 Thermal Environment

The material shall withstand the thermal environment at operating conditions without excessive degradation.

Excessive brittleness at low temperatures must be avoided for cryogenic applications. The titanium alloy Ti-5Al-2.5Sn ELI is recommended for liquid-hydrogen temperature (−423° F). Both Ti-5Al-2.5Sn ELI and Ti-6Al-4V ELI are recommended

at liquid-nitrogen temperature (−320° F). All the recommended aluminum alloys are satisfactory for operation from room temperature down to liquid-hydrogen temperature. If they are made of the recommended alloys, parts that are of suitable strength at ambient temperatures are still stronger at cryogenic temperatures.

3.5.3.3 Fabrication

The material shall be suitable for the intended manufacturing and fabrication method.

A cast-aluminum inducer would be the proper choice for low-stress applications when low cost is important. Aluminum is easy to forge and machine, but welding or brazing this material is not practicable.

Titanium alloy parts are more expensive to machine than comparable parts of aluminum alloys but are less expensive than alloys such as Inconel 718 or Rene' 41. The recommended titanium alloys can be welded readily by either gas-tungsten arc or electron-beam processes. Proper welding procedures should be observed for titanium alloys.

3.6 Vibration Considerations

3.6.1 High-Frequency Fatigue

The inducer blades shall not experience vibration amplitudes above the fatigue limit.

Design the inducer initially from strength considerations alone and then analyze (ref. 69) the vibration behavior of known problem areas of the blade, such as leading- and trailing-edge corner flap and flutter. To prevent fatigue failure, the blade should be sized so that oscillatory stresses are kept below the endurance limit.

3.6.2 Resonance

The blades shall not experience resonant vibration produced by fixed-wake forcing frequencies.

It is recommended that at least a 15-percent margin between blade frequency and wake frequency be maintained in the operating speed range. It is, however, sometimes difficult to achieve this margin. It is established practice to consider only first- and second-order harmonic vibration for inducer blades. Both upstream and downstream wakes should be considered as the source of forcing frequencies. The blade natural frequencies and fixed-wake forcing frequencies should be compared on

a Campbell diagram (ref. 89) to determine the critical speeds at which resonant vibration will occur. Where possible, obtain the recommended margin by changing the obstacle producing the wake. Otherwise, modify the blade to change its natural frequency.

3.6.3 Self-Induced Vibration

The blades shall not experience flutter resulting from self-induced oscillations.

Blade flutter should be alleviated by trimming back the leading or trailing edges or by adding a shroud to the inducer. The recommended trimming angles are 60° to 140° wrap for the leading edge and 20° to 40° for the trailing edge. If the blades are trimmed back, the axial length of the inducer should be increased to maintain adequate solidity of the blading.

3.6.4 Determination of Blade Natural Frequencies

The blade natural frequencies shall be determined by vibration analysis and by testing.

The initial vibration analysis should establish nominal values for blade frequencies based on blade geometry and material and nominal operating conditions. The effects of blade manufacture and actual conditions of use on the nominal values should be accounted for by following the practices set forth in sections 3.6.4.1 through 3.6.4.4. Because present analytical techniques give only approximate results, the values for blade frequencies must be verified by testing a prototype inducer as required in section 3.6.4.5.

3.6.4.1 Tolerance Bands

In the determination of the natural frequency bands, the vibration analysis of the blade shall take into account the blade dimensional tolerance bands.

The blade should be analyzed for the maximum root–minimum tip thickness and minimum root–maximum tip thickness to determine the natural frequency bands.

3.6.4.2 Centrifugal Stiffening

The vibration analysis shall consider the effect of centrifugal stiffening on the blade natural frequencies.

The restoring component of the centrifugal force should be added to the restoring force due to the blade elastic bending properties.

3.6.4.3 Temperature Effects

The vibration analysis shall account for the effect of the operating temperatures on the elastic properties of the material.

The effect of cryogenic temperatures on the elastic modulus of the material is to raise the natural frequency. If operation with a test fluid different from the design fluid is contemplated, the resulting frequency bands should be corrected by use of the relationship

$$\frac{n_{op}}{n_{test}} = \sqrt{\frac{E_{op}}{E_{test}}} \tag{80}$$

where n_{op} and n_{test} are frequencies under operating and test conditions, respectively, and E_{op} and E_{test} are the corresponding values for the material elastic modulus.

3.6.4.4 Virtual Mass Effect

The vibration analysis shall include the effects of the virtual mass of fluid moving with the blade under operating conditions.

The reduction in blade natural frequencies should be determined or verified by prototype testing. The following reductions (ref. 90) should be taken as order-of-magnitude values giving estimates of the effect: a 4-percent reduction of the fundamental frequency in liquid hydrogen, and a 24- to 31-percent reduction (two different designs) in liquid oxygen. The effect of the virtual mass may be estimated by the approximate relationship

$$n_F = \frac{n_0}{\sqrt{1 + K(\rho_F/\rho_{bl})}} \tag{81}$$

where n_F and n_0 are frequency with and without fluid, respectively, K is a constant factor characteristic of the blading considered, and ρ_F and ρ_{bl} are densities of fluid and blade material, respectively. The value of K should be determined in each case from test results. No analytical approach is recommended at present. The effect should be allowed for when the results of blade vibration tests in air are reduced to inducer operating conditions.

3.6.4.5 Natural Frequencies

Vibration tests on each prototype inducer design shall verify and accurately determine the blade natural frequencies.

The vibration tests should include excitation in air and in the pumping fluid medium if possible. The modes of vibration can be determined by fuller's earth, stroboscopic films, strain gages, or accelerometers during the shake test.

3.7 Structural Considerations

3.7.1 Blade Loading

The load analysis shall determine critical loads on blades for both steady-state and alternating conditions, encompassing all anticipated hydrodynamic and inertia loads in the operating and test range.

It is recommended that all loads and forces be calculated on the basis of a mechanical design speed that is 110 percent of the maximum speed or 120 percent of nominal speed, whichever is higher. The critical blade loadings should be based on the worst flow/NPSH/speed conditions that can occur during operation or testing. Particular attention should be paid to situations where test conditions differ from the design conditions.

The minimum flow–maximum NPSH condition should be used to define the leading-edge loading of the blades, and the minimum flow–minimum NPSH condition should be used to define blade loadings in the channel section of the blade. Use a computer program like that provided in reference 79 to calculate the leading-edge loading. The channel loading may be calculated by a computer program based on an axisymmetric or blade-to-blade solution of the noncavitating inducer flow, or it may be determined by using the theory of simple radial equilibrium to calculate the pressure distribution on the blades.

The study of oscillatory blade loads should include the effects of periodic flow fluctuations, circumferential nonuniformities of flow and pressure wakes from ribs or stator blades, and random vibrations. Since these effects are not predictable at the design phase, assume an alternating load equal to 20 to 30 percent of the steady-state hydrodynamic loads. Use accurate values for the important fluid properties that affect the structural analysis: density, temperature, pressure, and vapor pressure. These determine hydrodynamic forces and affect material properties and NPSH values.

If models of cryogenic pumps are to be tested in other fluids, attention should be directed to the change in stress level that results from the change in fluid density and pump speed. A stronger material may have to be used, or one of lower stress capability may be satisfactory for the model, depending on strength and cost considerations.

3.7.2 Blade Stress

The stress analysis shall determine critical values of stress and strain for both steady-state and alternating conditions, based on the established critical loads and inducer geometry with proper allowance for manufacturing tolerances.

It is recommended that the critical stress regions corresponding to potential failure lines be found by plotting the stress level at various locations on the blade. These stresses may be found by the methods described in section 2.7.2. Critical sections are normally at the root junction or close to it, or on bending lines for a blade corner. Blade corners may be rounded off to reduce bending stresses. The effect of manufacturing tolerances on blade dimensions should be evaluated by using minimum root thickness and maximum tip thickness.

3.7.2.1 Discontinuities

The stress analysis shall include the effect of stress concentrations due to discontinuities at bolt holes and keyways or splines in the inducer hub and at the blade-hub and blade-shroud junctions.

It is recommended that the stress-concentration factor for blade root fillets or other discontinuities be applied to the blade alternating stress before the Goodman diagram is used to determine the blade structural adequacy. The endurance limit is reduced by stress-concentration effects on the alternating stress but not by its effects on the mean stress for ductile materials. The full theoretical stress-concentration factor K_t should be used if actual stress-concentration factors K_{tf} are not available.

3.7.2.2 Load Concentrations

The stress analysis shall identify and analyze peak stress regions associated with hub-profile load concentrations.

The blade centrifugal pullout of the hub and reversals in the hub profile, together with discontinuities due to splines, keyways, and eccentric bolt holes, should be considered potential failure areas (refs. 83, 91-96). A special study of these local problem areas is recommended.

3.7.3 Hub Strength

Stress analysis shall verify that the disc burst speed for the inducer hub is at the level required.

The disc burst speed for the inducer hub should be determined from the relationship

$$n_{\text{burst}} = n \sqrt{\frac{\sigma_{\text{AT, burst}}}{\sigma_{\text{AT}}}} \tag{82}$$

where σ_{AT} is the average tangential stress in the disc at the speed n and $\sigma_{\text{AT, burst}}$ is the average tangential stress at the burst speed n_{burst}. The average tangential stress must be calculated for the weakest cross section of the disc according to equation (59):

$$\sigma_{\text{AT}} = \frac{1}{A'_H} \int \sigma_t \, dA_H$$

where A'_H is the meridional cross-sectional area of the disc (or hub) at its weakest section (i.e., allowing for bolt holes, splines, etc.), and the integral represents the total centrifugal force acting on one-half the disc (or hub); σ_t is the tangential stress at the speed considered acting on the area element dA_H.

The average tangential stress at burst $\sigma_{\text{AT, burst}}$ is obtained from the empirical relationship

$$\sigma_{\text{AT, burst}} = f_b \, F_{tu} \tag{83}$$

where F_{tu} is the material ultimate tensile strength from the guaranteed minimum properties and f_b is a so-called burst factor. The factor f_b has been established experimentally as a function of a disc design factor f_d, which represents the nonuniformity of the stress distribution existing in the disc in the unyielded state, and also as a function of the material's capability to yield; specifically, the elongation e measured on a test rod over a length equal to 4 diameters of the rod. This combined functional relationship is presented in figure 21. This relationship must be used to determine f_b from a knowledge of f_d for the disc in question.

The design factor f_d is defined by the ratio

$$f_d = \frac{\sigma_{\text{AT}}}{\sigma^*_{\text{MT}}} \tag{84}$$

calculated at some speed n, where σ^*_{MT} is the maximum tangential stress in the disc including stress-concentration effects at eccentric bolt holes and at the base of spline teeth in a central hole, i.e.,

$\sigma^*_{\text{MT}} = \sigma_{\text{MT}}$ times stress-concentration factor
σ_{MT} = maximum tangential stress obtained from the basic stress analysis for elastic deformation

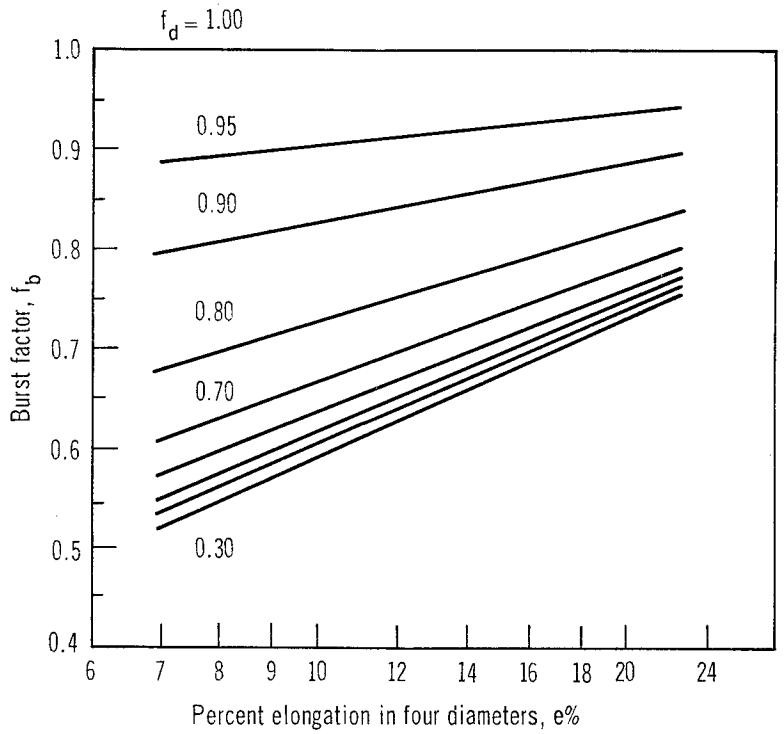

Figure 21.—Burst factor vs. elongation for various design factors.

3.7.3.2 Yield Speed

Stress analysis shall verify that the disc yield speed is at the level required.

The disc yield speed should be calculated from

$$n_{\text{yield}} = n\sqrt{\frac{F_{ty}}{\sigma_{\text{AT}}}} \tag{85}$$

where F_{ty} is the yield strength of the material. The calculation of σ_{AT} is described above. The value for n_{yield} is straightforward, as shown.

3.7.3.3 Safety Factors on Hub Speeds

The inducer burst speed and yield speed shall provide adequate safety factors relative to the mechanical design speed.

Recommended values of these safety factors are 1.20 for the inducer burst speed and 1.05 for the inducer yield speed. These values give the ratio of inducer burst speed or yield speed to mechanical design speed (sec. 3.7.1).

3.7.4 Shaft Shear Section Strength

The rotor shaft shear section shall be sized on the basis of the allowable shear stress for the compound stress condition.

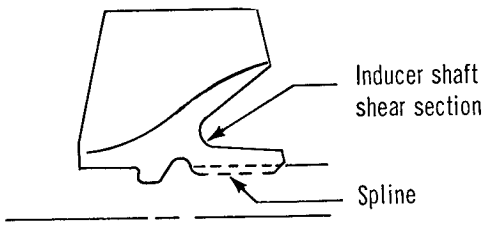

Figure 22.—Shear section.

The inducer shaft shear section (fig. 22) should be sized according to the following relationship (adapted from eq. (37) in ref. 56) for the allowable shear stress:

$$\tau_0 = \left(\frac{L_s F_{ty}}{n_{ult}\sqrt{3}} \right) \frac{\sqrt{1 - \left(\frac{n_{ult}\,\sigma_{ax}}{L_b F_{ty}} \right)^2}}{1 + \left(\frac{K_{tsf} L_s F_{ty}}{F_e} \right)\left(\frac{\tau_{alt}}{\tau_0} \right)} \tag{86}$$

where

$$L_b = (4/\pi) L_s \tag{86a}$$

$$L_s = 4/3\,[1 - (d_i/d_o)^3]/[1 - (d_i/d_o)^4] \tag{86b}$$

and

n_{ult} = safety factor against ultimate failure
K_{tsf} = fatigue notch factor for shear stress
F_e = material endurance strength, $lb_f/in.^2$
τ_0 = allowable shear stress, $lb_f/in.^2$
τ_{alt} = alternating shear stress, $lb_f/in.^2$
σ_{ax} = axial stress, $lb_f/in.^2$
d_i and d_o = inside and outside diameters of hub shear section, in.

Note: $L_b F_{ty} <$ material ultimate strength. Allowance for alternating shear should be made by assuming $\tau_{alt}/\tau_0 = 0.05$.

3.7.5 Safety Factors

Safety factors shall be based on the guaranteed minimum material properties at the operating condition.

The endurance limit, ultimate, and yield data should be modified to represent actual blade conditions considering the effects of temperature, surface finish, residual stress from the manufacturing processes, material grain size, heat treatment, and type of loading.

3.7.5.1 Fatigue Failure

The safety factor against fatigue failure shall be based on a Goodman diagram constructed from experimental values for material fatigue strength.

Because the nature of the blade alternating stress cycle generally is unknown, it is recommended that the endurance limit strength values be used in constructing the Goodman diagram (ref. 68), figure 23. In using the Goodman diagram, the stress-concentration factor should be applied for the alternating stress only. Peak stress points should be considered at all radii. In general, the blade root fillet tangent plane is most critical.

3.7.5.2 Ultimate Failure and Yielding

Safety factors against ultimate failure and yielding shall be based on the peak stress $(\sigma_{mean} + \sigma_{alt})$ *that includes the stress-concentration effects caused by discontinuities.*

The magnitude of the stress-concentration factor should be based on the ability of the material to yield. For brittle materials with low ductility and notched strength less than unnotched strength, the full theoretical value of the stress-concentration factor should be used in determining the peak stress. For materials with high ductility and notched strength greater than unnotched strength, the stress-concentration factor approaches 1 as yielding occurs and therefore can be neglected in the prediction of the peak stress.

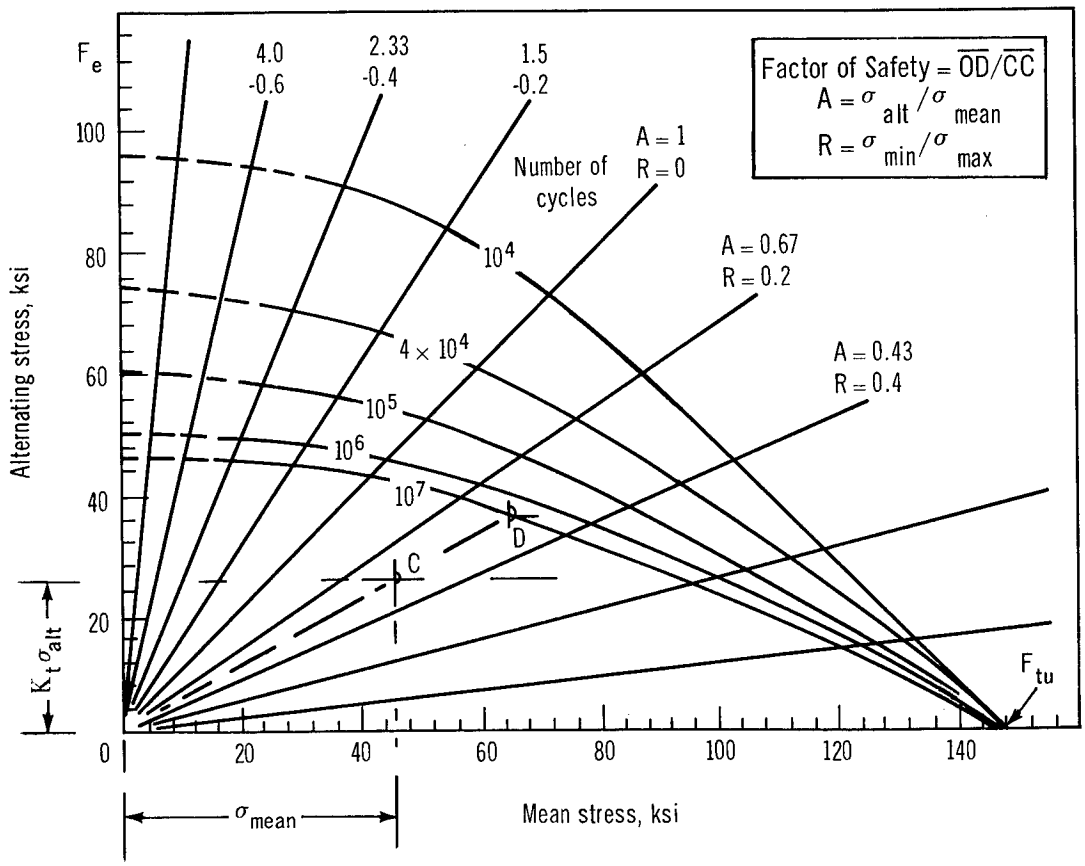

Figure 23.—Goodman diagram.

3.7.5.3 Values for Safety Factors

The safety factors on yield, ultimate, and fatigue strength shall be adequate for all stress conditions and shall be consistent with well-established design practice.

Experience indicates that the following safety factors have been adequate for successful inducer design:

Fatigue, $n_f = 1.5$
Ultimate, $n_{ult} = 1.5$
Yield, $n_y = 1.1$

These safety factors are based on stress levels obtained at the mechanical design speed.

If the alternating stress component is accurately determined, the fatigue safety factor could justifiably be reduced. The safety factors are highly dependent on strict quality control practices.

3.7.6 Hub Stress Verification

For high-speed inducer designs, the inducer spin test shall verify the predicted hub stress.

When centrifugal stresses govern the design, a prototype inducer should be run to destruction. Adequate instrumentation should be provided such that the stress distribution and critical deflections can be obtained to verify the calculations.

3.7.7 Inducer Proof Test

The inducer spin proof test shall verify the predicted structural capability of the inducer.

Spin testing is recommended when the mechanical design speed exceeds 60 percent of the burst speed in the operating environment. The proof-test spin speed should subject the inducer material to strains equal to or greater than the centrifugal strains it will experience during operation, and should demonstrate the same maximum centrifugal stress-to-available-strength ratio as that which will occur at the mechanical design operating conditions. The spin speed should not exceed the speed at which gross yielding will occur or induce partial failure by approaching the room-temperature burst speed. It is recommended that the spin speed have no less than 10-percent margin on the room-temperature burst speed. A spin duration of no less than 2 minutes is recommended.

REFERENCES

1. Gross, L. A.; and Miller, C. D.: A Performance Investigation of an Eight-Inch Hubless Pump Inducer in Water and Liquid Nitrogen. NASA TN D-3807, 1967.
2. Brumfield, R. G.: Optimum Design for Resistance to Cavitation in Centrifugal Pumps. P-10 Propulsion Memorandum, U. S. Naval Ordnance Test Station, Feb. 1948.
3. Ross, C. C.; and Banerian, G.: Some Aspects of High-Suction Specific Speed Pump Inducers. Trans. ASME, vol. 78, Nov. 1956, pp. 1715-1721.
4. Stripling, L. B.: Cavitation in Turbopumps—Part 2. J. Basic Eng., vol. 84, Sept. 1962, pp. 339-350.
5. Wislicenus, G. F.: Critical Considerations on Cavitation Limits of Centrifugal and Axial-Flow Pumps. Trans. ASME, vol. 78, Nov. 1956, pp. 1707-1714.
6. Lewis, G. W., Jr.; Sandercock, D. M.; and Tysle, E. R.: Cavitation Performance of an 83° Helical Inducer Operated in Liquid Hydrogen. NASA TM X-419, 1961.
7. Osborne, W. M.: Investigation of a Liquid-Fluorine Inducer and Main-Stage Pump Combination Designed for a Suction Specific Speed of 20,000. NASA TM X-1070, 1965.
8. Salemann, V.: Cavitation and NPSH Requirements of Various Liquids. J. Basic Eng., vol. 81, June 1959, pp. 167-180.
9. Stepanoff, A. J.: Cavitation Properties of Liquids. J. Eng. Power, vol. 86, Apr. 1964, pp. 195-200.
*10. Anon.: Evaluation of NPSH Performance of the Model Mark 3 LOX Turbopump Used in the Thor MB-3 Propulsion System. R-3995, Rocketdyne Div., North American Rockwell Corp. Unpublished, Apr. 1967.
*11. Iura, T.: Cavitation Performance of Pump With Inducer in Liquid Oxygen and Liquid Nitrogen. DDR 512-114, Rocketdyne Div., North American Rockwell Corp. Unpublished, Jan. 1956.
*12. Stremel, R. L.: Water Versus "Cold LOX" Performance Comparison Study for the Various Mark 4 LOX Pump Configurations. CEM 0125-15, Rocketdyne Div., North American Rockwell Corp. Unpublished, Apr. 1960.
*13 Walsh, J. K.: Mark 15 LOX Pump Calibration. TAMM 6115-50, Rocketdyne Div., North American Rockwell Corp. Unpublished, Aug. 1966.
*14. DiCristina, H.: Water, Alcohol, and JP-5 Tests of a Phase 5 Fuel Pump. PED 55-5807, Rocketdyne Div., North American Rockwell Corp. Unpublished, Dec. 1955.
15. Hammitt, F. G.: Observation of Cavitation Scale and Thermodynamic Effects in Stationary and Rotating Components. J. Basic Eng., vol. 35, Mar. 1963, pp. 1-16.
16. Jacobs, R. B.; Martin, K. A.; and Hardy, R. J.: Direct Measurement of Net Positive Suction Head. J. Basic Eng., vol. 81, June 1959, pp. 147-154.
17. Grindell, A. G.: Correlation of Cavitation Inception Data for a Centrifugal Pump Operating in Water and in Sodium-Potassium Alloy (NaK). J. Basic Eng., vol. 82, Dec. 1960, pp. 821-828.
18. Hollander, A.: Thermodynamic Aspects of Cavitation in Centrifugal Pumps. ARS J., vol. 32, no. 10, Oct. 1962, pp. 1594-1595.
19. Stahl, H. A.; and Stepanoff, A. J.: Thermodynamic Aspects of Cavitation in Centrifugal Pumps. Trans. ASME, Series D, vol. 78, Nov. 1956, pp. 1691-1693.
20. Jakobsen, J. K.: On the Mechanism of Head Breakdown in Cavitating Inducers. J. Basic Eng., vol. 86, June 1964, pp. 291-305.

*Dossier for design criteria monograph "Liquid Rocket Engine Turbopump Inducers." Unpublished, 1968. Collected source material available for inspection at NASA Lewis Research Center, Cleveland, Ohio.

21. Jacobs, R. B.; and Martin, K. B.: Cavitation Problems in Cryogenics. Technical Briefs, J. Basic Eng., vol. 82, Sept. 1960, pp. 756-757.

*22. Holl, J. W.: The Influence of Temperature, Size and Speed on NPSH. TSM 7115-2077, Rocketdyne Div., North American Rockwell Corp. Unpublished, Aug. 1967.

23. Ruggeri, R. S.; Moore, R. D.; and Gelder, T. F.: Method for Predicting Pump Cavitation Performance. NASA TM X-52316, 1967.

24. Moore, R. D.; and Ruggeri, R. S.: Prediction of Thermodynamic Effects of Developed Cavitation Based on Liquid-Hydrogen and Freon-114 Data in Scaled Venturis. NASA TN D-4899, 1968.

25. Ruggeri, R. S.; and Moore, R. D.: Method for Prediction of Pump Cavitation Performance for Various Liquids, Liquid Temperatures, and Rotative Speeds. NASA TN D-5292, 1969.

26. Gelder, T. F.; Ruggeri, R. S.; and Moore, R. D.: Cavitation Similarity Considerations Based on Measured Pressure and Temperature Depressions in Cavitated Regions of Freon-114. NASA TN D-3509, 1966.

27. Moore, R. D.; and Ruggeri, R. S.: Venturi Scaling Studies on Thermodynamic Effects on Developed Cavitation of Freon-114. NASA TN D-4387, 1968.

28. Meng, P. R.; and Moore, R. D.: Hydrogen Cavitation Performance of 80.6° Helical Inducer Mounted in Line with Stationary Centerbody. NASA TM X-1935, 1970.

29. Moore, R. D.; and Meng, P. R.: Thermodynamic Effects of Cavitation of an 80.6° Helical Inducer Operated in Hydrogen. NASA TN D-5614, 1970.

30. Bissell, W. R.; Wong, G. S.; and Winstead, T. W.: An Analysis of Two-Phase Flow in LH_2 Pumps for O_2/H_2 Rocket Engines. AIAA Paper No. 69-549, AIAA 5th Propulsion Joint Specialist Conference (U.S. Air Force Academy, Col.), June 1969.

31. Stripling, L. B.; and Acosta, A. J.: Cavitation in Turbopumps—Part 1. J. Basic Eng., vol. 84, Sept. 1962, pp. 326-338.

32. Wade, R. B.; and Acosta, A. J.: Investigation of Cavitating Cascades. J. Basic Eng., vol. 89, Dec. 1967, pp. 693-706.

33. Jakobsen, J. K.: Supercavitating Cascade Flow Analysis. J. Basic Eng., vol. 86, Dec. 1964, pp. 805-814.

34. Jakobsen, J. K.: Computer Program To Calculate Cavity on Inducer Blade. NASA Tech Brief, NAR 53852, 1968.

*35. King, W. S.: The Effect of Sweeping Back the Leading Edges of a 5.5 Inch Inducer. DDR 712-3003, Rocketdyne Div., North American Rockwell Corp. Unpublished, Oct. 1957.

*36. Iura, T.: Effect of Blade Leading Edge Modification on the Cavitation Performance of a Straight-Milled Inducer. DDR 512-61, Rocketdyne Div., North American Rockwell Corp. Unpublished, Sept. 1955.

37. Numachi, F.: Effect of Surface Roughness on Cavitation Performance of Hydrofoils—Part 3. J. Basic Eng., vol. 89, Mar. 1967, pp. 201-209.

38. Holl, J. W.: The Inception of Cavitation on Isolated Surface Irregularities. J. Basic Eng., vol. 82, Mar. 1960, pp. 169-183.

39. Acosta, A. J.: An Experimental Study of Cavitating Inducers. ACR 38, Second Symposium, Naval Hydrodynamics, Office of Naval Hydrodynamics, Office of Naval Research, 1958; Discussion by Toru Iura, p. 554.

*40. Rosenmann, W.: Results of Testing Three Experimental Model 17-Inch Mark 10 LOX Inducers at the CTL-I Water Tunnel Facility. TAMM 6115-54, Rocketdyne Div., North American Rockwell Corp. Unpublished, Aug. 1966.

*Dossier for design criteria monograph "Liquid Rocket Engine Turbopump Inducers." Unpublished, 1968. Collected source material available for inspection at NASA Lewis Research Center, Cleveland, Ohio.

*41. King, W. S.: Effect of Partial Blading on 5.5-Inch Inducer. DDM 712-3022, Rocketdyne Div., North American Rockwell Corp. Unpublished, Oct. 1957.

42. Montgomery, John C.: Analytic Performance Characteristics and Outlet Flow Conditions of Constant and Variable Lead Helical Inducers for Cryogenic Pumps. NASA TN D-583, 1961.

43. Sandercock, D. M.; Soltis, R. F.; and Anderson, D. A.: Cavitation and Non-Cavitation Performance of an 80.6° Flat-Plate Helical Inducer at Three Rotational Speeds. NASA TN D-1439, 1962.

44. Carter, A. D. S.; and Hughes, H. P.: A Theoretical Investigation Into the Effect of Profile Shape in the Performance of Aerofoils in Cascade. R&M 2384, British A.R.C., 1946.

45. Lieblein, S.: Incidence and Deviation Angle Corrections for Compressor Cascades. J. Basic Eng., vol. 82, Sept. 1960, pp. 575-587.

46. Lieblein, S.: Experimental Flow in Two-Dimensional Cascades; Chapter VI, Aerodynamic Design of Axial Flow Compressors. NASA SP-36, pp. 183-226.

*47. Rosenmann, W.: Mark 15 LOX Shrouded Inducer Test Report. TAMM 5115-103, Rocketdyne Div., North American Rockwell Corp. Unpublished, Dec. 1965.

*48. Schaffer, R. J.: Mark 10 Model LOX Inducer Performance With Shroud. CEM 0125-90, Rocketdyne Div., North American Rockwell Corp. Unpublished, Nov. 1960.

49. Wood, G. M.; Welna, H.; and Lamers, R. P.: Tip-Clearance Effects in Centrifugal Pumps. J. Basic Eng., vol. 87, Dec. 1965, pp. 932-940.

*50. Goff, L. R.: Backflow Deflector Influence on the Mark 10 LOX Pump Suction Performance Tests Conducted on CTL-V. TAMM 4115-86, Rocketdyne Div., North American Rockwell Corp. Unpublished, July 1964.

*51. Nielson, C. E.; and Fishburn, F. R.: The Effects of a Backflow Deflector Upon Mark 10 FRT Oxidizer Pump Head-Flow and Suction Performance and Pressure Oscillation at Bravo 2A. TAMM 6115-15, Rocketdyne Div., North American Rockwell Corp. Unpublished, Mar. 1966.

*52. Jackson, E.; and Goff, L.: Mark 10 LOX Pump Performance As Influenced by Inducer Diameter and by the Vaned Backflow Deflector. TAMM 5115-88, Rocketdyne Div., North American Rockwell Corp., Unpublished, Oct. 19, 1966.

*53. Hoshide, R. K.: Prewhirl Test Results on the Model Mark 10 LOX Pump. TAMM 2115-5, Rocketdyne Div., North American Rockwell Corp. Unpublished, Feb. 1962.

*54. Hoshide, R. K.: Test Results of the X-8 Pump Utilizing Prewhirl. TAMM 3115-2054, Rocketdyne Div., North American Rockwell Corp. Unpublished, Oct. 1963.

55. Wong, G. S.; MacGregor, C. A.; and Hoshide, R. K.: Suppression of Cavitation and Unstable Flow in Throttle Turbopumps. J. Spacecraft Rockets, vol. 2, no. 1, Jan.-Feb. 1965, pp. 73-80.

56. Peterson, R. E.: Stress Concentration Design Factors. John Wiley & Sons, Inc., 1962.

*57. Non-Ferrous Metallurgy Unit: Evaluation of Shot Peening as a Means of Increasing Life of F-1 Tens-50-T60 LOX Impellers at Cryogenic Temperatures. MPR 4-252-138, Rocketdyne Div., North American Rockwell Corp. Unpublished, June 1964.

58. Anon.: Compatibility of Materials With Rocket Propellants and Oxidizers. Memorandum 201, Defense Metals Information Center, Battelle Memorial Institute (Columbus, Ohio), Jan. 1965, pp. 5, 6, 17.

*59. Goff, L.; and Jackson, E.: Effect of Increased Inducer Radial Clearance on Low Frequency Pump Inlet Oscillations, H-Q and Suction Performance for the Mark 10 Fuel Pump. TAMM 6115-34, Rocketdyne Div., North American Rockwell Corp. Unpublished, June 1966.

*Dossier for design criteria monograph "Liquid Rocket Engine Turbopump Inducers." Unpublished, 1968. Collected source material available for inspection at NASA Lewis Research Center, Cleveland, Ohio.

*60. Jackson, E. D.: Mark 10 Quieting Program—Oscillation Reduction by Holes in the Inducer Blades. Phase I—Water Tunnel Study Using Mk 4 Inducers. TAMM 5115-23, Rocketdyne Div., North American Rockwell Corp. Unpublished, Feb. 1965.

*61. Jackson, E. D.; and Fishburn, F. R.: Test Results for the Model Mark 10 Fuel Pump With the 20-Inch Model Turbine Fuel Inlet Manifold, 6+6 Impeller and Tapered Inducer With and Without Holes. Unpublished, TAMM 5115-78, Rocketdyne Div., North American Rockwell Corp. Oct. 1965.

*62. Jackson, E. D.: Oscillation and Suction Performance Results of Test With Mark 10 Fuel Inducer and Modifications in Water Tunnel. TAMM 5115-80, Rocketdyne Div., North American Rockwell Corp. Unpublished, Sept. 1965.

*63. Stremel, R. L.: Elimination of Pressure Surges Occurring in the Mark 3 LOX Pump. CEM/FGD/925-2039, Rocketdyne Div., North American Rockwell Corp. Unpublished, May 1959.

*64. Jackson, E. D.: Oscillation and Suction Performance Results of Tests With Mark 10 LOX Inducers With and Without Holes in the Water Tunnel. TAMM 5115-91, Rocketdyne Div., North American Rockwell Corp. Unpublished, Nov. 1965.

*65. Rosenmann, W.: Results of Testing Gas Injection in Mark 10 Fuel Inducer. TAMM 5115-76, Rocketdyne Div., North American Rockwell Corp. Unpublished, Sept. 1965.

*66. Nielson, C.; and Fishburn, F.: POGO J-2 Oxidizer Pump Test Results—(a) Head Capacity and Suction Performance, (b) Gaseous Helium Injection, (c) LOX Warming. TAMM 5155-77, Rocketdyne Div., North American Rockwell Corp. Unpublished, Nov. 1965.

67. Jackson, E. D.: Final Report, Study of Pump Discharge Pressure Oscillations. NASA CR-80153, 1966.

68. Anon.: Metallic Materials and Elements for Aerospace Vehicle Structures. MIL-HDBK-5A, Department of Defense, Feb. 8, 1966.

69. Agricola, K. R.: The Usefulness of Materials Used in Booster Structures. Paper presented at the Symposium, The Application and Properties of Materials Used in Aerospace Vehicle Design, sponsored by The Martin Company (Denver, Colo.), May 4-6, 1960.

70. Anon.: 6000 Pound Thrust Jet Propulsion Unit; Part II, Materials Corrosion Data. Rep. SPD 121, Contract AF W33(038)-ac-13916, M. W. Kellogg Company, Mar. 1948.

71. Nelson, G. A.: Corrosion Data Survey. Shell Development Company (Emeryville, Calif.), 1960.

72. Ordin, P. M.; Miller, R. O.; and Diehl, J. M.: Preliminary Investigation of Hydrazine As a Rocket Fuel. NACA Rep. E7H21, May 1948.

73. Liberto, R. R.: Research and Development on the Basic Design of Storable High-Energy Propellant Systems and Components. Final Rep. TR 60-61, Contract AF 33(616)-6689, Bell Aerosystems Co. (Buffalo, N. Y.), May 1961.

74. Schmidt, H.: Fluorine and Fluorine-Oxygen Mixtures in Rocket Systems. NASA SP-3037, 1967.

75. Young, J. O.; and Holl, J. W.: Effects of Cavitation on Periodic Wakes Behind Symmetric Wedges. J. Basic Eng., vol. 88, Mar. 1966, pp. 163-176.

76. Yeh, H.; and Eisenhuth, J. W.: The Unsteady Wake Interaction in Turbomachinery and Its Effect on Cavitation. J. Basic Eng., vol. 81, June 1959, pp. 181-189.

*77. Lambert, R. B.: Vibration Tests of Mark 10 LOX Inducer. SM 4111-8057, Rocketdyne Div., North American Rockwell Corp. Unpublished, Dec. 1964.

*78. King, W. S.: Investigation of the Blade Failure on the Mark 6 Model Oxidizer Inducer. DDM 812-3025, Rocketdyne Div., North American Rockwell Corp. Unpublished, Mar. 1958.

*Dossier for design criteria monograph "Liquid Rocket Engine Turbopump Inducers." Unpublished, 1968. Collected source material available for inspection at NASA Lewis Research Center, Cleveland, Ohio.

*79. Stripling, L. B.: Digital Computer Program—Flat Plate Blade Loading Analysis. Free-Streamline-Wake Theory. IR 220, Rocketdyne Div., North American Rockwell Corp. Unpublished, 1962.

80. Herman, L. R.: Bending Analysis for Plates. Proceedings of the Conference on Matrix Methods in Structural Mechanics, Wright-Patterson AFB (Dayton, Ohio), Oct. 1965, AFFDL TR 66-80 (AD 646300), Nov. 1966, pp. 577-602.

81. Becker, E.; and Brisbane, J.: Application of the Finite Element Method to Stress Analysis of Solid Propellant Rocket Grains. Rep. S-76, Rohm & Haas Co., vol. I (AD 474031), Nov. 1965; vol. II, part 1 (AD 476515); vol. II, part 2 (AD 476735), Jan. 1966.

82. Lang, T. E.: Summary of the Functions and Capabilities of the Structural Analysis and Matrix Interpretive System Computer Program (SAMIS). Tech. Rep. 32-1075, Jet Propulsion Lab., NASA CR-83742, Apr. 1967.

83. Holms, A. G.; and Repko, A. J.: Correlation of Tensile Strength, Tensile Ductility, and Notch Tensile Strength With the Strength of Rotating Disks of Several Designs in the Range of Low and Intermediate Ductility. NACA TN 2791, 1952.

84. Rosenmann, W.: Experimental Investigations of Hydrodynamically Induced Shaft Forces With a Three Bladed Inducer. Symposium on Cavitation in Fluid Machinery, ASME Winter Annual Meeting (Chicago, Ill.), Nov. 1965, pp. 172-195.

85. Abbott, I. H.; and Von Doenhoff, A. E.: Theory of Wing Sections. Dover Pub., Inc., 1960.

*86. Goff, L. R.; and Gulbrandsen, N. C.: Results of the Suction Side Refaired Mark 10 LOX Pump Inducer Tests Conducted at CTL-V, Cell 4A and Bravo 2. TAMM 4115-138, Rocketdyne Div., North American Rockwell Corp. Unpublished, Nov. 1964.

*87. Dolony, J. F.: Axial Stack-up Analysis and Prestressed Bolts. Stress Note No. 15, Rocketdyne Div., North American Rockwell Corp. Unpublished, Oct. 1964.

88. Campbell, M.; Thompson, M. B.; and Hopkins, V.: Solid Lubricant Handbook for Use in the Space Industry. Contract NAS8-1540, Control No. TP85-137, Midwest Research Institute (Kansas City, Mo.), 1968.

89. Campbell, W.: The Protection of Steam Turbine Disc Wheels From Axial Vibration. Trans. ASME, vol. 46, 1924, pp. 31-140; Discussion, pp. 140-160.

*90. Turner, J. D.: The Effect of Fluid Density on Stator Blade Resonant Frequency. SM 3111-8073A, Rocketdyne Div., North American Rockwell Corp. Unpublished, Dec. 1963.

91. Anderson, R. G.: How To Design High Speed Rotating Parts for Maximum Burst Resistance. Mach. Design, vol. 29, no. 21, Oct. 17, 1957, pp. 148-156.

92. Holms, A. G.; Jenkins, J. E.; and Repko, A. J.: Influence of Tensile Strength and Ductility on Strengths of Rotating Disks in Presence of Material and Fabrication Defects of Several Types. NACA TN 2397, 1951.

93. Holms, A. G.; and Jenkins, J. E.: Effect of Strength and Ductility on Burst Characteristics of Rotating Disks. NASA TN 1667, 1948.

94. Winne, D. H.; and Wundt, B. M.: Application of the Griffith-Irwin Theory of Crack Propagation to the Bursting Behavior of Discs, Including Analytical and Experimental Studies. Trans. ASME, vol. 80, Nov. 1958, pp. 1643-1658.

95. Anon.: Mechanical Design Aspects of Centrifugal Impellers With High Tip Speed Capability (U). Rep. 7446-01F, Contract AF 04(611)-7446, Aerojet-General Corp. (AD 350716), Mar. 1963. Confidential.

96. Anon.: Mechanical Design Aspects of Centrifugal Impellers With High Tip Speed Capability: The Results of Experimental Program (U). Report Phase II Final. Rep. 7446-01F, Aerojet-General Corporation (AD 340146), Aug. 1963. Confidential.

*Dossier for design criteria monograph "Liquid Rocket Engine Turbopump Inducers." Unpublished, 1968. Collected source material available for inspection at NASA Lewis Research Center, Cleveland, Ohio.

GLOSSARY

Symbol	Definition	Remarks
A	inducer inlet flow area, ft^2	$\pi/4\ (D^2 - d^2)$
A_H	meridional cross-sectional area of inducer hub, in.^{2}	
a	mathematical expression, eq. (42)	defined in eq. (42b)
b	mathematical expression, eq. (42)	defined in eq. (42a)
b	exponent in eq. (48)	approx. value = 0.5
C	blade chord length, ft	
C	empirical constant, eq. (17)	
C_p	pressure coefficient, eq. (61)	defined in eq. (60)
C_ψ	constant of integration, eqs. (38) and (41)	defined in eq. (43)
c	absolute fluid velocity, ft/sec	
c	radial clearance, ft	eqs. (54) and (55)
c_L	specific heat of liquid, Btu/(lb-°R)	
$c_{m,\,max}$	maximum obtainable meridional fluid velocity, ft/sec	
D	inducer inlet tip diameter, ft	
D_c	cavity diameter, ft	
D_s	suction specific diameter	$D\,(\mathrm{NPSH})^{¼}/Q^{½}$
D'_s	corrected value of D_s (zero hub blockage)	fig. 1 $(1 - \nu^2)^{½} D_s$
d	inducer inlet hub diameter, ft	
d_i, d_o	inside and outside diameters of hub shear section, in.	
E	material modulus of elasticity	
ELI	extra-low-interstitial (content of interstitial elements)	
e	elongation in 4-diameter length of test rod	
F	mathematical expression, eq. (26)	defined in eq. (27)
F_e	material endurance limit strength, lb/in.^{2}	
F_{tu}	material ultimate tensile strength, lb/in.^{2}	
F_{ty}	material yield strength, lb/in.^{2}	

Symbol	Definition	Remarks
FLOX	mixture of liquid oxygen and fluorine	
f_b	disc burst factor	
f_d	disc design factor	
f_i	column matrix of nodal forces	
g	acceleration of gravity, 32.174 ft/sec^2	
H	total head, ft	
H_{loss}	line friction head loss, ft	
ΔH	local total head rise, ft	
ΔH_{net}	net total head rise per stage, ft	
Hz	Hertz, cps	
h	static head, ft	p_s/ρ
h_c	cavity height, ft	
I_{A1}	expression for integral, eq. (43)	defined in eq. (43a)
I_{A2}	expression for integral, eq. (43)	defined in eq. (43b)
I_{B1}	expression for integral, eq. (43)	defined in eq. (43c)
I_{B2}	expression for integral, eq. (43)	defined in eq. (43d)
IRFNA	inhibited red fuming nitric acid	
J	energy conversion factor	778.2 ft-lb/Btu
j	symbol for blade number in eq. (43)	
K	blade tip cavitation number	$\frac{p_s - p_v}{\frac{1}{2}\rho w_1^2/g}$
K	empirical constant, eq. (81)	
K^*	minimum value of cavitation number K at which blade will operate	
K_c	cavitation number based on cavity pressure p_c instead of fluid bulk vapor pressure p_v	$\frac{p_s - p_c}{\frac{1}{2}\rho w_1^2/g}$
K_{min}	cavitation number at supercavitation	
K_t	theoretical stress concentration factor	
K_{tf}	actual stress concentration factor	
K_{tsf}	fatigue notch factor for shear stress	
k	thermal conductivity, Btu/(sec-ft-°R)	
k_i	square symmetric element stiffness matrix	

Symbol	Definition	Remarks
k_s	empirical coefficient, eq. (54)	$k_s = 0.50$ to 0.65 experimentally
k_ψ	empirical coefficient, eq. (55)	$k_\psi = 1.0$
L	latent heat, Btu/lb, eq. (14)	
L	blade radial length, ft	
L_{ax}	axial length of blade, ft	
L_b	mathematical expression, eq. (86)	defined in eq. (87)
L_c	cavity length, ft	
L_s	mathematical expression, eq. (86)	defined in eq. (88)
l_w	length of blade wedge, ft	
M	coefficient, eq. (48)	has value $\approx$ 0.25 to 0.35
ms	mean or rms station	
$m1$, $m2$, $m3$	empirical exponents, eq. (17)	
N	blade number	
NPSH	net positive suction head, ft	$(p_{total} - p_v)/\rho_F$
$NPSH_{tank}$	minimum net positive suction head in tank at operating conditions, ft	
n	shaft or hub speed, rpm	
n	natural frequency of blade, Hz	measured at condition shown by subscript
n_f	safety factor for fatigue	
n_{ult}	safety factor against ultimate failure	
n_y	safety factor against yield failure	
n_0	natural frequency of blade in vacuum (or in atmosphere), Hz	
p_c	fluid vapor pressure in cavity at leading, edge, lb/ft^2	
p_s	fluid static pressure, lb/ft^2	
p_{total}	total fluid pressure at any point, lb/ft^2	$p_s + 1/2\rho_F c^2$
p_v	fluid bulk vapor pressure, lb/ft^2	
Q	flowrate, gpm	
Q'	corrected flowrate	$Q/(1 - \nu^2)$
R	radius of blade edge, in.	
R_C	Rockwell hardness C	

Symbol	Definition	Remarks
r	radial coordinate, ft	
r_{FSL}	radius of curvature of free streamline, in.	
rms	root mean square	$X_{rms} = \sqrt{\frac{X_1^2 + X_2^2 + \cdots + X_n^2}{n}}$
$r\theta$	blade wrap, ft	
$r\omega$	blade velocity, ft/sec	
S	blade or cascade spacing, ft	$\pi D/N$
S_s	suction specific speed	$nQ^{1/2}\ (\mathrm{NPSH})^{-3/4}$
$S_{s,0}$	suction specific speed for zero clearance	
S'_s	corrected suction specific speed	$S_s/(1 - \nu^2)^{1/2}$
$S'_s{}^*$	characteristic suction specific speed (determined in cold water)	
$S'_{s,\max}$	maximum suction specific speed obtainable with K^*	
T	fluid bulk temperature, °R	
TSH	thermal suppression head, ft	
t	blade thickness, in.	
U_c	fluid velocity on cavity boundary, ft/sec	
UDMH	unsymmetric dimethyl hydrazine	
u	blade tip speed, ft/sec	$\pi D\, n/60$
w	fluid velocity relative to blade at tip, ft/sec	$\sqrt{u^2 + c_m{}^2}$
w_c	fluid velocity on cavity boundary, ft/sec	
Z	NPSH factor	$2g\ (\mathrm{NPSH})_{\mathrm{tank}}/c_m{}^2$
z	axial coordinate, ft	
dz	change in z with change in $r\theta$, ft	
Δz	axial blade clearance, ft	
α	incidence angle of flow at blade leading edge, deg	
α	thermal cavitation parameter	defined in eq. (14), used in eq. (17)
α_{cant}	blade cant angle, deg	
α_{cone}	blade cone angle, deg	
α_w	wedge angle of blade, deg	

Symbol	Definition	Remarks
β	thermal factor, $sec^{1/2}$	defined in eq. (16)
β	blade angle, deg	
$\Delta\beta$	blade camber, deg	
β_w	blade angle measured to suction side of wedge, deg	
γ	fluid angle, deg	
$\Delta\gamma$	fluid turning angle, deg	
δ	deviation angle, deg	
δ_i	column matrix of modal deflections	
η	hydraulic efficiency	
θ	blade wrap angle (leading-edge sweep), rad	
K	thermal diffusivity, ft^2/sec	defined in eq. (15), used in eqs. (16) and (17)
Λ	blade lead, ft	
λ	blade lead per radian, ft/rad	
$\lambda\omega$	blade lead velocity, ft/sec	
ν	hub-to-tip diameter ratio	d/D
ρ	density, lb/ft^3	
Σ	mathematical expression, eq. (72)	defined in eq. (73)
σ	cascade solidity	
σ_{alt}	alternating stress, $lb/in.^2$	$(\sigma_{max} - \sigma_{min})/2$
σ_{AT}	average tangential stress at speed N, $lb/in.^2$	
$\sigma_{AT,\ burst}$	average tangential stress at burst speed, N_{burst}, $lb/in.^2$	
σ_{ax}	axial stress, $lb/in.^2$	
σ_{MT}	maximum tangential stress from basic stress analysis, $lb/in.^2$	
σ^*_{MT}	maximum tangential stress in disc including stress concentration effects, $lb/in.^2$	
σ_{mean}	average stress, $lb/in.^2$	$(\sigma_{max} + \sigma_{min})/2$
σ_t	local tangential stress, $lb/in.^2$	
τ	cavitation parameter	$(NPSH)/(u^2/2g)$
τ_{alt}	alternating shear stress, $lb/in.^2$	eq. (86)

Symbol	Definition	Remarks
τ_0	allowable shear stress, lb/in.^{2}	eq. (86)
ϕ	flow coefficient, ref. to inlet tip blade speed	c_m/u
ψ	head coefficient, ref. to inlet tip blade speed	$H/(u^2/g)$
ψ_l	head coefficient, local value at radius r	c_u/u
ψ_0	head coefficient for zero clearance	
ω	angular velocity, rad/sec	

Subscripts

1	inlet	m	meridional
2	outlet	ms	mean or rms station
a	axial component	op	operating conditions
bl	blade	opt	optimum
burst	burst speed	T	tip
d	design value	TE	trailing edge
F	fluid	test	test conditions
H	hub	u	tangential component
L	liquid	v	vapor
LE	leading edge	yield	yield speed
l	local station		

NASA SPACE VEHICLE DESIGN CRITERIA
MONOGRAPHS ISSUED TO DATE

ENVIRONMENT

SP-8005	Solar Electromagnetic Radiation, June 1965
SP-8010	Models of Mars Atmosphere (1967), May 1968
SP-8011	Models of Venus Atmosphere (1968), December 1968
SP-8013	Meteoroid Environment Model—1969 (Near Earth to Lunar Surface), March 1969
SP-8017	Magnetic Fields—Earth and Extraterrestrial, March 1969
SP-8020	Mars Surface Models (1968), May 1969
SP-8021	Models of Earth's Atmosphere (120 to 1000 km), May 1969
SP-8023	Lunar Surface Models, May 1969
SP-8037	Assessment and Control of Spacecraft Magnetic Fields, September 1970
SP-8038	Meteoroid Environment Model—1970 (Interplanetary and Planetary), October 1970

STRUCTURES

SP-8001	Buffeting During Atmospheric Ascent, revised November 1970
SP-8002	Flight-Loads Measurements During Launch and Exit, December 1964
SP-8003	Flutter, Buzz, and Divergence, July 1964
SP-8004	Panel Flutter, July 1964
SP-8006	Local Steady Aerodynamic Loads During Launch and Exit, May 1965
SP-8007	Buckling of Thin-Walled Circular Cylinders, revised August 1968
SP-8008	Prelaunch Ground Wind Loads, November 1965
SP-8009	Propellant Slosh Loads, August 1968
SP-8012	Natural Vibration Modal Analysis, September 1968
SP-8014	Entry Thermal Protection, August 1968
SP-8019	Buckling of Thin-Walled Truncated Cones, September 1968
SP-8022	Staging Loads, February 1969

SP-8029	Aerodynamic and Rocket-Exhaust Heating During Launch and Ascent, May 1969
SP-8031	Slosh Suppression, May 1969
SP-8032	Buckling of Thin-Walled Doubly Curved Shells, August 1969
SP-8035	Wind Loads During Ascent, June 1970
SP-8040	Fracture Control of Metallic Pressure Vessels, May 1970
SP-8046	Landing Impact Attenuation For Non-Surface-Planing Landers, April 1970
SP-8050	Structural Vibration Prediction, June 1970

GUIDANCE AND CONTROL

SP-8015	Guidance and Navigation for Entry Vehicles, November 1968
SP-8016	Effects of Structural Flexibility on Spacecrafe Control Systems, April 1969
SP-8018	Spacecraft Magnetic Torques, March 1969
SP-8024	Spacecraft Gravitational Torques, May 1969
SP-8026	Spacecraft Star Trackers, July 1970
SP-8027	Spacecraft Radiation Torques, October 1969
SP-8028	Entry Vehicle Control, November 1969
SP-8033	Spacecraft Earth Horizon Sensors, December 1969
SP-8034	Spacecraft Mass Expulsion Torques, December 1969
SP-8036	Effects of Structural Flexibility on Launch Vehicle Control Systems, February 1970
SP-8047	Spacecraft Sun Sensors, June 1970
SP-8058	Spacecraft Aerodynamic Torques, January 1971
SP-8059	Spcecraft Attitude Control During Thrusting Maneuvers, February 1971

CHEMICAL PROPULSION

SP-8025	Solid Rocket Motor Metal Cases, April 1970
SP-8041	Captive-Fired Testing of Solid Rocket Motors, March 1971
SP-8048	Liquid Rocket Engine Turbopump Bearings, March 1971
SP-8051	Solid Rocket Motor Igniters, March 1971